Variations in soil fluxes of methane and carbon dioxide in an immature deciduous forest

未成熟な落葉樹林におけるメタンと二酸化炭素の土壌フラックスの変動特性

Hokkaido University　Graduate School of Agriculture
Frontiers of Environment Sciences　Doctoral Course

Hu Rui

Academic supervisor: Prof. Hirano Takashi

Co-advisors: Prof. Toma Yo
Prof. Kato Tomomichi

Date of defense: 29th July, 2024

Abstract

Soil carbon flux is the primary pathway of carbon (C) cycling between the atmosphere and terrestrial ecosystems. It determines the rate at which soil absorbs C from the atmosphere or releases C back into the atmosphere. In terrestrial ecosystems, nearly half of the total organic C is stored in forest soils, highlighting the importance of forest soils in regulating soil C balance and global climate change. Soil carbon flux primarily refers to the flux of soil methane (CH_4) and carbon dioxide (CO_2), with the latter also known as soil respiration (RS). Soil CH_4 dynamics are primarily influenced by soil microbial processes. Soil respiration consists of two main components: heterotrophic respiration (RH) and root respiration (RR). RH is a result of the decomposition of soil organic matter (SOM), while RR is a result of root metabolism. Therefore, RH and RR respond differently to environmental factors. Accurately partitioning RS is crucial for understanding the dynamic changes in soil C stock. Gross primary production (GPP) provides the substrate for root metabolism, which significantly affects RR. However, since it is not possible to directly measure RR, the relationship between RR and GPP remains unclear.

The field experiment was conducted in a naturally regenerating immature open forest located in Tomakomai, southern Hokkaido, Japan (42°44′ N, 141°31′ E; elevation 125 m) after a severe blowdown caused by a typhoon in 2004. Soil CH_4 and CO_2 fluxes were continuously measured using an automated chamber system during the growing seasons in 2021 and 2022. The chamber system was composed of a control unit and transparent rectangular chambers with an open area of 0.9 m × 0.9 m and height of 0.5 m. Eighteen transparent chambers were randomly distributed within an area of 30 m × 30 m, among which 10 chambers were used in this study. The 10 chambers were allocated to two treatments: five trench chambers (no vegetation, corresponding to RH) and five root chambers (with root but no aboveground vegetation, corresponding to RR).

Among five root chambers, fine root biomass and production were measured by the soil core sampling and ingrowth core methods, respectively. Physicochemical properties of the surface soil and meteorological factors were used to explain the spatiotemporal variation in CO_2 and CH_4 fluxed. Soil carbon flux was predicted by environmental variables using RF and Gradient Boost Model (GBM) modelling algorithms, in which feature importance extracted from RF models was used to represent the controlling factors of soil CO_2 and CH_4 fluxes. Moreover, RS was separated using a conventional method according to an empirical equation: RR = RS − RH. Meanwhile, a high-accuracy RF model, which was developed from Trench chambers' flux data, was used to estimate RH in Root chambers. Thus, RR could be calculated as a difference between RS and the estimated RH using the RF model. RRs calculated using the two methods were fitted with soil temperature using an exponential regression. Moreover, the two types of RR were fitted with GPP, which was measured by the eddy covariance method at 11 m near the chambers, by a Cross Correlation Function (CCF) and wavelet cross power analysis to determine the time delay between ecosystem productivity and root respiration.

Results and conclusions of this study are summarized as follows:

Part 1: Soil carbon dynamics

For two years, mean daily CH_4 fluxes in Trench and Root chambers were −2.35 ± 0.47 nmol m^{-2} s^{-1} and −2.56 ± 0.61 nmol m^{-2} s^{-1} (± 1 standard deviation), respectively, and daily CO_2 flux was 2.14 ± 1.49 μmol m^{-2} s^{-1} and 2.67 ± 1.69 μmol m^{-2} s^{-1}, respectively, indicating that the forest soil functioned as a net CH_4 sink and CO_2 source in 2021 and 2022. Daily CH_4 and CO_2 fluxes showed a clear seasonal trend, and the peaks of CH_4 uptake and CO_2 emission appeared at around DOY of approximately 220, corresponding to the seasonality of soil moisture and temperature. The RF algorithm had a better performance in predicting soil C flux than the GBM algorithm; the RF

approach had higher R^2 and lower RMSE in both treatments. Models based on Root chambers data had higher accuracy than Trench chambers, and CO_2 models had higher accuracy than CH_4 models. The soil O_2 diffusion rate had the highest relative importance in CH_4 models in both treatments, followed by water-filled pore space (WFPS), suggesting that soil CH_4 uptake was controlled by soil moisture. In contrast, soil temperature was the dominant factor in CO_2 models, with relative influence of soil temperature contributed for around 35% of relative influence in both treatments, indicating soil temperature was the main factor to regulate soil CO_2 emission. Soil temperature had a positive effect on soil CH_4 uptake and CO_2 emission, while soil moisture posted a negative effect on soil CH_4 uptake, and a complex both positive and negative effect on soil CO_2 emission.

Part 2: Separation of soil respiration

Two-year mean daily RR separated using conventional method (RR_C) was 0.53 ± 0.39 μmol m^{-2} s^{-1}, which was significantly lower ($P < 0.05$) than that by RF modelling (RR_RF) (0.61 ± 0.50 μmol $m^{-2}s^{-1}$), suggesting conventional method tended to underestimate RR by 15% in this study. Significant spatial variation emerged among Root chambers in RR estimated by both methods, with unreasonable minus RR in R1 chamber (−0.069 ± 0.38 μmol m^{-2} s^{-1} for RR_C and −0.003 ± 0.45 μmol $m^{-2}s^{-1}$ for RR_RF). To ensure the credibility of data analysis, RR in chamber R1 and R2 was excluded from following analysis for low data quality and big data gap. Fitting between soil temperature and RR_RF was better than RR_C; R^2 of exponential regression was 0.52 and 0.44, respectively. Sensitivity to temperature (Q_{10}) of RR_RF was 2.43 ± 1.27, higher than that of RR_C (2.00 ± 0.98), suggesting root respiration estimated by RF modelling method was more sensitive to the change of soil temperature.

Part 3: Time lag estimation between GPP and RR

RS, along with separated RR in Part 2, was standardized and denoised for wavelet

analysis with processed GPP data. Hourly data was averaged for the diurnal trend of GPP, RS and RRs in different months, and results showed that GPP peaked at noon throughout the whole growing seasons and RS peaked at 15-18 PM, suggesting that time lag between GPP and root respiration was approximately 5-8 hours. RR_RF had a similar diurnal trend to GPP while RR_C showed a vague diurnal trend in some months. The result of wavelet power analysis showed that GPP, RS, and RRs had a significant one-day period, suggesting that GPP, soil respiration and root respiration had a clear diurnal trend in this study. However, diurnal trend of GPP and RS was more significant than RRs, especially RR_C did not show a clear trend in 2022. Two-year mean daily time lags estimated using wavelet cross power method and phase difference method was 6.56 ± 4.06 hours for GPP/RS, which means change of GPP led the change of soil respiration by about 6.5 hours. Time lag of GPP/RR_RF was estimated to be 5.12 ± 4.70 hours, significantly higher than that of RR_C (2.97 ± 5.00 hours). Significant seasonal variation ($P < 0.05$) appeared in GPP/RR_RF, but no significant interannual variation ($P > 0.05$) was found, which was considered to be reasonable in an undisturbed ecosystem. As a contrast, significant variation ($P < 0.001$) appeared both within each year and interannually in lags of GPP/RR_C, suggesting an unreliable result of time lag between GPP and root respiration estimated by the conventional method, which indicates RF modelling method was more reliable than the conventional method in estimating root respiration. In addition, RS and two RRs (RR_C and RR_RF) were normalized at a base temperature of 15 °C to exclude the impact from soil temperature on soil respiration and root respiration. However, fitting performance based on temperature-normalized data was poor and time lags estimated using normalized data were unreliable, with minus lags appeared commonly. As a result, time lag between GPP and soil respiration in Tomakomai site was estimated to be approximately 6.5 hours, longer than the lag between GPP and root respiration (around 5 hours).

Soil carbon dynamics are closely related to carbon cycling between terrestrial

ecosystem and atmosphere, which has widely acknowledged as one of the main factors to regulate future global climate change. Findings in this study could help to increase the understanding of mechanism of how the environmental factors interacted with soil carbon dynamics, and to quantify the lag between ecosystem production and root respiration, which has a great application potential in increasing the model accuracy in predicting soil respiration.

Keywords: Soil carbon flux; Machine learning models; Automated chamber system; Soil respiration separation; Wavelet cross power; Time lag.

Contents

1. General Introduction

1.1 Introduction

In this study, soil carbon (C) fluxes of carbon dioxide (CO_2) and methane (CH_4) were measured using an automated chamber system from 2021 to 2022 in a regenerating cool-temperate deciduous forest in Tomakomai, Japan. Large-quantity flux data were related to environmental variables using machine learning (ML) modelling methods. Results of ML models were further used to separate soil respiration (RS), and then separated root respiration (RR) was related to gross primary production (GPP) using wavelet analysis methods. In this part, research backgrounds and objectives are introduced. Background includes soil C cycling process and its important role in climate change, controlling factors of soil CO_2 and CH_4 fluxes, and measurement and analysis methods of soil C flux.

1.2 Backgrounds

1.2.1 Forest soil carbon stock and its role on global carbon cycles

Soil carbon flux is the primary pathway of the C cycle between soil and the atmosphere, determining how fast the soil fix C from the atmosphere or emit C to the atmosphere (Brevik, 2012; Trumbore, 2006). In terrestrial ecosystems, forests cover more than 4 billion hectares, nearly 30% of Earth's land surface, accounting for 75% of gross primary production (GPP, Mukul et al., 2021; Beer et al. 2010) and containing more carbon in biomass and soils than which is stored in the atmosphere (Pan et al. 2013; Jhariya et al., 2019). Forest ecosystems play a crucial role in regulating the global climate by acting as significant carbon sinks. Generally, carbon cycling in forest ecosystems can be divided into two processes: the photosynthesis of vegetation, which transfers carbon absorbed from atmosphere to the stems, roots, fruits, and leaves for growth and maintenance (Kondo et al., 2018), and the respiration of plants and microbes, which releases the C stored in forests back to the atmosphere (Janzen et al., 2006). Forests are also considered as one of the main global anthropogenic carbon sources

(second to the fossil fuel combustion), primarily through deforestation and forest degradation (Malhi et al., 2002; Gatti et al., 2021).

Forest carbon stock can be mainly divided into five pools: 1) aboveground biomass; 2) belowground biomass; 3) litter; 4) deadwood / woody debris (coarse woody debris: CWD); and 5) soil (Zhang et al., 2013; Latte et al., 2013). Forest soil C stock refers to the amount of C stored in the soil of forested areas, which can be recognized in two forms: organic and inorganic C (Tan et al., 2014). Organic C is the dominant form of soil C that is available in soil organic matters (SOM). Inorganic C, on the other hand, is the mineral form of C that is originated from Earth's parent materials primarily through weathering (Das et al., 2023; Azam et al., 2020). Forest soils store 400–800 Pg soil organic C (SOC) out of a global total of 1200-1600 Pg SOC (Hiederer et al., 2011; Yu et al., 2020; Díaz-Hernández et al., 2010). When it comes to the CH_4 cycle, forest soil is reported to account for up to 62% of global soil CH_4 sink (Lee et al., 2023).

The size of the forest soil C stock is influenced by the interacting driving factors that determine the fertility and productivity of the whole ecosystems, including climate patterns, vegetation communities, local topography, soil chemical, physical and biological properties, and the land-use and management practices (Mayer et al., 2020; Chen et al., 2018; Noormets et al., 2015). Natural and anthropogenic disturbances influence forest soil C stocks by affecting rates of organic matter input and decomposition (Jandl et al., 2007). Natural disturbances such as wildfire, pests, diseases and windthrow can temporarily reduce soil C stocks (Lindgren, 2011), while anthropogenic disturbance relates to both conversion of forests to other land uses and modifications of forests involved in the provision of forest products and services (Nave et al., 2010; Payn et al., 2015). In the context of global climate change, influences from increasing temperature and atmospheric greenhouse gas (GHG) concentration on forest soil C stock are complex. On one hand, continuous increase of temperature led to increasing C loss of forest soil through enhancing soil microorganism activities and decomposition of SOM (Ramesh et al., 2019). Increased C release from soil rises the atmospheric concentration of GHGs, leading to higher temperature and more carbon

loss from forest soil (known as a positive feedback, Stuart Chapin et al., 2019). On the other hand, increased CO_2 concentration improved plant photosynthesis which helped forest ecosystems fix more atmospheric C into plant biomass and soil (CO_2 fertilization effect), resulting in the mitigation of global climate change (known as a negative feedback, Walker et al., 2021; Launiainen et al., 2022). Thus, comprehensive understanding of certain quantity and dynamics of forest soil C stock is a key when formulating sustainable development strategies in the future.

1.2.2 Controlling factors of soil carbon dioxide flux

Soil CO_2 flux is the basic form of RS (Jian et al., 2022), which can be divided into two parts: autotrophic respiration (RA) and heterotrophic respiration (RH). RA mainly originates from the metabolic activities of plant fine root (Gessler et al., 2024), thus RA is also widely acknowledged as RR. RH primarily comes from the activities of soil microorganisms (Suseela et al., 2012). These two components have different sources and respond differently to changes in environmental factors (Hu et al., 2018; Savage et al., 2013). Therefore, accurately separating RS into RH and RR is crucial for understanding the feedback of soil C storage on global climate (Phillips et al., 2017). However, it is very difficult to measure RR directly in the field for the long term. Exploring a reliable and convenient method to separate RS has become an urge need in the context of global climate change.

The factors influencing forest soil CO_2 flux can be broadly categorized into biotic and abiotic components. Biotic factors include the types and activities of soil organisms, from microorganisms such as bacteria and fungi to larger soil fauna, and the plant roots that interact with and modify the soil environment (Pritchard et al., 2011; Drigo et al., 2008). These biological activities are instrumental in the decomposition of SOM, which significantly influences CO_2 emissions through respiration processes (Li et al., 2018).

Abiotic factors encompass a wide range of physical and chemical soil properties, and environmental conditions. Soil texture, moisture, temperature, and pH levels play critical roles in determining CO_2 flux (Iqbal et al., 2008; Feizienė et al., 2010; Wu et al.,

2010). For example, soil temperature affects soil CO_2 flux through five ways: 1) The rate of microbial metabolism increases with temperature, following a roughly exponential relationship up to a certain threshold (Mikan et al., 2002). As soil temperature rises, the activity of microorganisms increases, leading to faster decomposition of organic matter and subsequently higher RH (Fang et al., 2001); 2) RR increases with soil temperature because metabolic processes in plant tissues speed up as temperatures rise, which contributes to higher CO_2 fluxes from the soil (Dusenge et al., 2019; Hopkins et al., 2013); 3) Enzymatic reactions which decompose SOM will be enhanced when soil temperature rises, leading to higher RH (Wang et al., 2020; Davidson et al., 2006); 4) Soil temperature interacts with soil moisture levels to affect CO_2 flux especially when drought events occur. High temperatures can lead to soil drying, which might limit microbial activity and reduce CO_2 emissions (Schaufler et al., 2010); 5) Higher temperatures can change the physical structure of the soil (e.g. soil porosity), potentially increase the diffusion rate of CO_2 from the soil to the atmosphere (Ganot et al., 2014).

Additionally, human activities and natural disturbances significantly impact forest soil CO_2 flux. Land use changes, such as deforestation, afforestation, and agricultural practices, will alter soil structure, composition, and the organic matter content, thereby affecting soil CO_2 dynamics (Ahirwal et al., 2021; Ramesh et al., 2019). Similarly, natural disturbances like wildfires, extreme weathers, and pest plagues can lead to significant changes in soil C stocks and CO_2 flux patterns (Koulelis et al., 2023).

1.2.3 Controlling factors of soil methane flux

Methane in forest soils is primarily produced and consumed by microbial processes. Methanogens produce CH_4 under anaerobic conditions, typically found in waterlogged or saturated deep soil layers where oxygen (O_2) is limited (Wilmoth et al., 2021; Kluber et al., 2020). Conversely, methane-oxidizing bacteria (MOB) consumes CH_4, predominantly in more aerobic or O_2-rich soil layers (Reay et al., 2001). The balance between these two processes determines the net CH_4 flux between forest soils

and the atmosphere.

The dynamics of forest soil CH_4 cycling are influenced by a complex interplay of environmental factors. Soil moisture and temperature are among the most critical; wetter and warmer conditions generally enhance the reaction rate of methanogenesis (Feng et al., 2020; Zhang et al., 2024). The physical structure of the soil, including porosity and water retention capacity, also affects the extent of anaerobic conditions, thereby influencing CH_4 production (van Verseveld et al., 2020; Busman et al., 2021). Generally, CH_4 production is enhanced in soils with high temperature and high moisture. On this occasion, activities of CH_4-producing bacteria (MPB) can reach to a such high level; thus, the production rate of CH_4 is accelerated. For example, tropical rainforest and peat forest soils were reported to emit more CH_4 in rainy seasons (Wong et al., 2018; Yuping et al., 2008).

In principle, soil CH_4 uptake is directly controlled by the gas diffusion rate in the soil, which affects the transport of atmospheric CH_4 and O_2 to MOB (Liu et al., 2019). The soil gas diffusion rate is mainly controlled by air-filled porosity, which is determined by the soil porosity and volumetric water content. In addition, previous studies have revealed the importance of many environmental factors, such as soil physical and chemical properties, soil microbial activity, and climatic factors (Figure 1) (Castaldi and Fierro, 2005; Feng et al., 2020; Subke et al., 2018). These factors can affect soil CH_4 uptake directly and indirectly. For example, the growth of fine roots changes the soil texture and influences the transport of CH_4 and O_2 from the atmosphere to soil profiles (Eviner and Chapin, 2003). Decomposable carbon nutrients produced through litter decomposition can affect the activities of methanotrophs, which are directly related to CH_4 uptake (Xiong et al., 2024). The direction and rate of soil CH_4 flux result from the dynamic balance of several biotic and abiotic factors.

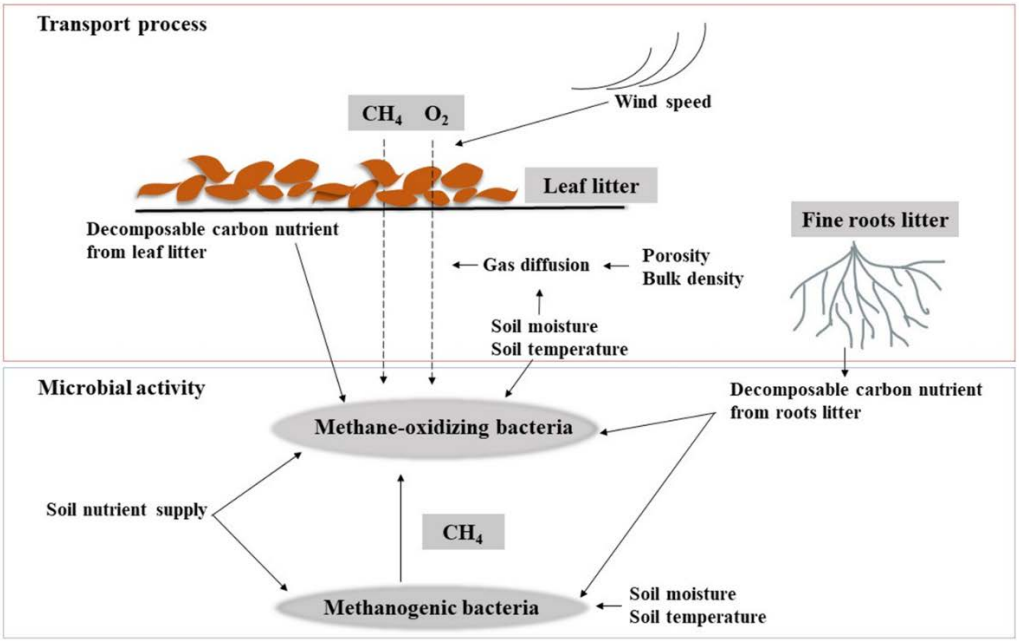

Figure 1. Illustration of biotic and abiotic controlling factors of soil CH_4 dynamics

1.2.4 Methods to measure and analyze soil carbon flux

Commonly used soil carbon flux measurement techniques include 1) chamber methods, 2) eddy covariance methods, 3) isotopic methods (^{13}C or ^{14}C route tracking methods), 4) remoting sensing (RS) methods, and 5) laboratory incubation methods (Smith et al., 2020). Chamber methods refer to placing a chamber over a soil surface to measure the releasing or absorbing rate of CO_2 and CH_4 by the soil, and thus soil carbon flux can be calculated from the mass balance inside the chamber. Chambers can be divided into static and dynamic ones, depending on the method to measure gas concentration in chamber headspace. In the static chamber method, air is periodically sample from the headspace manually and later analyzed for gas concentration, while gas concentration is continuously measured using gas analyzers in the dynamic chamber method (Sha et al., 2021; Wang et al., 2023). In recent years, automated chamber techniques have been developed as the dynamic method and widely used for its convenience, continuity, precision of soil carbon flux measurement (Basri et al., 2024; Yu et al., 2021; Yao et al., 2022).

The eddy covariance method is widely used for larger-scale and continuous monitoring of ecosystem-scale energy and mass balance (Baldocchi, 2008; Baldocchi,

2014). This method provides a big data quantity of trace gas fluxes, ecosystem production and environmental variables, providing an overall understanding of carbon and energy fluxes between terrestrial ecosystems and the atmosphere over large areas and long timescales (Kang et al., 2021). However, when it comes to small spatial scale study, chamber method will be a more suitable choice than eddy covariance technique.

Classical statistics are insufficient to quantitatively understand the spatiotemporal variation in soil carbon flux caused by the nonlinear interaction between flux and environmental factors (Ludwig et al.,2022). Compared with traditional linear models, main advantages of the Machine Learning (ML) approaches are (1) high fitting accuracy, (2) quantitative interpretation of the relative importance of observed environmental drivers, and (3) flexible data analysis, including regression and classification questions (Tavares et al., 2018). Recently, the Random Forest (RF) algorithm and other KL methods have been widely used to analyze soil greenhouse gases (GHGs) fluxes (Tavares et al., 2018; Hamrani et al., 2020; McCandless et al., 2018). However, to apply ML approaches, a large quantity of measured data is required for model training (Vogelsang and Borg, 2019).

Wavelet analysis has been demonstrated as an effective tool to resolve the role of variable carbon sources for RS through the transformation of time series measurements into different frequency sub-signals (Torrence and Compo, 1998; Vargas et al., 2011). Using wavelet cross power and coherence analysis, the phase relationship (i.e., the differences in the frequency distribution) between two time series can be used to establish possible cause-effect relationships between RS and environmental variables (Vargas et al., 2010). In this study, thus, wavelet analysis was used as a useful tool to help identifying the relationship between RS, RR and GPP. Photosynthate translocated from leaves is the main substrate of RR. Thus, RR links to GPP with some delay.

1.3 Objectives

The main objectives of this study are 1) to investigate the dynamic variations of soil CO_2 and CH_4 fluxes, including their small-scale spatial variations, and seasonal and

diurnal variations, and to determine the controlling factors of the soil carbon fluxes using ML modelling methods, 2) To separate RS into RH and RS using a conventional trenching method and RF modelling method, and to compare the performance of the two methods, and 3) To estimate the time delay between GPP and RR using wavelet analysis and phase difference methods.

2. Materials and methods

2.1 Study site description

The study was conducted in a naturally regenerating immature open deciduous forest located in southern Hokkaido, Japan (42◦44′ N, 141◦31′ E; elevation 125 m) after a severe blowdown caused by a typhoon in 2004. The terrain was almost flat with a slope of less than 2◦. The study site had been a mature Japanese larch (*Larix kaempferi*) plantation before disturbance. After the disturbance, all tree trunks were harvested in 2005; however, branches, leaves, and stumps remained at the site (Sano et al., 2010; Wu et al., 2019). The soil was classified as an immature volcanogenous regosol with high water permeability and poor nutrient content. A thin litter layer (1–2 cm) overlaid an approximately 10–15 cm thick organic soil layer (A horizon). Volcanic pumice stones (C horizon) underlay the A horizon, because the B horizon was absent (Liang et al., 2010). The surface soil profile was patchily disturbed by the logging. In mid-September 2021, the total biomass of trees taller than 2 m was estimated to be 13.2 Mg ha^{-1} from diameter at breast height (DBH) and tree height, using allometric equations (Yazaki et al., 2016). The forest was dominated by *Betula platyphylla Sukaczev*, followed by *Betula ermanii*, *Larix kaempferi*, *Magnolia Kobus*, and *Maackia amurensis*, which accounted for 62.2%, 9.7%, 7.6%, 6.7%, and 5.6% of the total tree biomass, respectively. In addition, the total biomass of understory species was estimated to be 1.97 Mg ha^{-1} from harvesting in mid-September, 2021, of which *Solidago gigantea* accounted for 93.7%. The mean annual temperature and precipitation were 8.2 ◦C and 1327 mm, respectively, in the last decade (2012-2021), with mean monthly temperatures ranging from 3.8 ◦C in January to 21.0 ◦C in August at the Tomakomai observatory 14 km from the study site. Snow usually covers the ground between early December and early April. Please refer to Sano et al. (2010) and Hirano et al. (2017) for further information regarding the study site.

2.2 Automated chamber system

2.2.1 System Design

Soil carbon flux was measured by means of chamber-based techniques. Liang et al. (2017) designed a multichannel automated chamber system to continuously measure soil carbon flux in non-snowing seasons in this study. Briefly, the system comprised a control unit (controlling box) inside a field-accessible case and up to 18 automated chambers. The control unit's main components were a datalogger (CR1000, Campbell Scientific Inc., Logan, Uath, USA), two valve-manifold (CKD-LAC-V-4SB010, CKD Corp., Nagoya, Japan), a laser-based $CH_4/CO_2/H_2O$ trace gas analyzer (LI-7810, LI-COR Corp., Lincoln, Nebraska, USA), a none-dispersive infrared CO_2 gas analyzer (LI-820, LI-COR Corp., Lincoln, Nebraska, USA), and a home-made sensor multiplexer. The chambers (0.9 m × 0.9 m × 0.5 m, length × width × height) were constructed of PVC plastic sheets (2 mm thick) glued to aluminum frames. To minimize the chamber effects and accurately estimate soil carbon flux, chamber size was designed to be as large as possible (Remy E et al., 2017). The chamber lids were raised and closed by two pneumatic cylinders (CKD-LAC-C-20B, CKD Corp., Komaki, Aichi, Japan) that operated at a pressure of about 0.2 MPa, which was generated by a micro-compressor (0.2LP-7s, Hitachi Ltd., Tokyo, Japan). In the none-measuring periods, the two sections of the chamber lid were raised (Figure 3 (a)) to keep the air condition inside the chamber as the same as that outside. In addition, leaf litter could also normally reach the enclosed soil surface, thus keeping the soil conditions as natural as possible. During the measurement periods, the chamber lids were closed and the chamber air was mixed by two micro fans (MF12B, Kyoei Tsushin Kogyo Ltd., Tokyo, Japan). The chamber air was circulated through the gas analyzers by a 5 L min^{-1} diaphragm pump (CM-50, Enomoto Micropump Ltd., Tokyo, Japan), and the change in the CO_2/CH_4 concentration over time was measured by the analyzers. Opening and closing of the chambers were controlled by a home-made relay board that was controlled by the datalogger. Further information on the automated chamber system can be referred to Liang et al. (2003, 2017).

During the growing seasons (from mid-April to mid-November) in 2021 and 2022, 18 chambers were distributed randomly on the forest floor within an area of 30 m × 30 m (Figure 2). All chambers were allocated to three treatments (Figure 3 (c)): five Root chambers (R1-R5, with roots but no aboveground plants), five Trench chambers (T1–T5, without both roots and aboveground plants) and eight Plant chambers (with both underground roots and aboveground plants). However, Plant chambers were not involved in this study. In Trench chambers, four PVC boards (4 mm thick) were installed into the soil at a depth of 30 cm to prevent outside roots from invading into inside chamber area. To precisely measure soil carbon flux, maintenance was conducted at intervals of 3-5 weeks in the growing seasons, including clipping aboveground new-emerging plants in Root chambers, testing gas tightness of chambers and pipes, and checking data records.

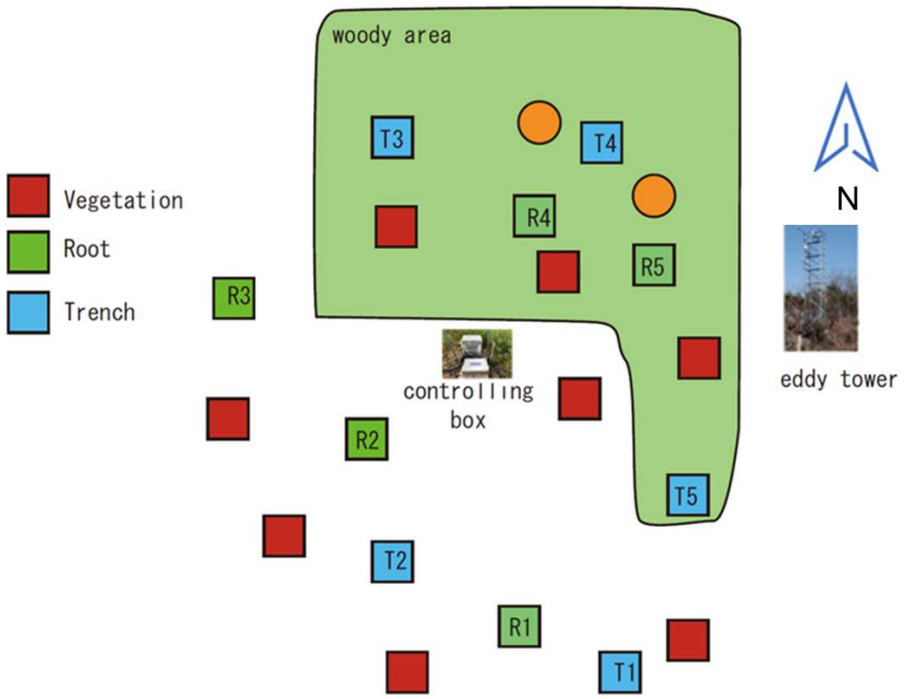

Figure 2. Illustration of chamber distribution. The relative size of the chamber is enlarged in the figure for the ease of viewing. Vegetation chambers (red chambers in the figure) were not used in this thesis.

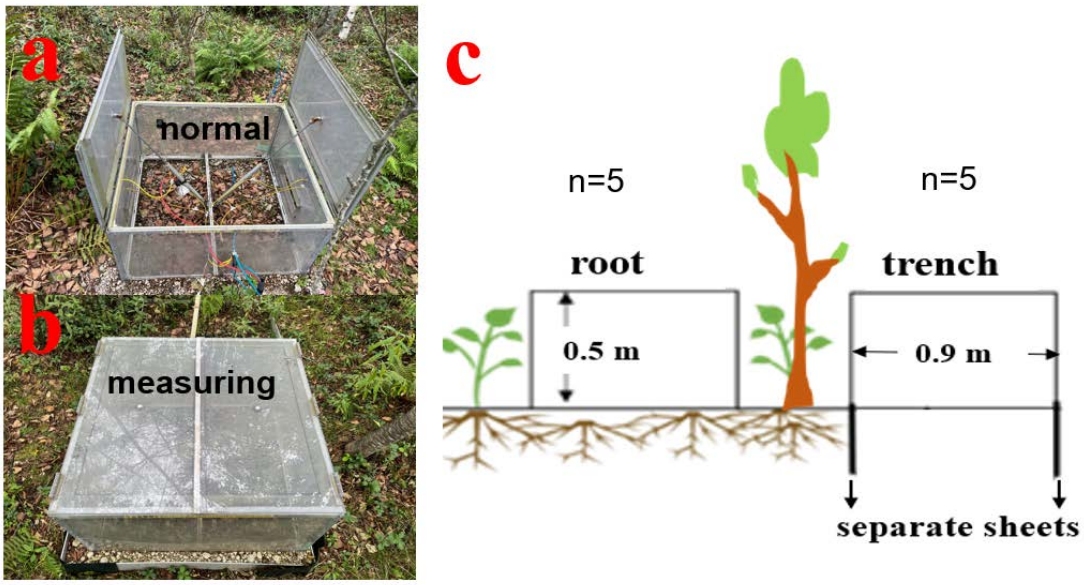

Figure 3. Chamber condition during non-measuring period (a) and measuring period (b), and illustration of two treatments (c).

2.2.2 Carbon flux calculation and processing

Each of 18 chambers was automatically closed for 200 s, one after the other, for one hour. During chamber closure, air was circulated between the closed chamber (Figure 3 (b)) and control unit with an air pump at a flow rate of 5.0 L min^{-1} and bypassed into the gas analyzer at 0.35 L min^{-1}. The soil carbon concentration (CO_2: μmol CO_2 mol (dry air)$^{-1}$; CH_4: nmol CH_4 mol (dry air)$^{-1}$) in the closed chamber headspace was measured every 5 s, and the change rate of CO_2/CH_4 concentration (slope, μmol/nmol mol^{-1} s^{-1}) was determined using the least-squares method. The soil CO_2/CH_4 flux (F, μmol m^{-2} s^{-1} for CO_2 and nmol m^{-2} s^{-1} for CH_4) was calculated using the following simple mass balance equation (1) (Liang et al., 2017)

$$F = \frac{P * H}{R * (T_a + 273.15)} slope \qquad (1)$$

where P is the air pressure (Pa), H is the chamber height (0.5 m), R is the gas constant (8.314 Pa m^3 K^{-1} mol^{-1}), and T_a is the air temperature in each chamber (◦C). The precision (1 standard deviation (SD)) of the gas analyzer is 0.25 ppb for CH_4 concentration with 5-s averaging from an instruction manual. Based on the error

propagation law, 1 SD of the slope of the temporal change in CH_4 concentration is estimated to be 0.015 nmol mol^{-1} s^{-1}. Finally, according to *t*-test, the detection limit in a single CH_4 flux measurement is calculated to be 0.10 nmol mol^{-1} s^{-1} (95% confidence intervals) from the estimated SD of the slope using Eq. (1) at 20 ◦C and 1013 hPa.

Ideally, CO_2/CH_4 concentration is expected to change linearly with time after chamber closure. However, some data points deviated from linearity, especially immediately after closing, because of the replacement of the sampling air in the tubing. Therefore, to exclude such outliers and control flux quality, linear regression was applied to the time course of the CO_2/CH_4 concentration, which was measured 40 times during a chamber closure for 200 s, and residuals from the regression were calculated. If the residual was beyond the mean ± 3 × SD, the data point was excluded as an outlier. This procedure was repeated twice, using the remaining data points (Liang et al., 2017). If the final coefficient of correlation (*R*) was > 0.9, the flux was calculated using the slope (Eq. (1)). Valid data quantity after data quality control. Data gaps were not filled before ML modelling to maintain the original changing trend of soil fluxes and to avoid potential biases from gap-filling algorithms (Yuan et al., 2022).

In each chamber, volumetric soil water content (SWC, m^3 m^{-3}) at a depth of 10 cm was monitored with time-domain reflectometry (TDR) sensors (CS616, Campbell Scientific Inc. Logan, Utah, USA), and soil temperature (◦C) at a depth of 5 cm and air temperature (◦C) at a height of 25 cm were monitored with thermocouple thermometers, which were recorded every 5 s simultaneously with gas concentration monitoring.

The field experiment was conducted in the growing season (mid-April to mid-November) of 2021 and 2022. Data gaps appeared because of power failure or mechanical disorders caused by unexpected bad weather conditions (e.g. High temperature and thunder stroke).

2.3 Environment variables measurement and calculation

2.3.1 Soil properties measurement and calculation

Physicochemical properties of the surface soil, fine root dynamics, and meteorological factors were used to explain the spatiotemporal variation in CO_2 and

CH_4 fluxes. Surface soil was separately sampled from 0-5 and 5-10 cm depths at four points in each chamber using core samplers of 100 cm^3 in 2020 or 2021. The total volume (TV) of solid and liquid phases in each sample was measured with a digital actual volumenometer (DIK-1150, Daiki, Kusatsu, Japan), and then core samples were dried at 105 ◦C for 48 h and weighed. Bulk density (kg m^{-3}) was determined from the dry weight, and liquid volume was calculated from the weight loss of soil samples through oven-drying assuming that liquid specific weight is one. Soil porosity (φ, m^3 m^{-3}) was determined by subtracting solid volume (= TV – liquid volume) from the sampler capacity (100 cm^3). Using the soil samples, carbon (C) content (kg kg^{-1}) and nitrogen (N) content (kg kg^{-1}) were analyzed with a CN analyzer (FlashEA 1112, Thermo Fisher Scientific, Waltham, Massachusetts, USA). Finally, the physicochemical properties of the two depths were averaged at each point (n = 4 per chamber). The water-filled pore space (WFPS, %) was determined hourly as the ratio of SWC to φ (WFPS = SWC / φ). The soil O_2 diffusion coefficient (DO_2, m^2 s^{-1}) was estimated hourly from the relative gaseous diffusion coefficient (D / D_0) using the following empirical equation (Campbell, 1985):

$$DO_2 = 1.62 \times 10^{-5} \frac{D}{D_0} \left(\frac{T_S + 273.15}{273.15}\right)^{1.75} \left(\frac{1013}{P}\right) \quad (2)$$

where D_0 is the gaseous diffusion coefficient in the atmosphere at 1013 hPa and 273.15 K, Ts is the soil temperature at a depth of 5 cm (◦C), and P is the air pressure (hPa). The D / D_0 was calculated using the following equation:

$$\frac{D}{D_0} = 0.82\varepsilon^{2.03} \quad (3)$$

where ε is the air-filled porosity (= φ – SWC). Eq. (3) was determined from a laboratory experiment (Currie, 1960) using soil core samples extracted from the same area as this study area (Kim, 2005). The ε was calculated from hourly SWC measured in each chamber.

In each Root chamber, the biomass and production of fine roots (< 2 mm in

diameter) in 10 cm thick surface soil were measured at six points at intervals of 6-8 weeks using soil core sampling using a stainless-steel edged tube with an inner diameter of 2.4 cm and the ingrowth core method, respectively. Living fine roots were visually extracted from the soil core samples dispersed in tap water, dried at 70 ◦C for 48 h, and weighed to determine biomass. As ingrowth cores, plastic hair curlers with an outer diameter of 2.3 cm were used. The ingrowth cores were filled with air-dried root-free soil, which was collected from the study site and sieved through 2 mm meshes. In each Root chamber, six ingrowth cores were inserted down to 10 cm into the pit dug through soil core sampling, and the six ingrowth cores installed the previous time were collected (Sakaguchi, 2023). Ambient CH_4 concentration was determined hourly from the mean CH_4 concentrations 25-40 s after chamber closing, when the concentration peaked in each measurement. For ML modeling, periodic biomass data was linearly interpolated on a daily basis in each chamber, whereas production data was fixed between two successive sampling dates.

2.3.2 Gross Primary Production measurement

Half-hourly gross primary production (GPP, μmol m^{-2} s^{-1}) or ecosystem gross photosynthesis was determined from net ecosystem CO_2 exchange (NEE, μmol m^{-2} s^{-1}) measured on a tower near the chambers by the eddy covariance method. GPP was calculated as the sum of daytime NEE and ecosystem respiration (RE), which was estimated from the nighttime. Half-hourly data were adjusted to hourly resolution in wavelet analysis.

Please refer to Hirano et al. (2017; 2024) for further information regarding the eddy covariance method.

2.3.3 Other environmental variables and data processing

Site common variables, including wind speed (m s^{-1}) and precipitation (mm h^{-1}), were measured on the tower and on the ground near chambers, respectively. Real-time wind speed was put into ML modelling as an explanatory parameter.

Data processing of flux and environmental variables was conducted using R 4.2.2 (R core team, https://www.r-project.org/), with R packages. “lubridate”, “stats”, and “dplyr” were used for data filtering and primary processing. R package “ggplot2” and Origin 2023 Learning ver. (Origin Lab, Northampton, Massachusetts, USA) were used for graphing.

2.4 Machine learning models

Two supervised ML algorithms of Random Forest (RF) and Gradient Boosting Machine (GBM) were used for modeling soil carbon fluxes. Since ML models are built on black box algorithm, it is impossible to show specific fitting equations. Conceptual formula is shown as follows:

$$F \sim x1 + x2 + x3 \ldots (4)$$

where F indicates CO_2 or CH_4 flux, x1, x2, x3…indicate different environmental variables. Hourly flux data and corresponding environmental variables were used for modelling, with 80% of raw data was set as a training dataset and 20% for testing. Used variables can be found in Table 1.

Table 1 Used explanatory variables in ML models for soil CH_4 and CO_2 flux fitting

Variables	Unit	Abbreviation	Timescale
Soil temperature	°C	Ts	Hourly
Water filled pore space	%	WFPS	Hourly
Air temperature	°C	Ta	Hourly
Wind speed	m s^{-1}	ws	Hourly
Ambient CH_4 concentration [a]	nmol CH_4 mol (dry air)$^{-1}$)	CH_4.con	Hourly
Soil O_2 diffusion rate [a]	m^2 s^{-1}	DO_2	Hourly
Carbon/Nitrogen	–	C/N	Fixed
Bulk density	kg m^{-3}	BD	Fixed
Fine root biomass [b]	g m^{-2}	Root.bio	Daily
Fine root production [c]	g m^{-2} day^{-1}	Root.pro	Daily

[a] CH_4.con and DO_2 were only used in CH_4 flux fitting.

[b] Root.bio was only used in Root chambers, and was linearly interpolated on a daily basis in each chamber.

[c] Root.pro was only used in Root chambers, and was fixed between two successive sampling dates.

The RF algorithm is a bootstrap aggregating (“bagging”) ML technique that belongs to the family of ensemble learning methods, where many models, often called “decision trees”, are combined to solve a particular computational problem more effectively than a single model could. At its core, RF constructs a multitude of decision trees during training. Each tree is built from a random subset of the training data and during the growth of each tree, at each node, a random subset of features is chosen to decide the split. The final result is an average of the results from each decision tree (“voting from each tree”, Breiman, 2001). Two important parameters needed to be tuned in this study are:

“n.trees”: the number of decision trees, which was set at 70% of the quantity of training dataset.

“mtry”: the number of variables used in each decision tree, which was set at a half of the quantity of variables combination.

Similar with RF, GBM is one of the decision trees algorithm family. However, GBM builds on the logic of boosting, which is a method of converting a collection of weak learners into a strong learner (“boosting”). Procedures of GBM models include: 1) Building an initial “weak” model (basic decision tree model), 2) Computing residuals of each instance in the initial model, 3) Using residuals as targets to train new basic models as new base learners, 4) Updating predictions of existing models based on results of new base learners, 5) Repeating above procedures until the prediction bias reaches to presupposed level (Cai et al., 2022; Burges et al., 2010). In GBM models, four main parameters needed to be tuned:

“n.trees”: the number of decision trees, which was set at 70% of the quantity of training dataset.

“interaction.depth”: The complexity of each decision tree, which was set at 2, representing a two-way interactions.

“n.minobsinnode”: the number of observations of the final decision tree, which was set at 100, representing the quantity of observations in the last tree node.

“shrinkage”: the learning rate or step-size reduction, which was set at 0.1 to control the fitting quality of each tree.

Differences between RF and GBM algorithms can be concluded as follows: 1) RF uses a replacement sampling method, and each sampling is independent from each other. GBM uses an unchanged dataset in each boosting round, with the weight of each sample is decided by results from the last round; 2) Result of each decision tree has the same weight in RF models, while results with lower errors have higher weight in GBM models; 3) Each decision tree in RF models can calculate synchronously, while

calculation in GBM model must follow step-by-step order because results from the last learners are the targets of following learners; 4) RF models focus more on the variation of the distribution of original dataset, while GBM models concentrate on the bias of original dataset (Golden et al., 2019; Cha et al., 2021).

Model performance was evaluated using determination coefficients (R^2) and root-mean-square error (RMSE). A 10-fold cross-validation method was used to avoid overfitting. To avoid model bias caused by random data selection, each model was run 10 times using different random seeds. The model performance was determined based on the best result of these 10 trials. R packages "caret", "caretEnsemble", "randomForest", "gbm" were used for building models. R packages "pdp", "DALEX" and "iml" were used for interpreting and visualizing ML models.

2.5 Separation of soil respiration

Commonly used conventional methods to separate RS use the trenching method to exclude RR and measure RH, and then RR (RR_C) is estimated as a difference between mean RS measured in Root chambers and mean RH measured in Trench chambers.

$$conventionlRR = mean(RS_{1\sim5}) - mean(RH_{1\sim5}) \quad (5)$$

where $RS_{1–5}$ indicates CO_2 flux of Root chambers, $RH_{1–5}$ indicates CO_2 flux of Trench chambers. However, spatial variation of each chamber was ignored during averaging process. To solve this problem, a RF-model-based estimating method was developed in this study. Flux data from Trench chambers were used to build a RH-estimation model with environmental variables; then environmental variables from Root chambers were introduced into the RH-estimation model to calculate corresponding RH in Root chambers. Thus, RF-model-based RR (RR_RF) was calculated as:

$$RFRR_i = mean(RS_i - RH_i) \quad (6)$$

where *i* denotes the chamber number of Root chambers. In this way, the spatial variation of RR was taken into consideration.

To illustrate the relationship between RR and soil temperature, two types of RR (RR_C and RR_RF) were fitted with soil temperature using an exponential equation shown as follows (Liang et al., 2004):

$$RR = a1 * \exp\ (a2 * T) \quad (7)$$

where $a1$ and $a2$ are fitting parameters. T (°C) is soil temperature. In addition, temperature sensitivity Q_{10} (=exp (10*$a2$), Van't et al., 1900) was calculated by the fitting parameter $a2$ determined from Eq. (7).

2.6 Wavelet analysis

Typical time-series data analysis methods, including wavelet analysis, do not allow data gaps in the dataset. Thus, gaps in GPP data were filled by an RF algorithm from environmental variables of day length (h), air temperature (°C), vapor pressure deficit (VPD, hPa), and photosynthetic photon flux density (PPFD, μmol $m^{-2}s^{-1}$). Similarly, RS and RR data were gap-filled from the gap-filled GPP, global radiation (W m^{-2}), precipitation (mm h^{-1}), wind speed (m s^{-1}), soil temperature (°C), and soil moisture (%).

Wavelet power analysis was used to check the periodicity of GPP, RS and two RRs (RR_C and RR_RF), with wavelet cross-power analysis to determine the correlation strength of significant common periods of GPP/RS, GPP / RR_C and GPP / RR_RF.

R package "mice" was used to fill data gaps. R package "WaveletComp" was used to conduct wavelet analysis.

2.7 Time delay analysis between GPP and root respiration

In principle, it takes time for carbohydrate generated by photosynthesis to be transported from the canopy to the roots. That is to say, time delay exists between GPP and RR, indicating that RR links to GPP with some delay. Length of time delay depends on many factors, including plant species, age, height, disturbance, etc.

Cross correlation function (CCF) is a widely used method to estimate period difference between two time series. In essence, CCF quantifies the similarity between two signals as a function of their relative time delay, and a specific delay time

corresponding to the highest correlation would be considered as the time lag between two signals. (Shen C et al., 2015; Zhang et al., 2006). In this study, an autocorrelation factor (ACF) between GPP and RRs (RR_C and RR_RF) with different lags was calculated, and the lag with the highest ACF will be considered as the most possible time delay between GPP and RR

Wavelet cross power method was another method to estimate time lag between two time series. To conduct the wavelet cross power analysis, GPP, RS and RR data were firstly standardized and de-noised using the Z-score method and Loess regression method (Grinsted A et al., 2004). Significant phases of two time series data with significant wavelet cross power ($P < 0.05$) were extracted independently using the "white noise" method. Then difference of two phases was calculated using the empirical Eq. (8), and significant phase differences were considered as time lags. Compared with CCF method, wavelet cross power method could describe time lag in a more intuitive way, and microcosmic or long-term changing trends can also be extracted if time lags exist in a long-term observation dataset with a high time resolution.

$$Phase.diff = 2\pi\left(\frac{\Delta t}{ft}\right) \quad (8)$$

where *Phase.diff* (radian, rad) denotes the hourly instant phase difference between two time series. Δt (h) indicates time lag between two time series (GPP vs. RS or RR). *ft* (h) denotes a frequency period which was set at 24 hours (1 day). π was set to 3.1416 in this study.

For those phase differences which were over the range of one period (−π to π), the corresponding phase differences within one period would be calculated. For example, the original instant phase difference between GPP and RR_C at 2:00 AM on May 1, 2022 was –4.78 rad (< -π), and it was transformed to −1.64 rad (–4.78 + π); thus, time lag between GPP and RR_C was controlled within the range of −12 to 12 hours (Cazelles et al., 2008; Veleda et al., 2012). Negative lags mean that RR led the changing trend (change of RR led to the change of GPP) while positive lags represented GPP led the trend (change of GPP caused the change of RR). Hourly flux data from May to

October (six full-length months) in two years was used for CCF analysis and wavelet analysis. The first 12 hours and the last 12 hours in wavelet cross power analysis were excluded to prevent edge effect (Carmona et al., 1998; Aguiar-Conraria and Soares, 2011). Hourly valid instant time lags were finally averaged to calculate the daily lags.

In addition, to exclude the impacts of soil temperature, soil respiration and root respiration were normalized with Eq. (9) (Law et al., 1999; Hirano et al., 2003).

$$F_{nor} = F \cdot \exp\left[a2(T_b - T)\right] \quad (9)$$

where F_{nor} is normalized CO_2 flux (F, nmol $m^{-2}s^{-1}$) at T_b, and T_b is the base temperature, which was set to 15 °C. *a2* is the fitting parameter in Eq. (7). T (°C) is the real-time soil temperature.

Normalized RS and RRs were fitted with GPP to calculate time lags without being affected by temporal variation of soil temperature.

R package “astsa” was used for CCF analysis, and R packages “WaveletComp” was used for wavelet cross power method. Please refer to the manual of package “WaveletComp” for detailed information of building of wavelet cross power between two sets of time series data, extraction of phase differences and calculation process of time lags (http://www.hs-stat.com/WaveletComp/).

3. Results

3.1 Environmental variables

3.1.1 Soil physical properties

Porosity, C content, and N content showed a significant difference within each treatment, except for bulk density for Root chambers (Table 2), which means that such soil physicochemical properties varied spatially in each treatment. The spatial variation was more significant in Trench chambers with lower *P* values. Between treatments, only porosity was significantly different (Table 3, $P < 0.05$).

Table 2 Soil physical properties of each chamber (mean ± SD)

Treatment	Bulk density ($kg\ m^{-3}$)	Porosity ($m^3\ m^{-3}$)	C content ($kg\ kg^{-1}$)	N content ($kg\ kg^{-1}$)
Trench				
T1	0.660 ± 0.046	0.421 ± 0.027	4.220 ± 0.438	0.220 ± 0.027
T2	0.764 ± 0.072	0.735 ± 0.021	3.210 ± 0.360	0.174 ± 0.025
T3	0.621 ± 0.119	0.767 ± 0.045	6.90 ± 0.161	0.400 ± 0.011
T4	0.711 ± 0.095	0.734 ± 0.036	5.963± 0.597	0.367 ± 0.045
T5	0.871 ± 0.087	0.680 ± 0.032	6.221 ± 0.436	0.353 ± 0.022
P [a]	0.043*	$< 2e^{-16}$	$< 2e^{-16}$	$< 2e^{-16}$
Root				
R1	0.688 ± 0.064	0.772 ± 0.017	4.732 ± 0.405	0.283 ± 0.027
R2	0.752 ± 0.028	0.700 ± 0.026	3.494 ± 0.494	0.190 ± 0.034
R3	0.791 ± 0.076	0.693 ± 0.027	5.711 ± 0.898	0.324 ± 0.058
R4	0.627 ± 0.060	0.765 ± 0.028	7.784 ± 0.936	0.491 ± 0.084
R5	0.664 ± 0.107	0.768 ± 0.046	5.189 ± 0.332	0.290 ± 0.022
P [a]	0.082	0.009	$< 2e^{-16}$	$< 2e^{-16}$

[a] One-way ANOVA ($n = 5$) in each treatment.

Table 3 Soil physical properties of two treatments (mean ± SD)

Treatment	Bulk density ($kg\ m^{-3}$)	Porosity ($m^3\ m^{-3}$)	C content ($kg\ kg^{-1}$)	N content ($kg\ kg^{-1}$)
Trench	0.718 ± 0.119	0.667 ± 0.134	5.23 ± 1.39	0.299 ± 0.091
Root	0.704 ± 0.093	0.740 ± 0.047	5.38 ± 1.56	0.315 ± 0.111
P [a]	0.693	0.031	0.627	0.757

[a] *t*-test between two treatments (two-tailed).

3.1.2 Metrological variables

Mean daily precipitation and air temperature were shown in Figure 4 and Table 4. Typical seasonal trend appeared in mean air temperature in growing seasons of 2021, while mean air temperature increased from spring to summer, and appeared at DOY of approximate 200, then decreased from summer to autumn. Differently, air temperature of 2022 did not peak at around DOY of 200, but mean air temperature kept at a relatively high level during the period of around DOY of 190 and 240 (Figure 4). Max and minimum daily air temperature shared a similar trend with mean daily air temperature (Figure 4). Significant seasonal variation ($P < 0.001$) existed in mean air temperature in both years, but no significant interannual variation emerged between two years ($P > 0.05$, Table 4). Neither within year nor interannual variation appeared in mean daily precipitation ($P > 0.05$, Table 4), but distribution of precipitation in two years was different. Rainfall in summer in 2021 was a bit lower than that of 2022, with mean daily precipitation during DOY of 200-250 was 2.79 ± 7.96 mm day^{-1} in 2021 and 4.21 ± 8.37 mm day^{-1} in 2022, respectively (Table 4). Although the variation was not significant ($P > 0.05$, *t*-test), this result suggested a wetter summer in 2022 than in 2021. Two-year mean daily air temperature was 14.70 ± 5.43 °C and precipitation was 2.94 ± 7.35 mm day^{-1} (Table 4).

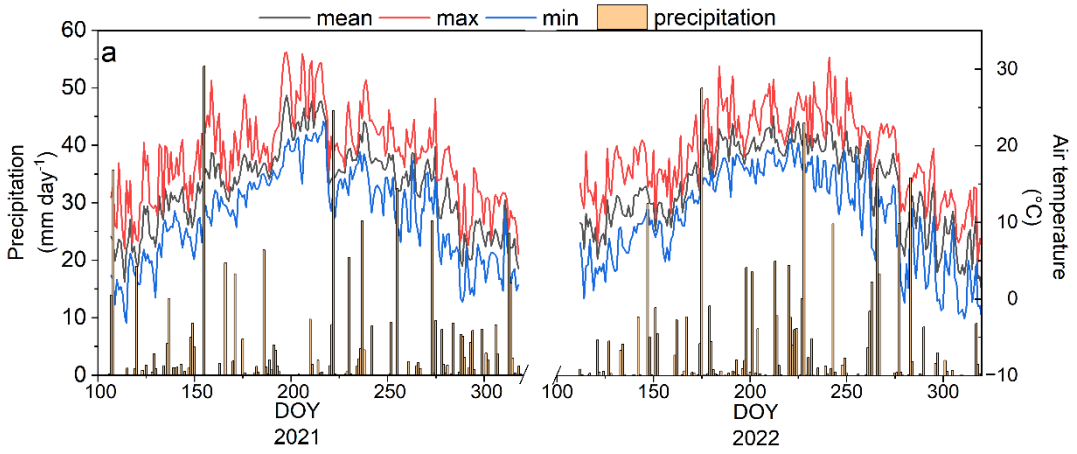

Figure 4. Seasonal variations in daily precipitation and daily mean, maximum, and minimum chamber air temperatures in 2021 (a, from April 17th to November 15th) and 2022 (b, from April 22nd to November 16th). Since no significant spatial variation was found in air temperature among chambers, air temperatures of 10 chambers were averaged.

Table 4 Mean daily precipitation and air temperature in each month of growing seasons in two years (mean ± SD)

Month	Precipitation (mm day^{-1})	Air temperature (°C)
2021		
Apr [a]	4.75 ± 10.32	6.27 ± 2.06
May	1.83 ± 3.09	11.30 ± 2.34
Jun	3.41 ± 10.53	16.19 ± 1.76
Jul	1.70 ± 4.25	20.99 ± 3.37
Aug	4.21 ± 9.86	19.46 ± 3.15
Sep	2.54 ± 7.61	16.40 ± 1.78
Oct	2.53 ± 3.30	9.78 ± 3.47
Nov [a]	3.87 ± 7.27	7.70 ± 2.21
Mean	2.93 ± 7.34	14.64 ± 5.43
P [b]	0.787	$< 2e^{-16}$
2022		
Apr [a]	0.19 ± 0.36	9.21 ± 1.44
May	2.69 ± 6.02	11.48 ± 2.44
Jun	3.59 ± 9.45	14.46 ± 3.13
Jul	1.82 ± 4.70	20.25 ± 1.72
Aug	5.84 ± 9.91	20.65 ± 1.37
Sep	3.08 ± 7.79	17.66 ± 2.48
Oct	2.69 ± 7.70	10.39 ± 3.95
Nov [a]	0.78 ± 2.27	5.77 ± 3.22
Mean	2.96 ± 7.39	14.76 ± 5.45
P [b]	0.298	$< 2e^{-16}$
2-y Mean	2.94 ± 7.35	14.70 ± 5.43
P [c]	0.962	0.828

[a] Precipitation and air temperature data in April and November were around half-month long. High mean daily precipitation in April 2021 was caused by a heavy precipitation event happened in 19th April (35.7 mm).

[b] One-way ANOVA within growing seasons in a year (n = 213 in 2021, n = 209 in 2022).

[c] *t*-test between daily precipitation and air temperature of growing seasons in two years (two-tailed).

3.1.3 Soil temperature and moisture

Mean daily soil temperature and WFPS in two years were shown in Figure 5 and Figure 6. To note, WFPS of R2 was excluded from data processing because SWC of 2021 and the period before Jul. 15th, 2022 in R2 was not recorded, which was caused by mechanical disorders. Seasonal trends appeared in soil moisture and temperature in 2021. Soil temperature increased and WFPS decreased from spring to summer, and then soil temperature decreased and WFPS increased from summer and autumn (Figures 5 and 6). The peak of soil temperature and the bottom of WFPS appeared at around DOY of 220 in 2021. Compared with 2021, seasonality of soil moisture was weak in 2022, especially no significant seasonal trend could be found in WFPS in both treatments (Figures 6 c and d), which might be caused by different distribution patterns of precipitation in two years. Higher mean daily precipitation in summer of 2022 reduced the seasonal variation of soil moisture (see 3.1.2).

Significant spatial variation of soil temperature appeared among five chambers in each treatment (Table 5, $P < 0.01$), but no significant difference of two-year mean soil temperature appeared between two treatments (Table 6, $P > 0.05$). In contrast, significant variation of WFPS not only emerged within two treatments (Table 5, $P < 0.01$), but also appeared between two treatments (Table 6, $P < 0.01$). Root chambers had a significant higher soil moisture (27.90 ± 6.94%) than that of Trench chambers (24.97 ± 6.84%).

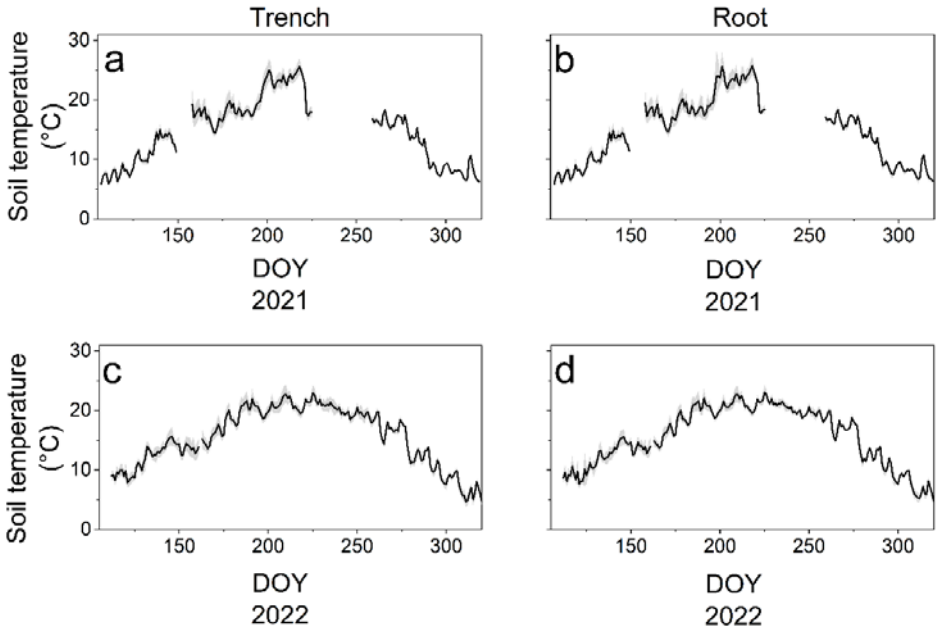

Figure 5. Seasonal variations in mean daily soil temperature in 2021 (a and b, from April 17th to November 15th) and 2022 (c and d, from April 22nd to November 16th). Shaded areas denote SD of five chambers in each treatment.

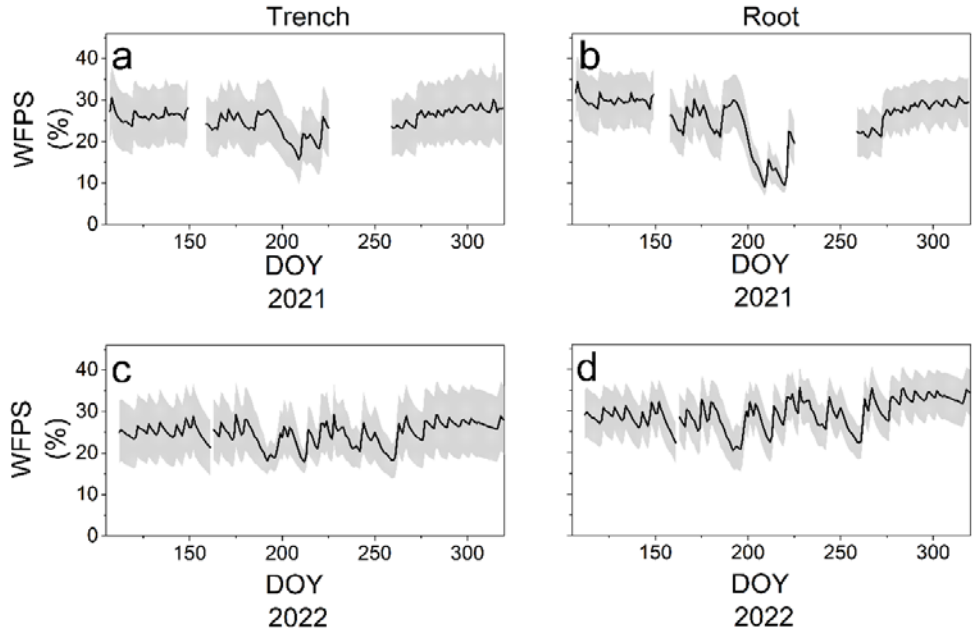

Figure 6. Mean daily WFPS in 2021 (a and b, from April 17th to November 15th) and 2022 (c and d, from April 22nd to November 16th). Shaded areas denote SD of four or five chambers in each treatment. Data from R2 chamber was excluded from (b) because of many data gaps.

Table 5. Mean daily soil temperature and WFPS for two years in each chamber in two treatments (mean ± SD)

Treatment	Soil temperature (°C)	WFPS (%)
Trench		
T1	16.25 ± 5.51	15.84 ± 1.31
T2	15.67 ± 5.36	24.37 ± 2.60
T3	14.84 ± 4.91	21.64 ± 2.61
T4	14.75 ± 4.96	32.98 ± 4.25
T5	14.46 ± 5.08	30.03 ± 4.01
P [a]	$< 2e^{-16}$	$< 2e^{-16}$
Root		
R1	15.72 ± 5.34	26.74 ± 5.10
R2	16.15 ± 5.99	32.06 ± 2.77 [b]
R3	14.96 ± 5.17	20.78 ± 3.94
R4	14.57 ± 4.77	34.68 ± 5.46
R5	14.99 ± 5.02	28.06 ± 5.57
P [a]	$< 2e^{-16}$	$< 2e^{-16}$

[a] *P* values of one-way ANOVA (n=5) in each treatment.

[b] WFPS of R2 was the mean of daily data from Jul. 15th to Nov. 16th, 2022.

Table 6. Mean soil temperature and WFPS for two years in two treatments (mean ± SD)

Treatment	Soil temperature (°C)	WFPS (%))
Trench	15.19 ± 5.21	24.97 ± 6.84 [b]
Root	15.26 ± 5.29	27.90 ± 6.94
P [a]	0.793	0.003

[a] *t*-test between two treatments (two-tailed).

[b] WFPS of Trench treatment was the mean of four chambers except for R2 which had many data gaps.

3.1.4 Root dynamics

The seasonal trend of fine root biomass and production were shown in Figure 7. In 2021, peak of fine root biomass was observed around July in the summer. However, no significant seasonal trend of biomass appeared in 2022. Root biomass was significantly higher in R4 and R5 than in other chambers (Table 7, $P < 0.05$). Root production increased from June to August in four chambers except for R5 in 2021, while a similar seasonal variation emerged in four chambers except for R4 in 2022. (Figure 7).

Table 7. Fine root biomass (dry weight, mean ± SD)

Chamber	Fine root biomass [a] (g m^{-2})
R1	101.0 ± 30.4
R2	48.3 ± 27.6
R3	63.8 ± 41.6
R4	161.2 ± 50.2
R5	129. 3 ± 43.8

[a] Mean dry weight of nine samples during experiment period.

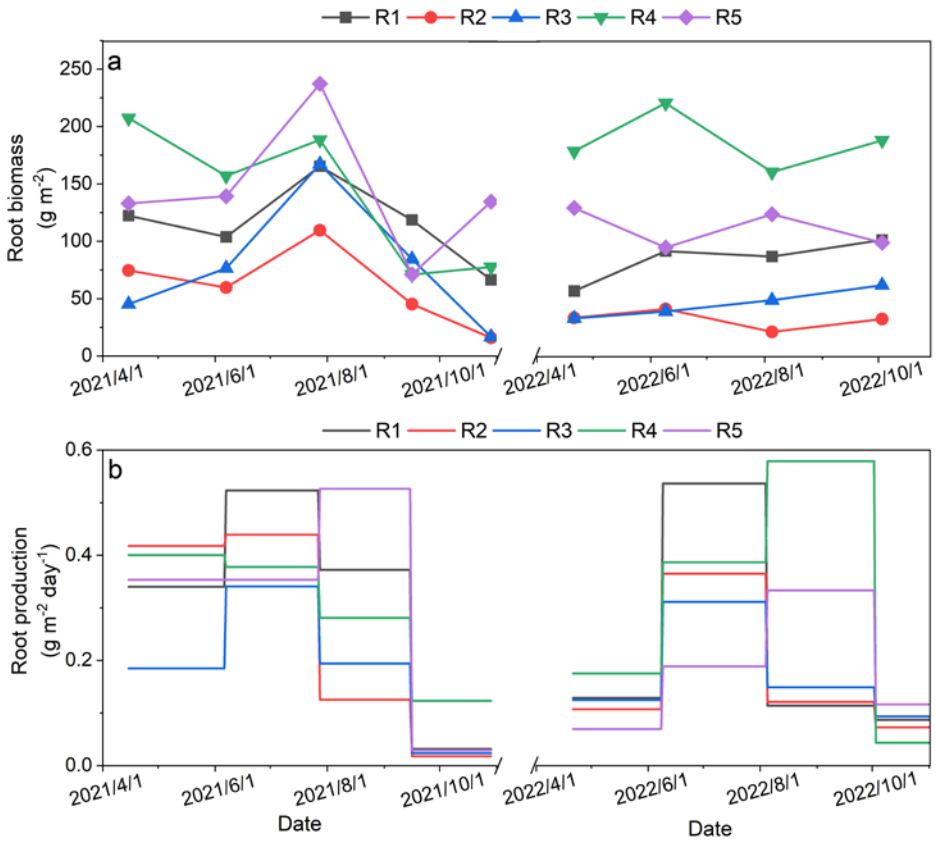

Figure 7. Seasonal variations in fine root biomass (a) and fine root production in five Root chambers for two years.

3.2 Soil methane flux

3.2.1 Spatiotemporal variation of soil methane flux

Soil CH_4 flux was always negative in all chambers, indicating that the soils with high water permeability functioned as a net CH_4 sink over the growing season (Figure 8). In both treatments, CH_4 flux varied seasonally in almost parallel with WFPS (Figure 6). The seasonal trend of CH_4 flux in 2022 was more not clear because of almost no seasonal trend of WFPS in 2021 (Figure 8). In addition, CH_4 flux negatively peaked in early August in synchronization with the peaks of soil temperature (Figure 5). Soil CH_4 flux showed significant spatial variation within each treatment (Table 8, Figure 9). The CH_4 flux of Trench chambers ranged from −1.99 ± 0.40 nmol m^{-2} s^{-1} (T2) to −2.62 ± 0.47 m^{-2} s^{-1} (T3), that of Root chambers ranged from −2.11 ± 0.48 nmol m^{-2} s^{-1} (R4) to −3.07 ± 0.40 nmol $m^{-2}s^{-1}$ (R1) (Table 8). Seasonal mean CH_4 flux in Root chambers (−2.56 ± 0.61 nmol m^{-2} s^{-1}) was significantly more negative (by 8.2 %, $P < 0.001$) than

that of Trench chambers (−2.35 ± 0.47 nmol m^{-2} s^{-1}) (Table 8), which means that more CH_4 was absorbed in Root chambers.

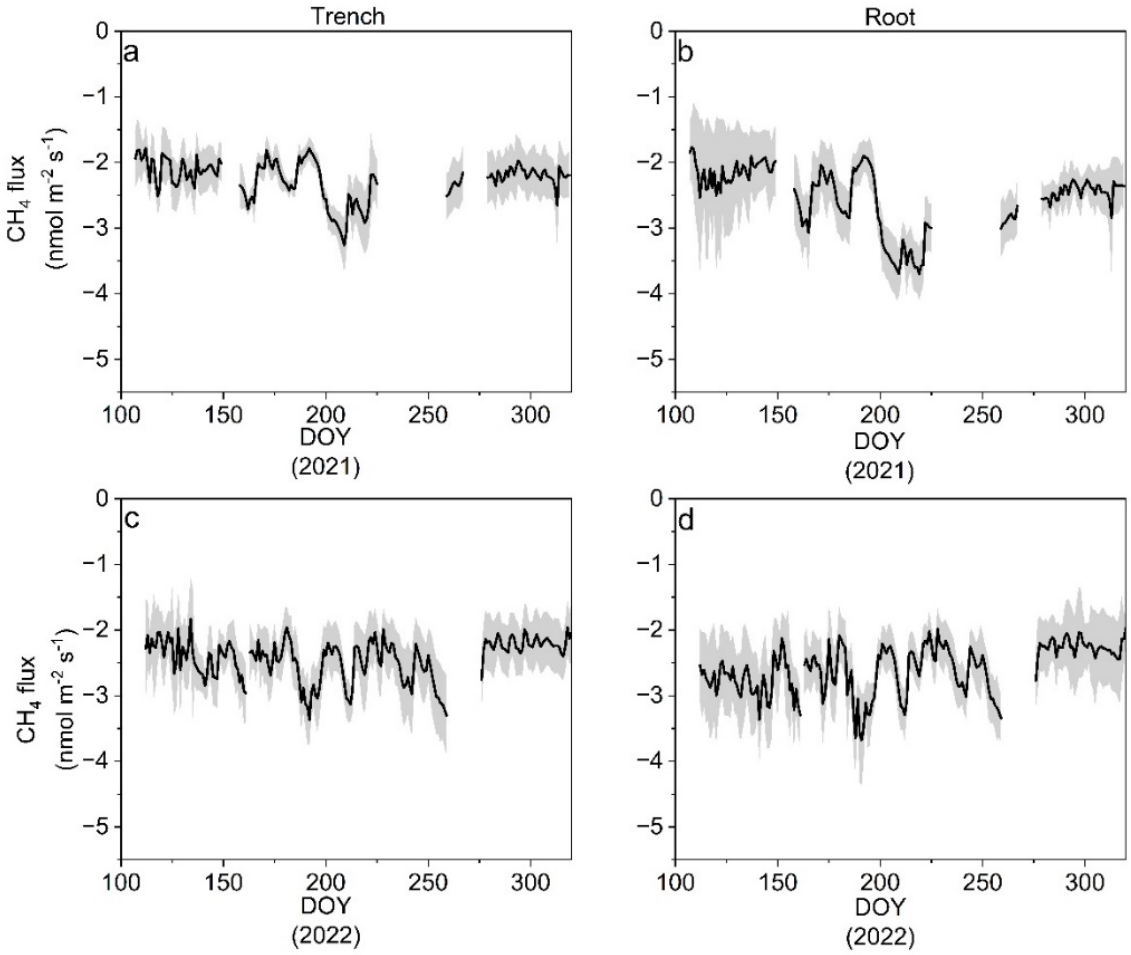

Figure 8. Seasonal variations in mean daily CH_4 flux in two treatments in 2021 (a and b, from April 17th to November 15th) and 2022 (c and d, from April 22nd to November 16th). Shaded areas denote SD of five chambers in each treatment.

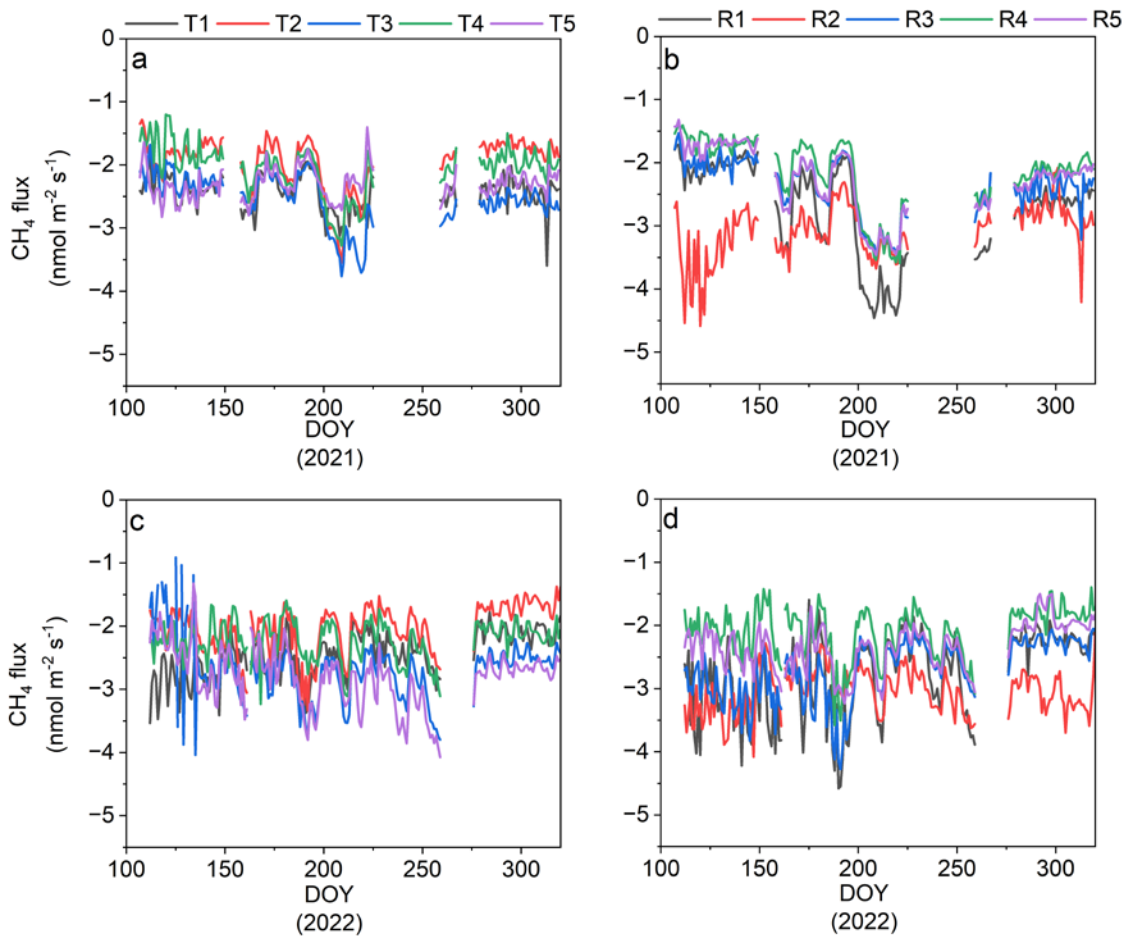

Figure 9. Seasonal variations in mean daily CH_4 flux in each chamber in 2021 (a and c, from April 17th to November 15th) and 2022 (c and d, from April 22nd to November 16th). T1-T5 represent Trench chambers (a and c) while R1-R5 represent Root chambers (b and d).

Table 8. Two-year mean daily CH_4 flux in each chamber (mean ± SD)

Treatment	CH_4 flux (nmol $m^{-2}s^{-1}$)
Trench	
T1	−2.44 ± 0.33
T2	−1.99 ± 0.40
T3	−2.62 ± 0.47
T4	−2.15 ± 0.36
T5	−2.57 ± 0.45
P [a]	$< 2e^{-16}$
Root	
R1	−2.76 ± 0.69
R2	−3.07 ± 0.40
R3	−2.58 ± 0.49
R4	−2.11 ± 0.48
R5	−2.30 ± 0.45
P [a]	$< 2e^{-16}$

[a] One-way ANOVA (n=5) in each treatment.

Table 9. Two-year mean daily CH_4 flux in two treatments (mean ± SD)

Treatment	CH_4 flux (nmol $m^{-2}s^{-1}$)
T	−2.35 ± 0.47
R	−2.56 ± 0.61
P [a]	$< 2e^{-1}$

[a] *t*-test between two treatments (two-tailed).

3.2.2 Fitting of machine learning models

Eight and ten explanatory variables (Table 1) were used to build ML models using RF and GBM algorithms. RF models had a higher R^2 and a lower RMSE than that of

GBM models in both treatments, suggesting that RF algorithm was more reliable to predict CH_4 flux (Table 10). The accuracy of Trench models was lower than Root models, even though Trench models used more observations than Root models (Table 10).

Table 10. Performance of RF and GBM models for CH_4 flux

Treatment	Observation quantity [a]	Algorithm	R^2 [b]	RMSE (nmol $m^{-2}s^{-1}$)
Trench	37063	RF	0.731	0.299
		GBM	0.649	0.421
Root	32772	RF	0.788	0.263
		GBM	0.672	0.415

[a] Chamber R2 data in 2021 were excluded from modelling because of the lack of soil moisture data.

[b] Models were repeated 10 times using different seeds, and the best result was shown.

3.2.3 Feature importance of models

O_2 diffusion rate had the highest influence in regulating CH_4 flux, followed by WFPS. The relative importance of O_2 diffusion rate was 19.69% and 18.38% in Trench and Root models, respectively, slightly higher than that of WFPS (17.72% in Trench model and 17.93% in Root model) (Figure 10). Generally, soil physical properties of bulk density and C/N ratio had higher importance ranking in Trench models than in Root models. In contrast, root dynamics showed high importance in Root models; root biomass and root production were the second and fourth most important variables, respectively. Ambient CH_4 concentration had a higher importance than soil temperature in both models, and both of these two features contributed to approximately 10% of relative influence, followed by air temperature and wind speed.

The influence of O_2 diffusion rate was positive, while WFPS had a negative impact. In Trench models, ambient CH_4 concentration shared a positive influence with soil temperature, whereas soil temperature had both effects and ambient CH_4 concentration

rate showed a positive effect in Root models. The bulk density, C/N ratio, air temperature and wind speed influenced the CH_4 flux both positively and negatively. Additionally, root biomass and root production showed both positive and negative effects, suggesting root dynamics influenced CH_4 uptake in both positive and negative ways.

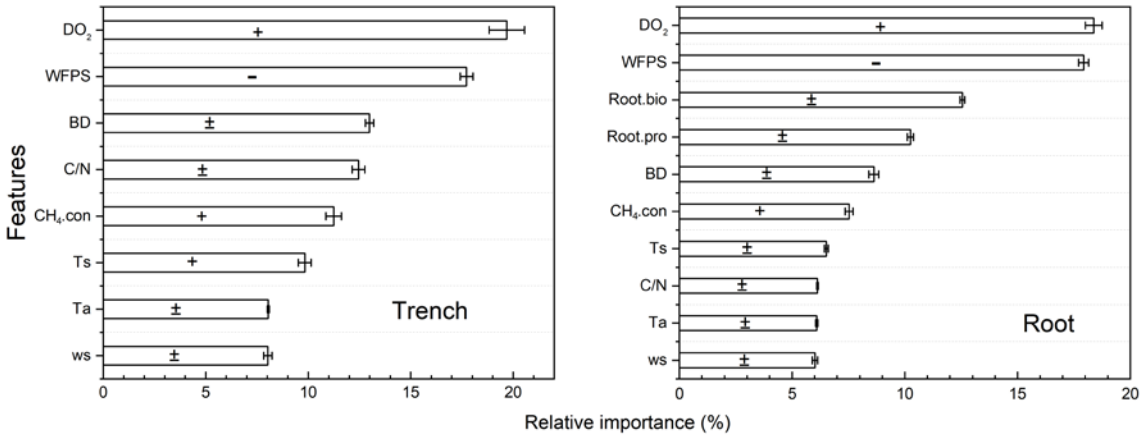

Figure 10. Feature importance of variables in RF models for two treatments. Relative importance (total to 100%) was used to represent the importance of each feature. Mean ± SD of 10 replicates with different seeds were shown. The symbols of +, − and ± represent positive, negative and both impacts of different features on CH_4 flux.

3.2.4 Relationship between soil methane flux and soil moisture and temperature

Figure 11 is the partial dependence of CH_4 flux on soil moisture and temperature. Generally, CH_4 flux is positively correlated with WFPS in the range of 15-30%. Compared with WFPS, the relationship of CH4 flux with soil temperature is more complex, especially in Trench models. Although soil temperature had an enhancing influence on CH_4 uptake in both models, CH_4 uptake was discontinuously decreased by soil temperature in the range of 10-15 °C in Trench models. Linearity of the relationship of CH_4 flux with soil temperature was weaker than that with WFPS (Figure 11).

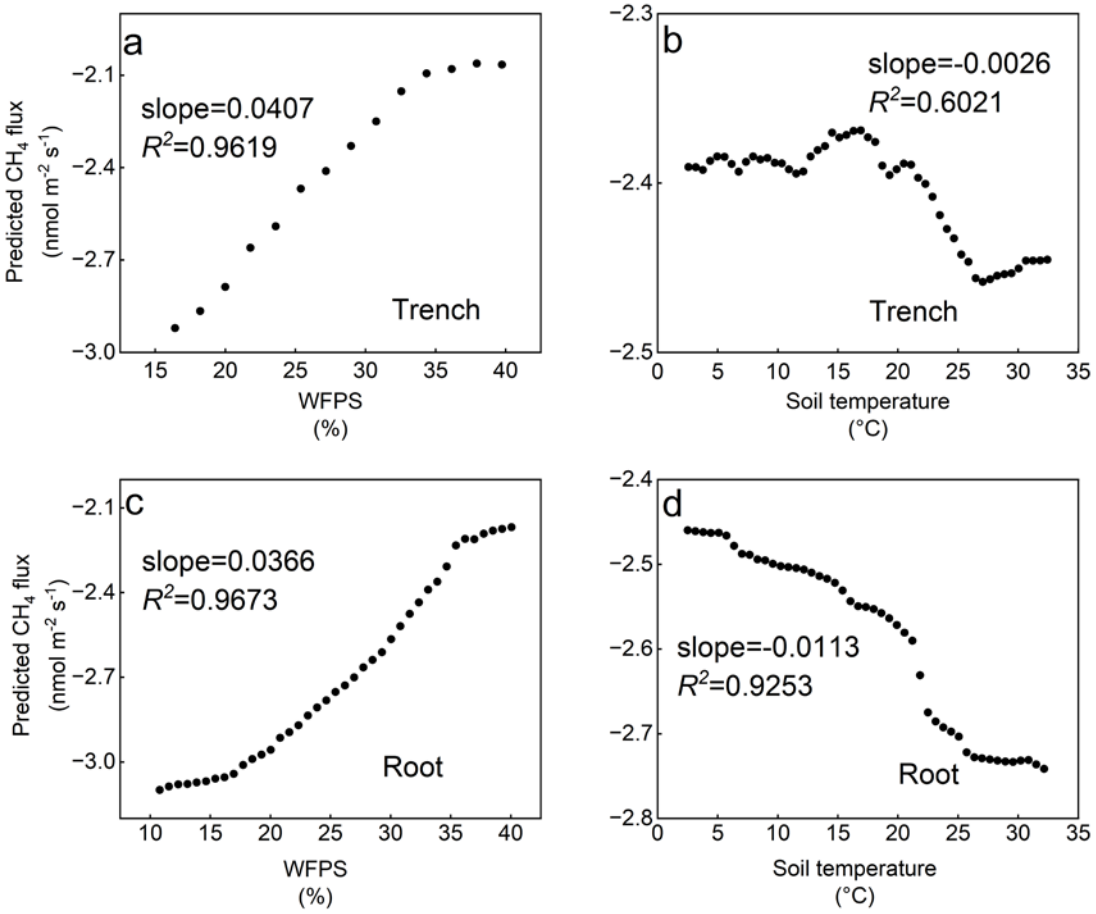

Figure 11. Partial dependence plot between predicted CH_4 flux and WFPS (a and c) or soil temperature (b and d) in RF models.

3.3 Soil carbon dioxide flux

3.3.1 Spatiotemporal variation of soil respiration

Soil CO_2 flux was always positive in all chambers, indicating that the forest soil was a continuous CO_2 source over the growing season (Figure 12). In both treatments, CO_2 flux changed seasonally, almost synchronously with soil temperature with a peak in August (Figure 5). Soil CO_2 flux had significant small-scale spatial variation within each treatment (Table 11). Chamber T3 (3.05 ± 1.01 μmol $m^{-2}s^{-1}$) and R4 (3.01 ± 1.89 μmol $m^{-2}s^{-1}$) had the highest CO_2 flux in each treatment, respectively. The coefficients of variation (CV) of Trench and Root chambers were 53.3% and 39.1%, respectively, suggesting that CO_2 flux in Trench chambers had a larger spatial variation than in Root chambers (Table 11, Figure 13). Also, two-year mean daily CO_2 flux in Root chambers

(2.67 ± 1.69 μmol m^{-2} s^{-1}) was significantly higher (by 19.9%, $P < 0.001$) than that of Trench chambers (2.14 ± 1.49 μmol m^{-2} s^{-1}) (Table 12), which means Root chambers were emitting CO_2 faster than Trench chambers by approximately 20% on average.

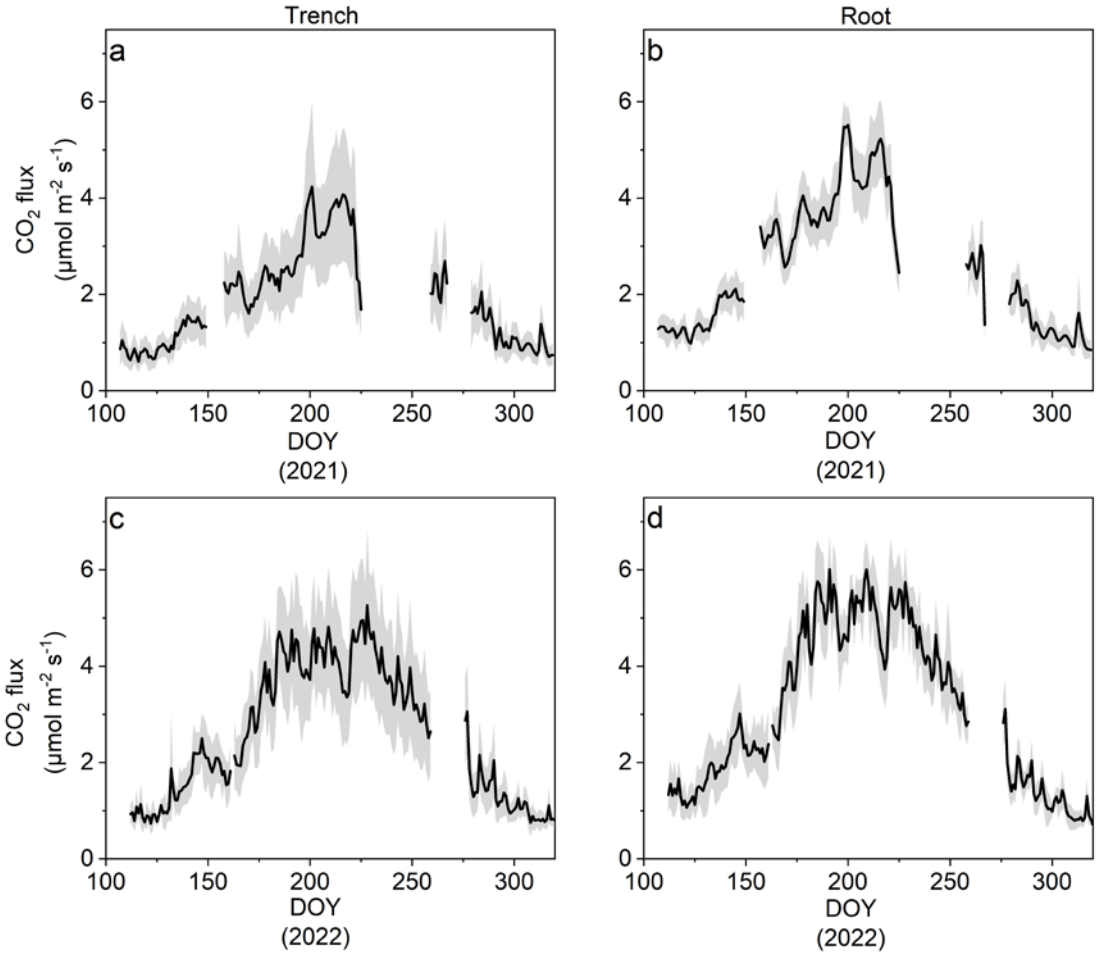

Figure 12. Seasonal variations in mean daily CO_2 flux in two treatments in 2021 (a and b, from April 17th to November 15th) and 2022 (c and d, from April 22nd to November 16th). Shaded areas indicate SD of five chambers in each treatment.

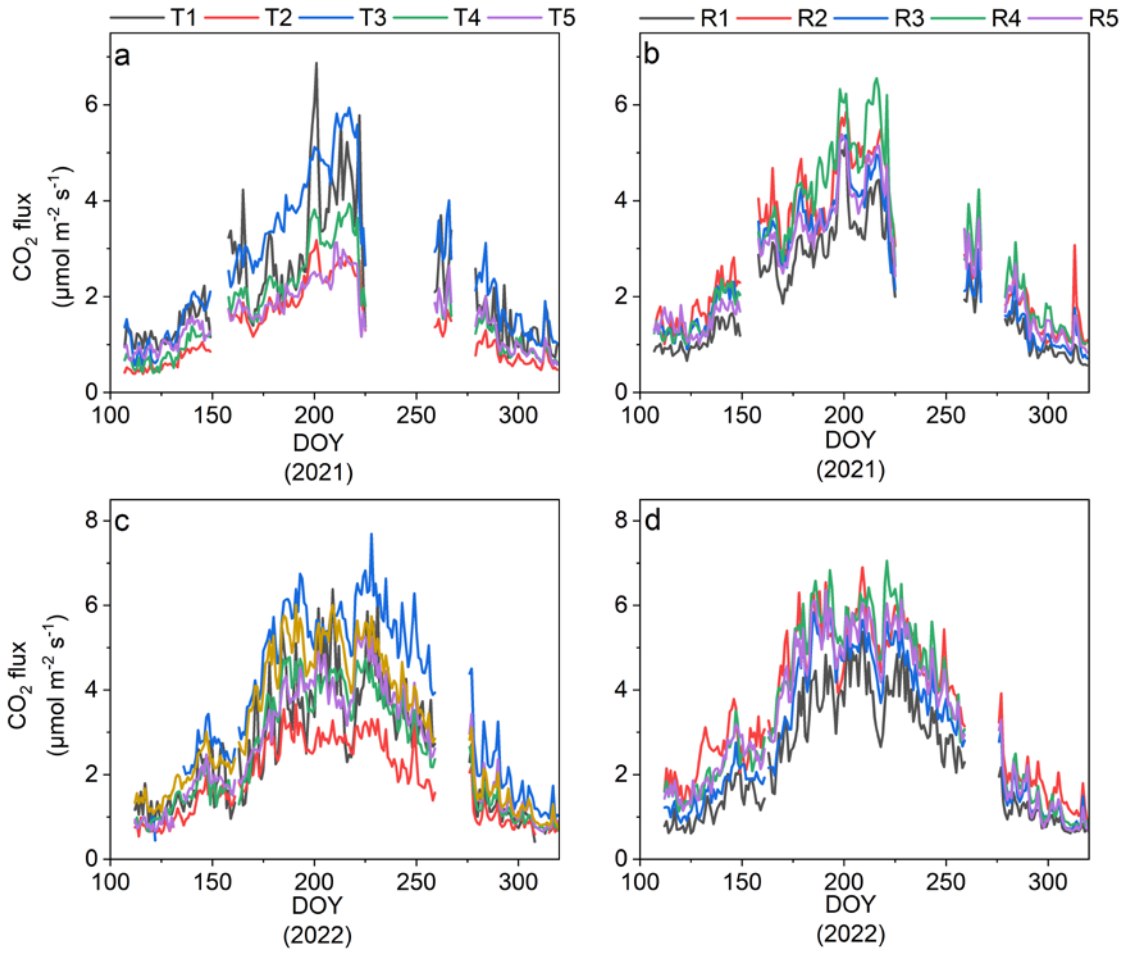

Figure 13. Seasonal variations in mean daily CO_2 flux in each chamber in 2021 (a and b, from April 17th to November 15th) and 2022 (c and d, from April 22nd to November 16th). T1-T5 represent Trench chambers (a and c) while R1-R5 represent Root chambers (b and d).

Table 11. Two-year mean daily CO_2 flux in each chamber (mean ± SD)

Treatment	CO_2 flux ($\mu mol\ m^{-2}s^{-1}$)
Trench	
T1	2.25 ± 1.44
T2	1.50 ± 0.92
T3	3.05 ± 1.01
T4	1.97 ± 1.31
T5	1.98 ± 1.18
P [a]	$< 2e^{-16}$
Root	
R1	2.05 ± 1.35
R2	3.01 ± 1.70
R3	2.52 ± 1.59
R4	3.01 ± 1.89
R5	2.74 ± 1.67
P [a]	$< 2e^{-16e}$

[a] One-way ANOVA (n=5) in each treatment.

Table 12. Two-year mean daily CO_2 flux in two treatments (mean ± SD)

Treatment	CO_2 flux ($\mu mol\ m^{-2}s^{-1}$)
T	2.14 ± 1.49
R	2.67 ± 1.69
P [a]	$< 2e^{-16}$

[a] *t*-test between two treatments (two-tailed).

3.3.2 Fitting of machine learning models

CO_2 models used the same variables combination with CH_4 models except for ambient CH_4 concentration and O_2 diffusion rate (Table 1). Similar to CH_4 models, RF

models had higher accuracy than GBM models in both treatments (Table 13). Root models had a better performance than Trench models. Although observations used for modeling were fewer than that of CH_4 modeling in both treatments because of data quality control, CO_2 models showed higher accuracy than CH_4 models (Table 10), indicating the combination of explanatory variables is more appropriate for CO_2 flux modeling.

Table 13. Performance of RF and GBM models in predicting CO_2 flux

Treatment	Observation quantity [a]	Algorithm	R^2 [b]	RMSE ($\mu mol\ m^{-2}s^{-1}$)
Trench	35379	RF	0.933	0.40
		GBM	0.861	0.51
Root	31591	RF	0.973	0.28
		GBM	0.892	0.33

[a] Chamber R2 data in 2021 were excluded from modelling because of the lack of soil moisture data.

[b] Models were repeated 10 times using different seeds, and the best result was shown.

3.3.3 Feature importance of models

Soil temperature was considered as the main controlling factor for CO_2 emission; the relative influence of soil temperature was approximately 35% in both treatments (Figure 14). Root biomass and production showed high importance in Root models, suggesting the important role of root dynamics in regulating CO_2 emission. Bulk density contributed to approximately 13% in both models, followed by WFPS. However, WFPS was more important in Trench models than in Root models, partly because the number of variables was smaller in Trench models. Wind speed still had the lowest importance in both models.

Soil temperature had a positive promoting effect on soil CO_2 emission, whereas bulk density, WFPS, C/N ratio, air temperature and wind speed had both positive and negative influences (Figure 14). Root production had a positive influence, while root

biomass influenced CO_2 flux both negatively and positively.

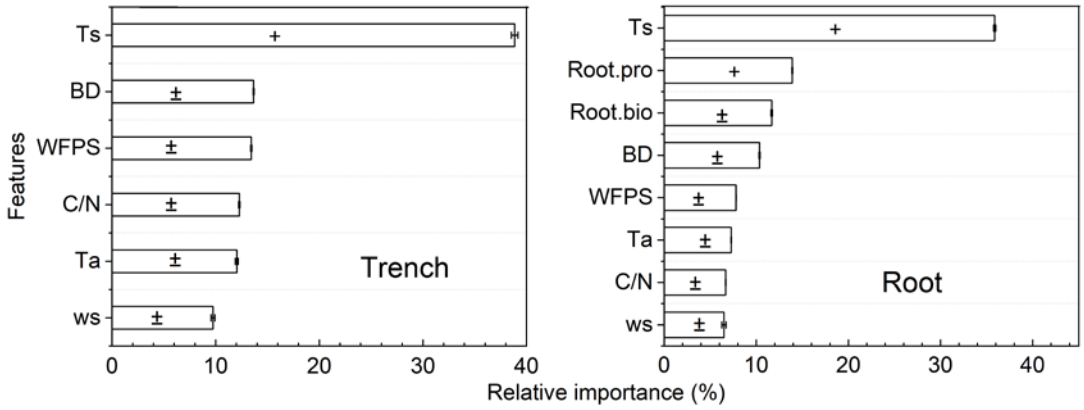

Figure 14. Feature importance of variables in RF models for two treatments. Relative importance (total to 100%) was used to represent the importance of each feature. Mean ± SD of 10 replicates with different seeds were shown. The symbols of + and ± represent positive and positive/negative impacts of different features on CO_2 flux.

3.3.4 Relationship between carbon dioxide flux and soil moisture and temperature

Partial dependence plot (Figure 15) revealed the complex relationship between CO_2 flux and WFPS, especially in Trench models, indicating complex interactions between soil moisture and CO_2 emission. In Root models, sudden drops appeared at WFPS of 20% and 30% in the linear regression. On the contrary, CO_2 flux showed a positive linear relationship ($R^2 > 0.9$) with soil temperature in the range of 10-25 °C in both models.

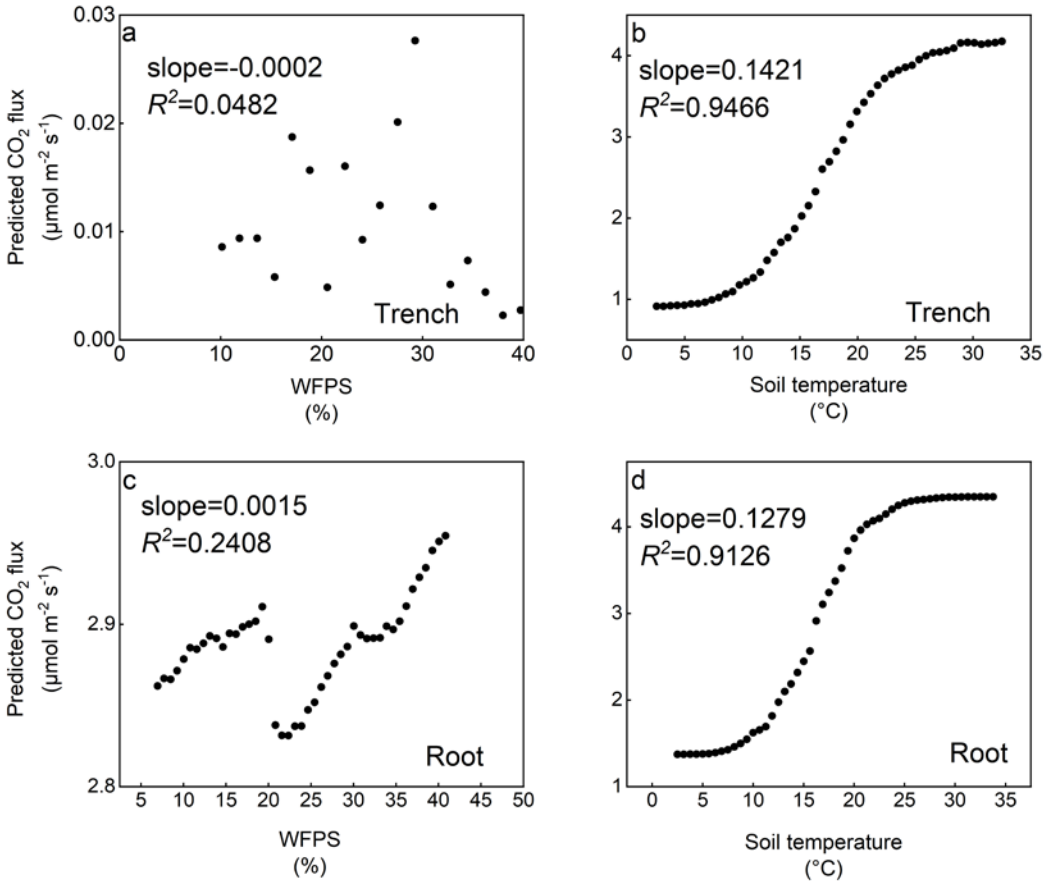

Figure 15. Partial dependence plot between predicted CO_2 flux and WFPS (a and c) or soil temperature (b and d) in RF models.

3.4 Separation of soil respiration

3.4.1 Root respiration estimated by a conventional method

Usually, RR is estimated as the difference of mean values of Root chamber CO_2 flux (corresponding to RS) and Trench chamber CO_2 flux (corresponding to RH) using a trenching method. RR estimated by the conventional method showed a clear seasonal trend (Figure 16). Unnaturally larger RR appeared in the spring between late April and early May.

For each Root chamber, conventional RR ranged from −0.069 ± 0.38 μmol m^{-2} s^{-1} (R1) to 0.95 ± 0.49 μmol m^{-2} s^{-1} (R2) (Table 14). Since RS in R1 was relatively low compared to that in other chambers, especially in 2022, it was difficult to separate RS

precisely using this method. Minus RR also appeared even in other chambers especially in October when RS decreased.

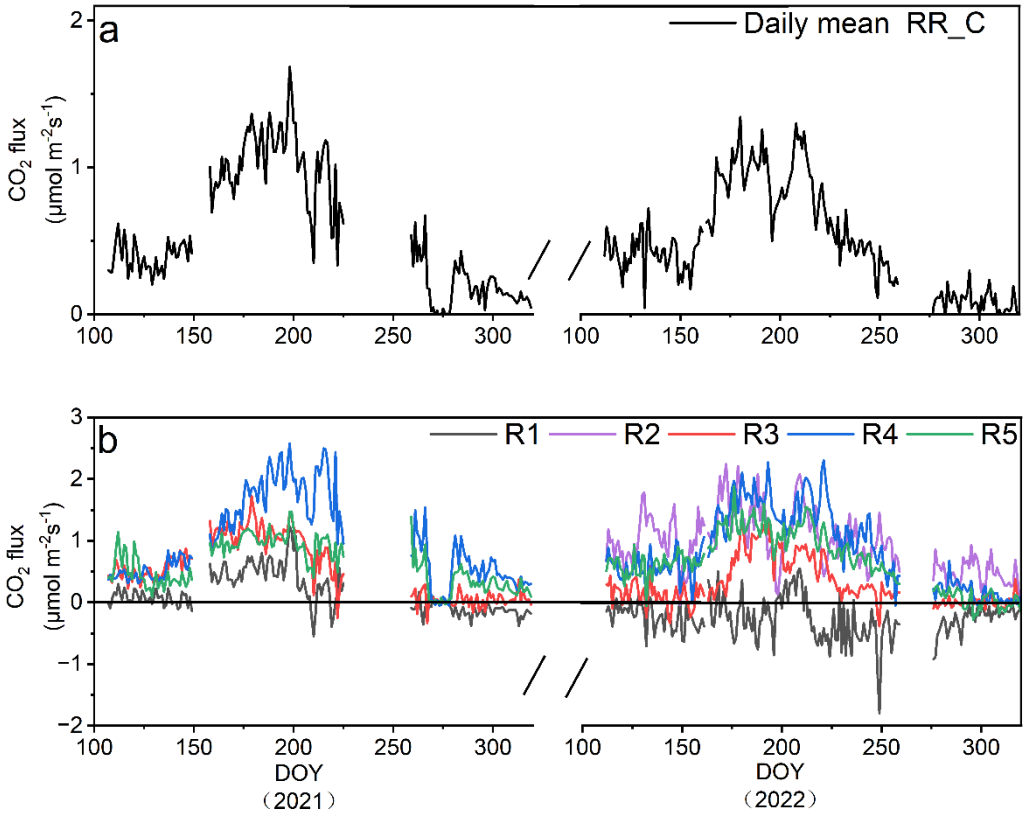

Figure 16. Seasonal variations in daily mean root respiration calculated by the conventional method on average (a) and in each Root chamber (b) in 2021 (from April 17th to November 15th) and 2022 (from April 22nd to November 16th).

3.4.2 Root respiration estimated by RF modelling

Six variables, excluding fine root biomass and production (Table 1), from Root chambers were put into the RF model trained using Trench chamber data to predict the RH in Root chambers. Using the estimated RH of each Root chamber, RR (RR_RF) was calculated as the difference between measured RS and estimated RH in each Root chamber. Like conventional RR, RR_RF showed seasonality with a peak before DOY 200 (Figure 17). Unnaturally larger RR in the spring, which was found in RR_C (Figure 16), did not appear in RR_RF, and the frequency of minus values decreased than that RR_C except for R1 chamber (Table 14). The highest RR_RF emerged in R4 chamber

(0.95 ± 0.75 μmol m^{-2} s^{-1}). RR_RF in R2 was shown from July in 2022, because soil moisture was not available before. Mean daily RR_RF (0.61 ± 0.50 μmol m^{-2} s^{-1}) was significantly larger than RR_C (0.53 ± 0.39 μmol m^{-2} s^{-1}) (by 15.1%, $P < 0.05$) (Table 14). In addition, CV was larger in RR_RF (72.6%) than in RR_C (62.1%) (Table 14).

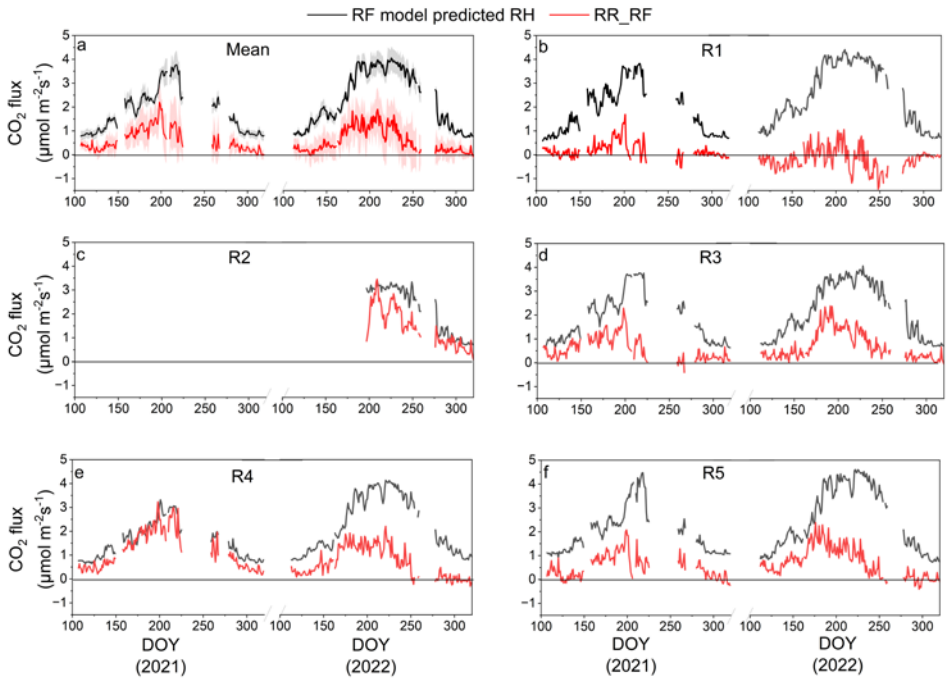

Figure 17. Root respiration estimated by the RF modelling method. Black lines denote RH predicted by RF models on average (a) and in each Root chamber (b−f), while red lines denote RR. Shaded areas (a) denote SD of five chambers.

Table 14. Two-year mean daily root respiration estimated by two methods (RR_C and RR_RF, mean±SD)

Chamber	RR_C ($\mu mol\ m^{-2}\ s^{-1}$)	RR_RF ($\mu mol\ m^{-2}\ s^{-1}$)
R1	−0.069 ± 0.38	−0.003 ± 0.45
R2 [a]	0.95 ± 0.49	0.80 ± 0.94
R3	0.41 ± 0.44	0.66 ± 0.55
R4	0.92 ± 0.66	0.95 ± 0.75
R5	0.64 ± 0.42	0.64 ± 0.58
P [b]	$< 2e^{-16}$	$< 2e^{-16}$
Mean	0.53 ± 0.39	0.61 ± 0.50
P [c]	0.023	
Q_{10} [d]	2.00 ± 0.98	2.43 ± 1.27
P [e]	0.567	
CV	62.1%	72.6%

[a] RRs of R2 chamber were calculated using only 2022 data.

[b] One-way ANOVA within each treatment.

[c] *t*-test between two-year mean daily RR calculated by two methods (Two-tailed).

[d] Q_{10} was the mean of five chambers.

[e] *t*-test between Q_{10} of two RRs (Two-tailed).

3.4.3 Relationship between root respiration and soil temperature

RR_C and RR_RF of chamber R3, R4, R5 was averaged to fit with average soil temperature (Eq. (7)), respectively (Figure 18). Chamber R1 was excluded because of low data quality. Fitting performance with soil temperature was better in RR_RF than that of RR_C, with R^2 was 0.54 and 0.44 in RR_RF and RR_C, respectively (Figure 18). Sensitivity of RRs to soil temperature was determined by temperature coefficient Q_{10}, which was calculated using the fitting parameter a2 in Eq. (7) using daily data. Q_{10} of RR_RF (2.43 ± 1.27, mean of five chambers) was higher than RR_C (2.00 ± 0.98,

mean of five chambers), indicating RR estimated by RF modelling method was more sensitive to change of soil temperature, but this kind of variation was not significant ($P > 0.05$, Table 14). Small-scale spatial variation in RR_RF was more significant than RR_C, with CV of RR_RF and RR_C was 72.6% and 62.1%, respectively.

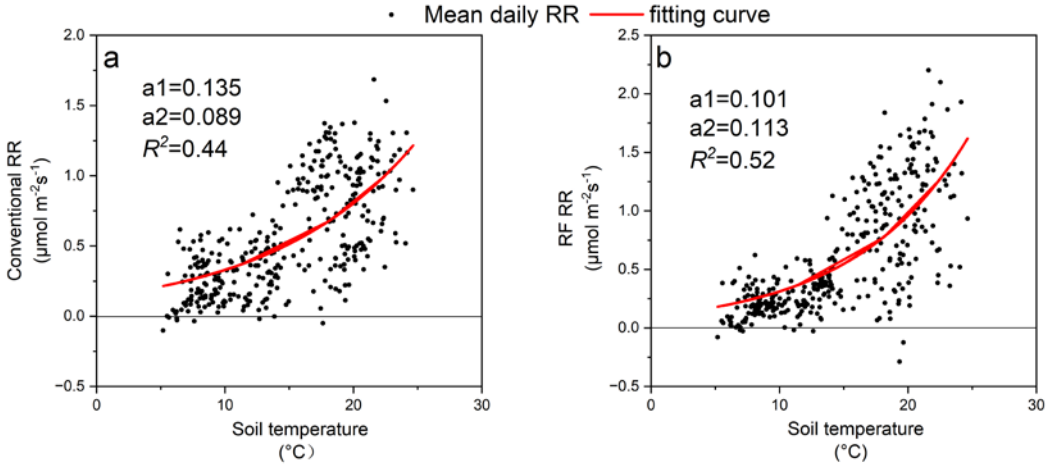

Figure 18. Exponential regression between root respiration and soil temperature for RR_C (a) and RR_RF (b). Daily mean data were plotted using the data from chamber R3, R4, and R5.

3.5 Relationship between root respiration and GPP

3.5.1 Seasonal trend of GPP

Gap-filled 30-min GPP data was averaged to daily scale to illustrate the seasonal trend of GPP. Generally, GPP increased from around DOY of 110 to 150, and changed frequently until around DOY of 220, then showed a decreasing trend to the DOY of 320 (Figure 19). Seasonal trend in two years was similar.

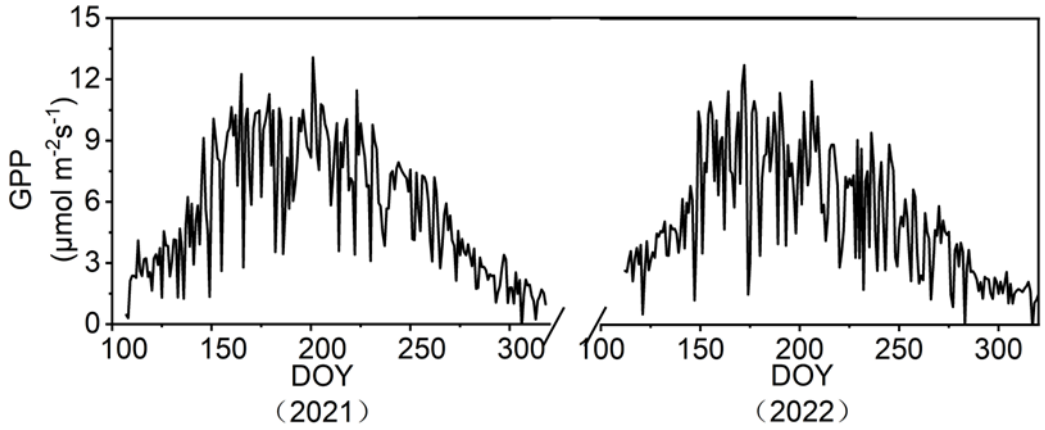

Figure 19. Seasonal variation in mean daily gross primary production (GPP) measured by the eddy covariance method in 2021 (from April 17th to November 15th) and 2022 (from April 22nd to November 16th).

3.5.2 Gap-filling of root respiration

To apply wavelet analysis, data gaps of hourly RS, RR_C and RR_RF were filled using an RF algorithm. RS and RR data from chambers R3, R4, and R5 were averaged and used for wavelet analysis. RR_RF had more data gaps in the summer of 2021 (Figure 20 c), because soil water content was not measured during this period owing to system malfunction. Gap filling seems to be successful, but some spiky data were produced (Figure 20).

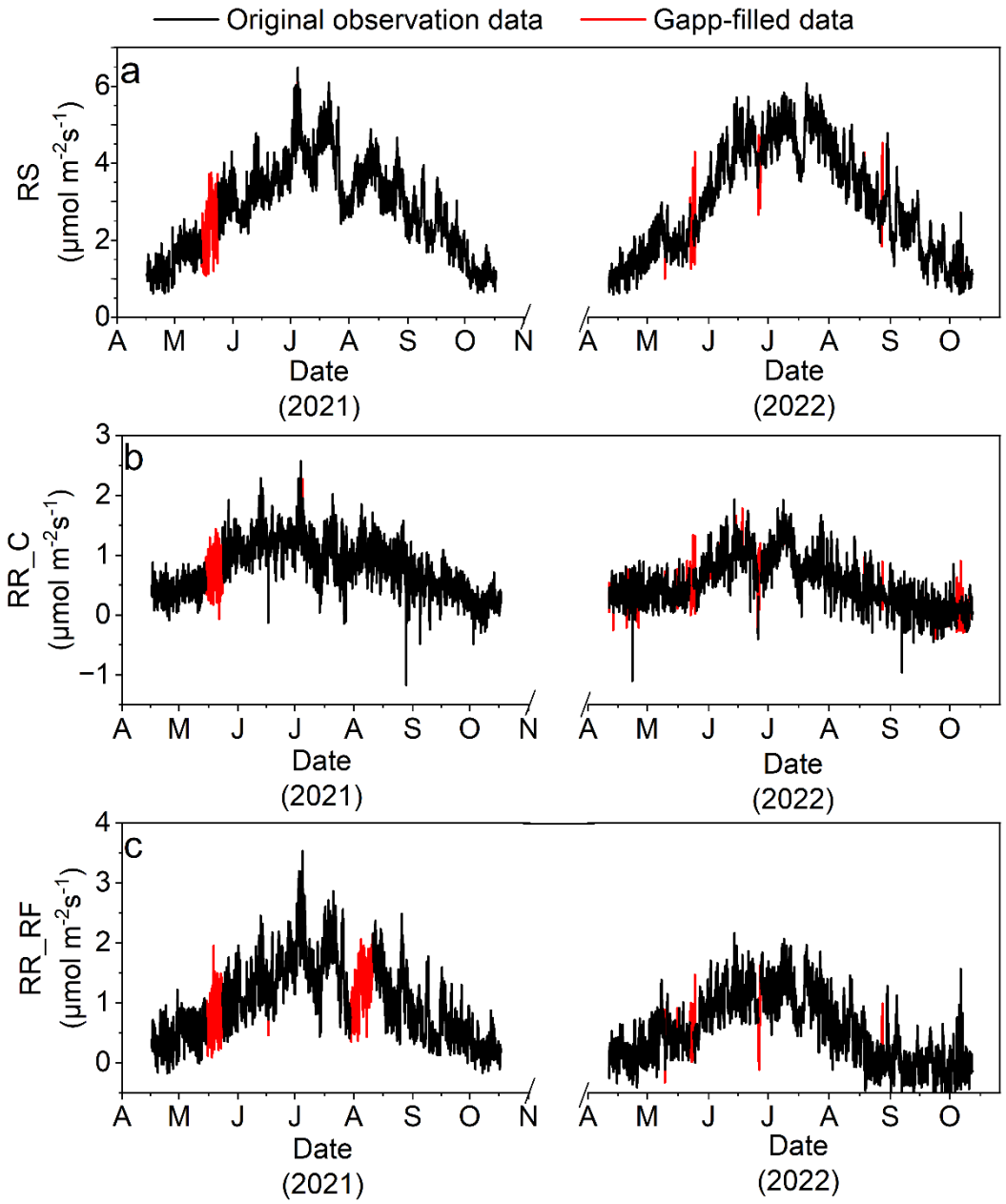

Figure 20. Gap-filled hourly data of RS (a), RR_C (b) and RR_RF (c) using RF algorithm. Black lines denote original observed data and red lines denote gap-filled data. Hourly data was averaged from chamber R3, R4 and R5. R1 and R2 were excluded from data analysis because of low data quality and many data gaps.

3.5.3 Wavelet power of two types of RR, RS and GPP

Z-score standardized, de-noised GPP, RS, RR_C and RR_RF data were used for wavelet power analysis and wavelet cross power analysis, respectively. Time resolution

was set at 1/24 day (one hour), consistent with the hourly GPP, RS and RR dataset. Frequency resolution was set at 1/120 day, and Fourier period was set from 1 / 8 day to 32 days. “White noise” method was used to generate the surrogate time series data of GPP, RS and RR. Strength of wavelet power indicates the strength of period. For example, significant wavelet power at a period of 24 hours denotes a diurnal trend.

Spectrum of wavelet power of GPP, RS, RR_C and RR_RF were shown in Figures 21 to 24. Generally, GPP and RS had a significant one-day period, especially continuous ridges appeared in GPP wavelet spectrum in both years, suggesting a typical diurnal trend of GPP (Figure 21). As a contrast, ridges of one-day period were not continuous in RS spectrum, indicating an unstable diurnal trend of RS (Figure 22). Wavelet power of GPP and RS became stronger in summer (June-August), indicating the diurnal trend of GPP and RS was more obvious in summer. Although significant one-day period appeared in RR_C and RR_RF, this kind of diurnal trend was not continuous in both kinds of RR (Figures 23a and Figure 24). No significant period was found in RR_C wavelet power spectrum in 2022, indicating that RR_C had no typical short-term temporal trend in 2022 (Figure 23b). Overall, diurnal trend of RR_RF was more significant than that of RR_C (Figures 23 and 24).

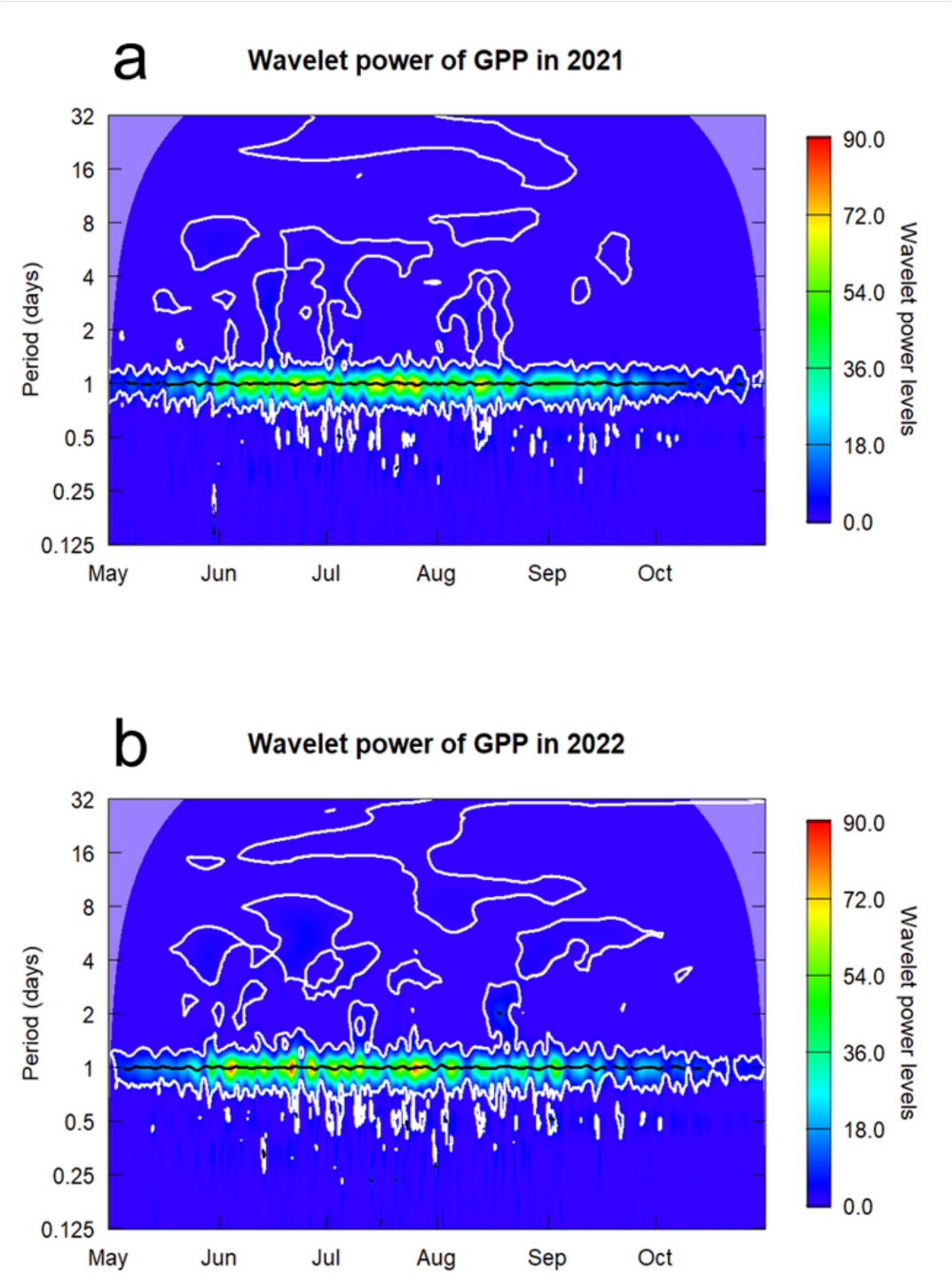

Figure 21. Spectrum of wavelet power of GPP in 2021 (a) and 2022 (b) from May 1st to October 31st. Light blue part is the cone of influence (COI) where edge effects might distort the picture (95% confidence). White lines denote significant periods ($P < 0.05$) and black line is the ridge of period, representing the general trend of periods. Color of significant period indicates the strength of wavelet power.

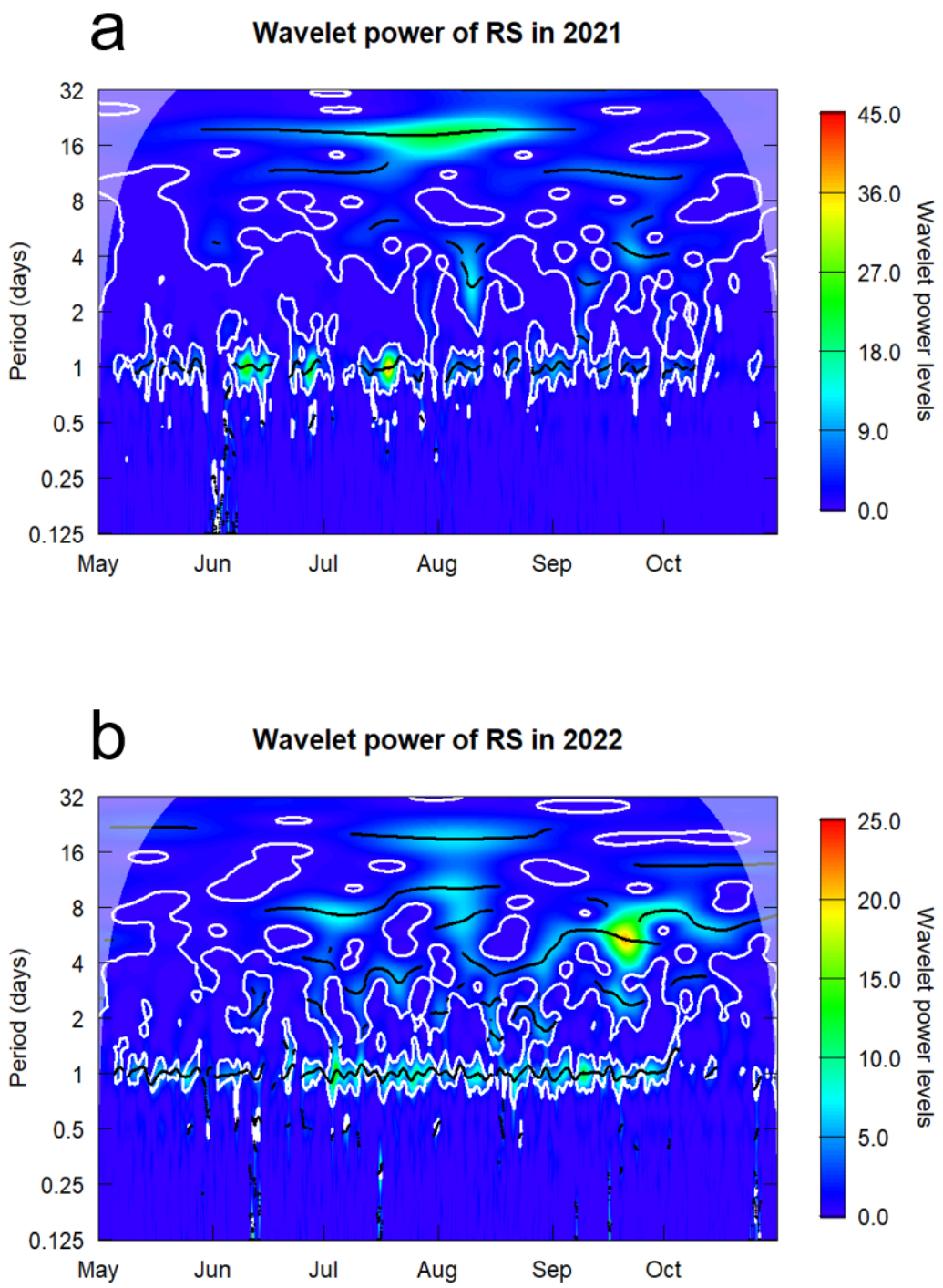

Figure 22. Spectrum of wavelet power of RS in 2021 (a) and 2022 (b) from May 1st to October 31st. Light blue part is the cone of influence (COI) where edge effects might distort the picture (95% confidence). White lines denote significant periods ($P < 0.05$) and black lines are the ridge of periods, representing the general trend of periods. Color of significant period indicates the strength of wavelet power.

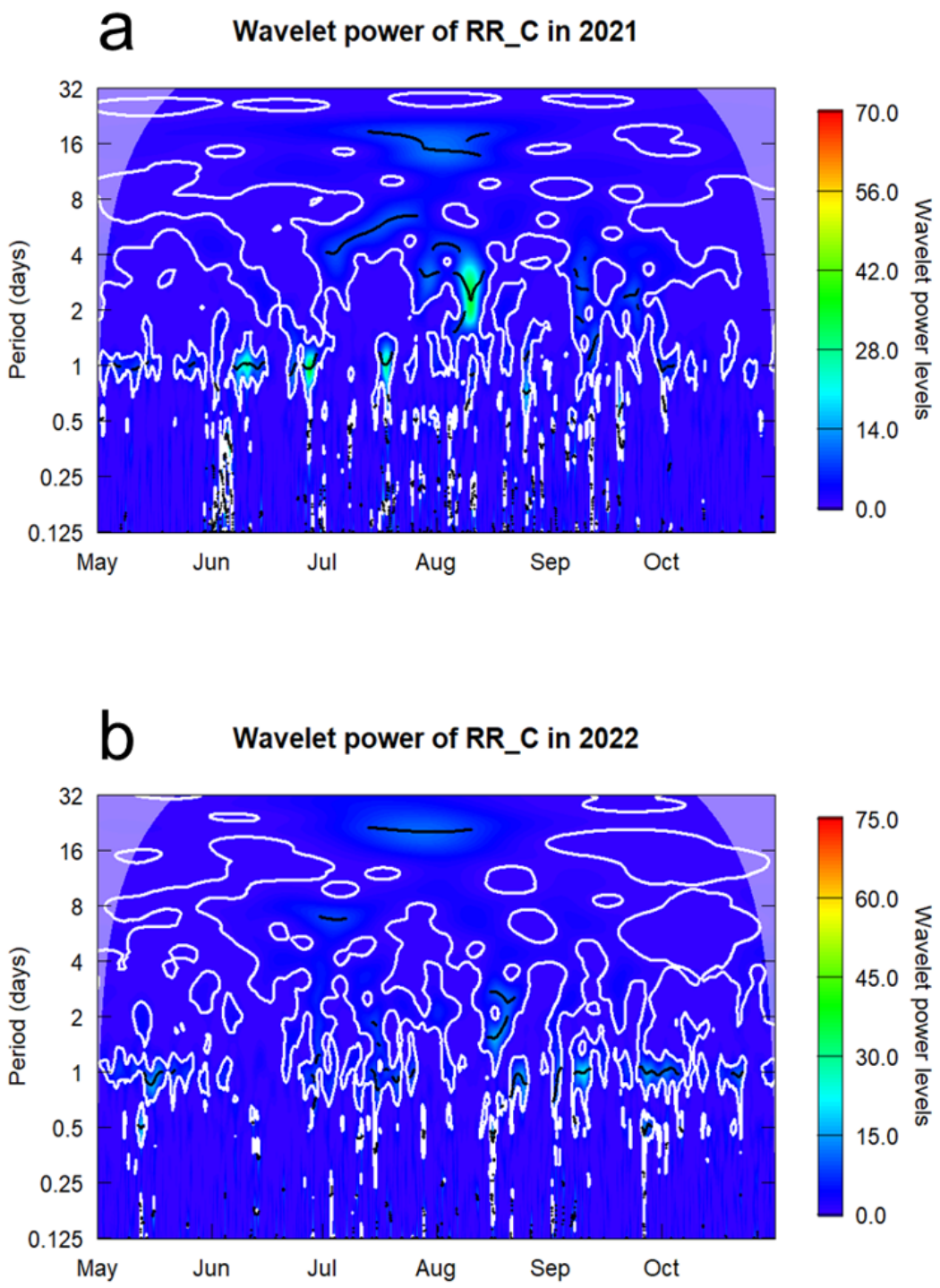

Figure 23. Spectrum of wavelet power of RR_C in 2021 (a) and 2022 (b) from May 1st to October 31st. Light blue part is the cone of influence (COI) where edge effects might distort the picture (95% confidence). White lines denote significant periods ($P < 0.05$) and black lines are the ridge of periods, representing the general trend of periods. Color of significant period indicates the strength of wavelet power.

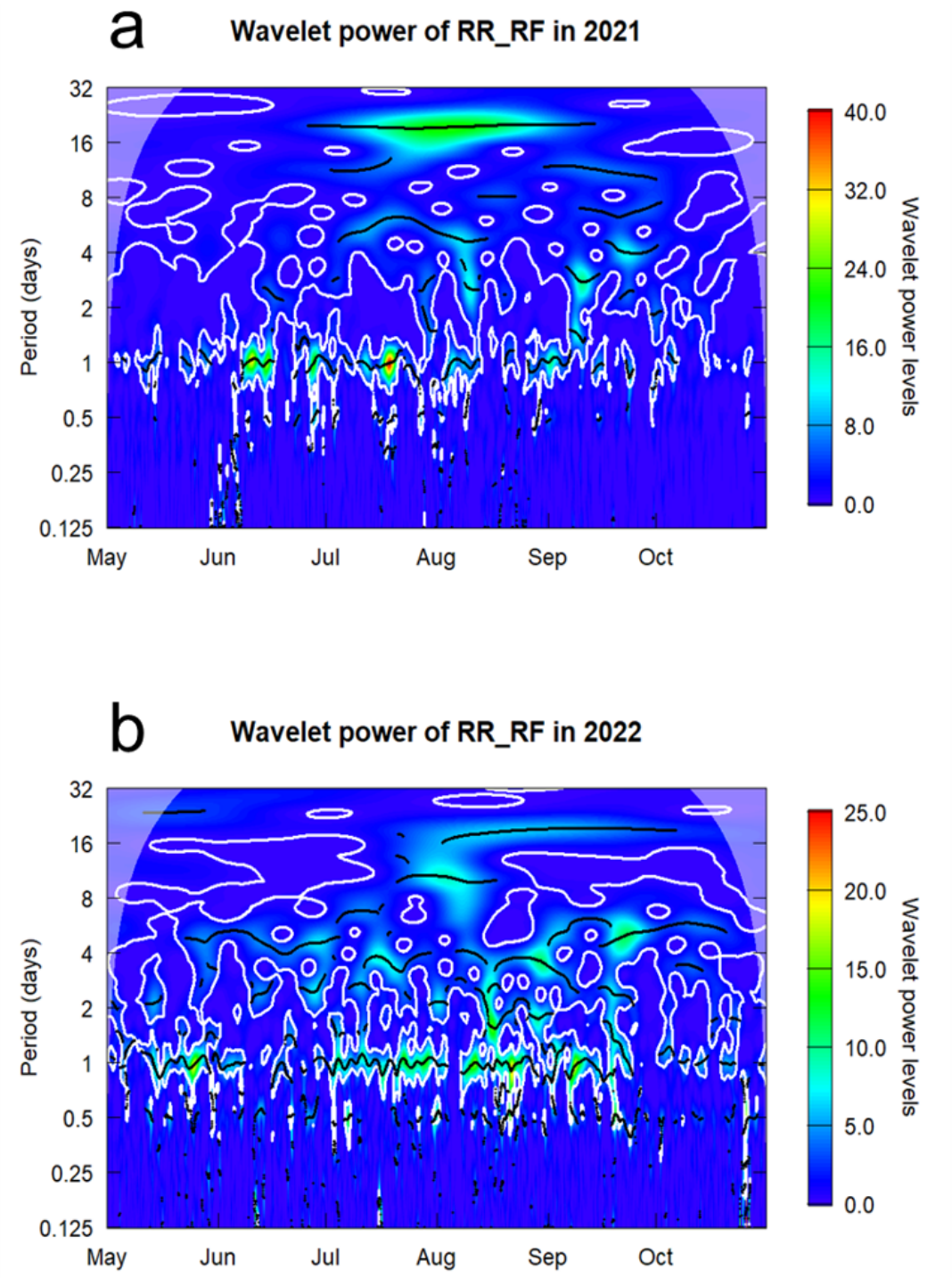

Figure 24. Spectrum of wavelet power of RR_RF in 2021 (a) and 2022 (b) from May 1st to October 31st. Light blue part is the cone of influence (COI) where edge effects might distort the picture (95% confidence). White lines denote significant periods ($P < 0.05$) and black lines are the ridge of periods, representing the general trend of periods. Color of significant period indicates the strength of wavelet power.

3.5.4 Wavelet cross power of GPP/RS, GPP/RR_C and GPP/RR_RF

Parameters of wavelet cross power analysis were set at the same as wavelet power analysis. Strength of wavelet cross power represents the intensity of synchronize change of two time series datasets. For example, significant cross power at a period of 24 hours represents both two datasets have a diurnal trend and change synchronously, but this kind of the common period was not a completely synchronized period and time lag (shorter than the common period) might exist between two datasets.

Overall, GPP had a significant common one-day period with RS and both types of RR in each year (Figures 25-27), which indicates that RS and RR were changing synchronously with GPP at a one-day period. Compared with cross power between GPP and RR_C, power of one-day common period between GPP and RR_RF was stronger and more stable especially in 2021 (Figures 26 a and 27a), indicating that RR estimated by RF modelling method corresponded to GPP more sensitively than by the conventional method. Stronger power of one-day period appeared from June to August in all three cross power spectrums, suggesting that correlation between GPP and RS, RRs became stronger in summer (Figures 25-27).

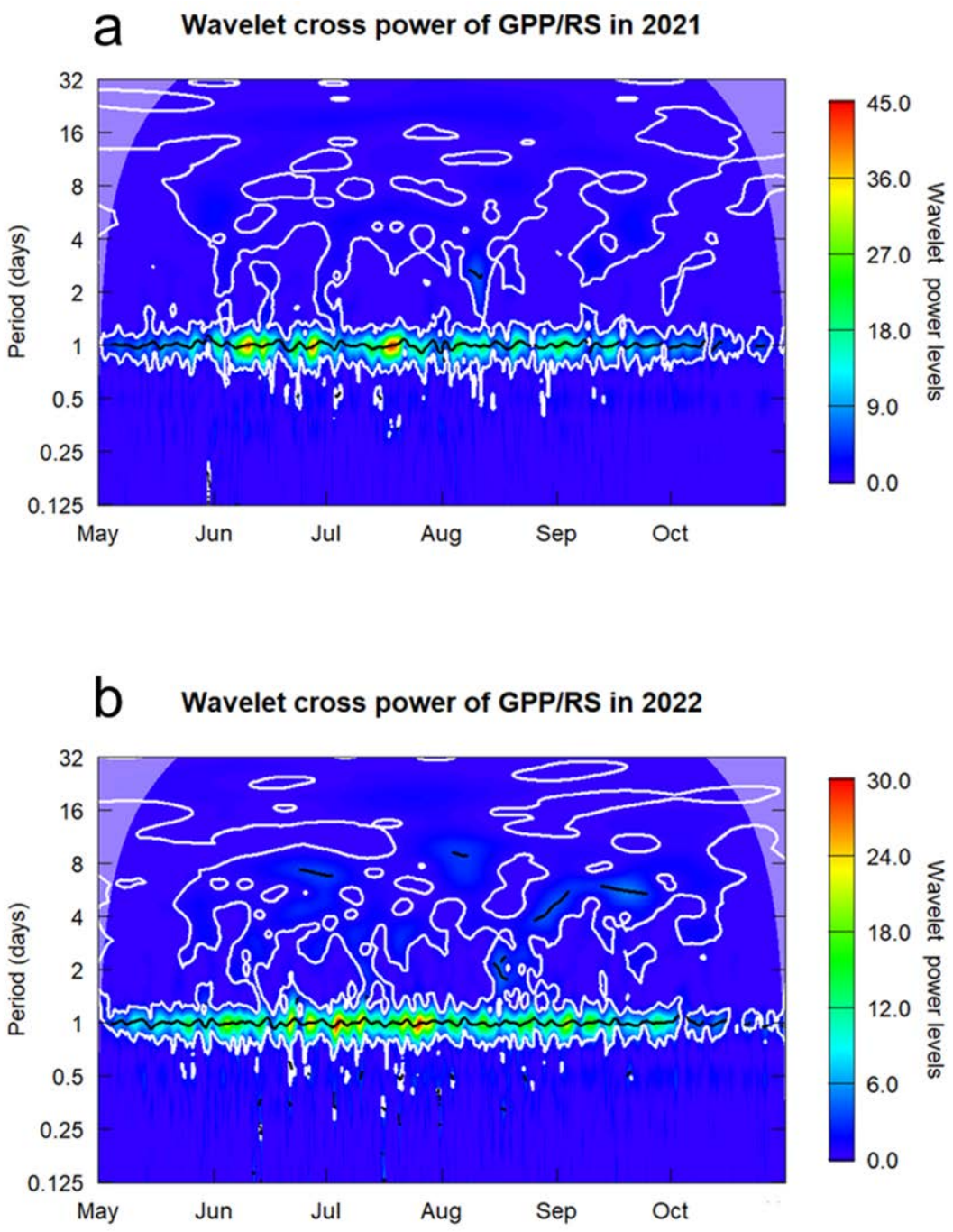

Figure 25. Spectrum of wavelet cross power of GPP over RS in 2021 (a) and 2022 (b) from May 1st to October 31st. Light blue part is the cone of influence (COI) where edge effects might distort the picture (95% confidence). White lines denote significant common periods ($P < 0.05$) and black lines are the ridge of common periods, representing the general trend of common periods. Color of significant common period indicates the strength of cross power.

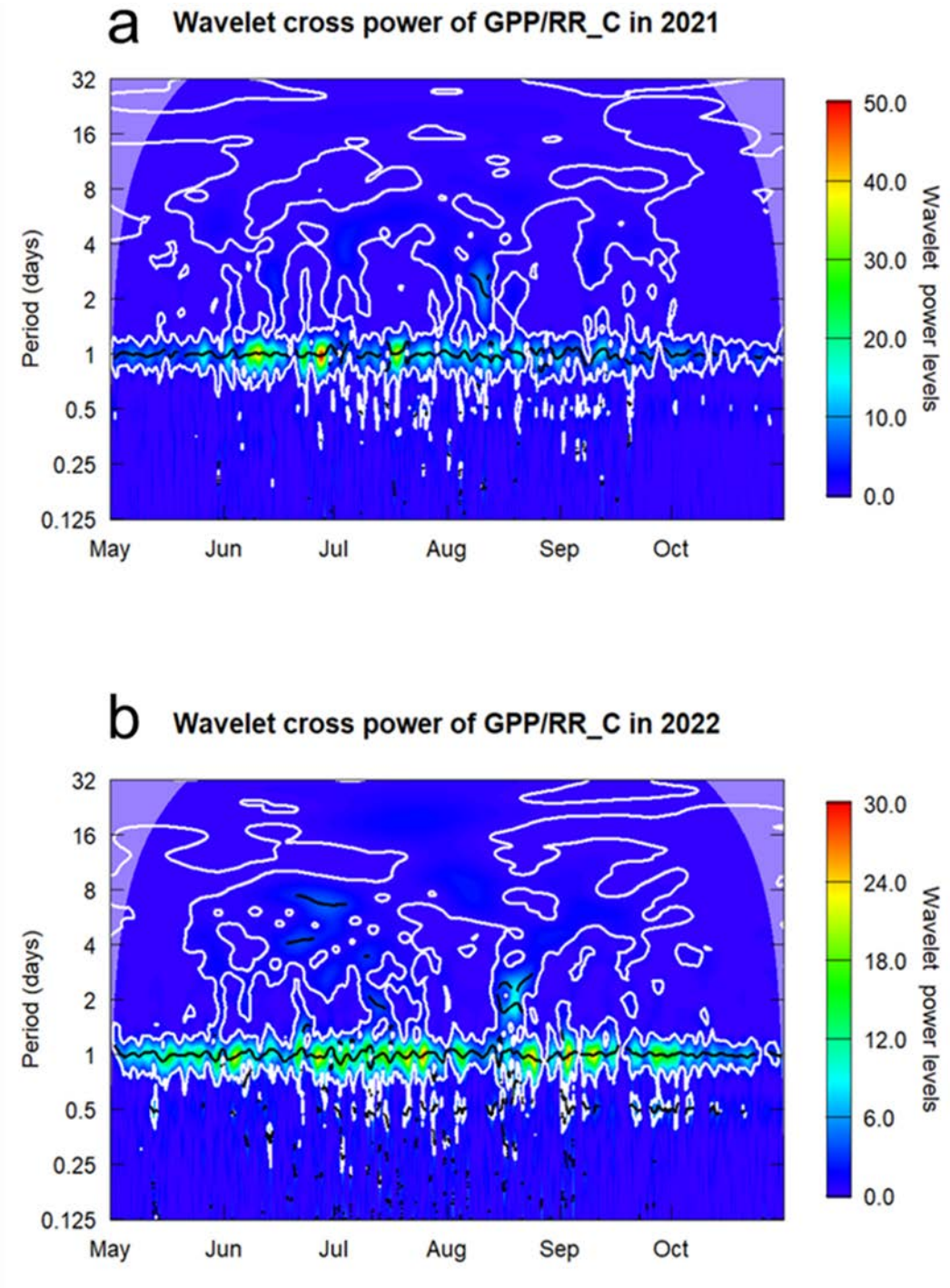

Figure 26. Spectrum of wavelet cross power of GPP over RR_C in 2021 (a) and 2022 (b) from May 1st to October 31st. Light blue part is the cone of influence (COI) where edge effects might distort the picture (95% confidence). White lines denote significant common periods ($P < 0.05$) and black lines are the ridge of common periods, representing the general trend of common periods. Color of significant common period indicates the strength of cross power.

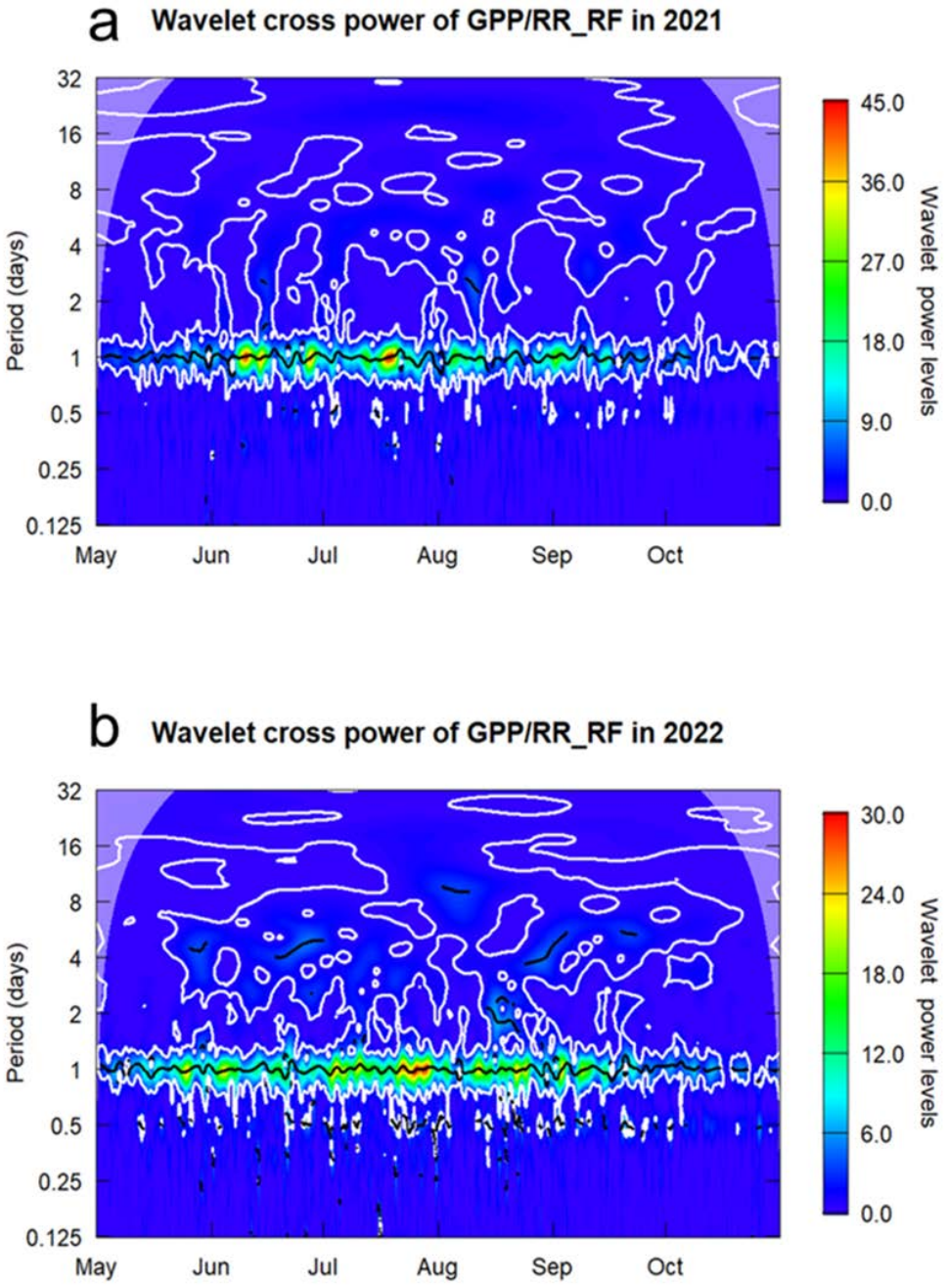

Figure 27. Spectrum of wavelet cross power of GPP over RR_RF in 2021 (a) and 2022 (b) from May 1st to October 31st. Light blue part is the cone of influence (COI) where edge effects might distort the picture (95% confidence). White lines denote significant common periods ($P < 0.05$) and black lines are the ridge of common periods, representing the general trend of common periods. Color of significant common period indicates the strength of cross power.

3.6 Time lag between root respiration and GPP

3.6.1 Diurnal trend of GPP, RS and RR

Hourly data of GPP, RS and two RRs, which were averaged from R3, R4, and R5 chambers, were ensemble-averaged in each month to acquire diurnal variations (Figures 28 and 29). To reflect the real trend of GPP and RR, data were not de-noised. GPP showed a clear diurnal variation with a peak just at noon. Overall, RS showed a similar variation to the GPP variation, but the diurnal variation became less significant in July and August (Figures 28 c, 28 d and Figures 29 c, 29 d). RR_RF had a similar diurnal trend corresponding to RS, while RR_C showed a vague diurnal variation, especially in July, August and September in 2021, and in June, July and August in 2022 (Figures 28 c, 28 d, 28 e and Figures 29 b, 29 c, 29 d). Minus values appeared in both RRs in October 2022 (Figure 29 f). As a whole, RS and RR peaked at around 15-18 PM with approximately 5-8 hours delay from the GPP peak.

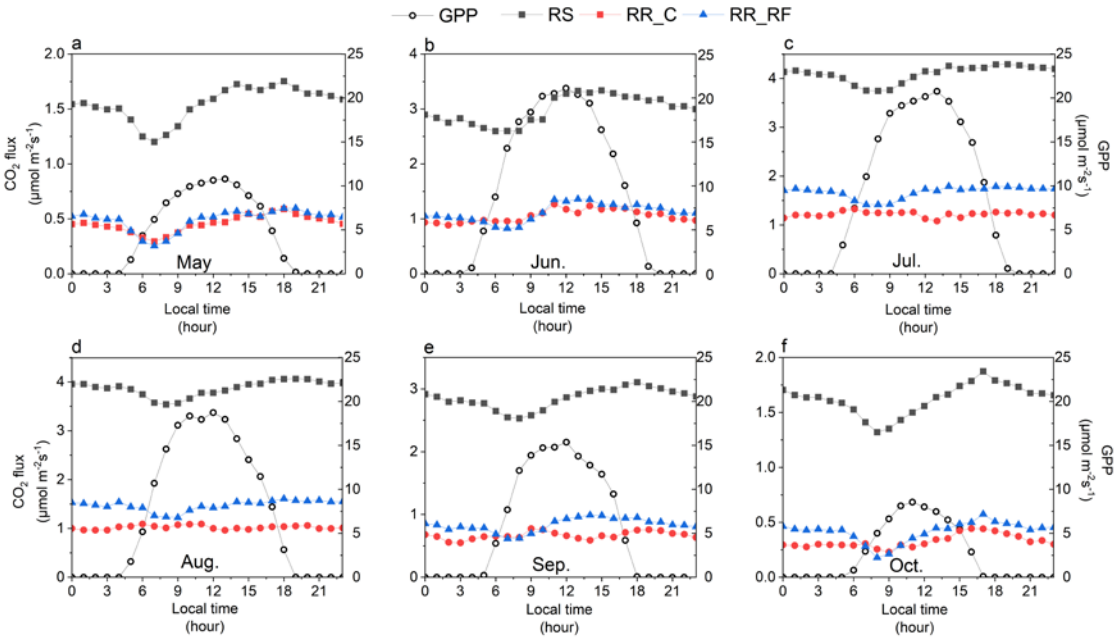

Figure 28. Diurnal trend of GPP, RS, RR_C and RR_RF in 2021. Black, red, and blue points demote RS, RR_RF, and RR_C, respectively. Hollow points indicate GPP.

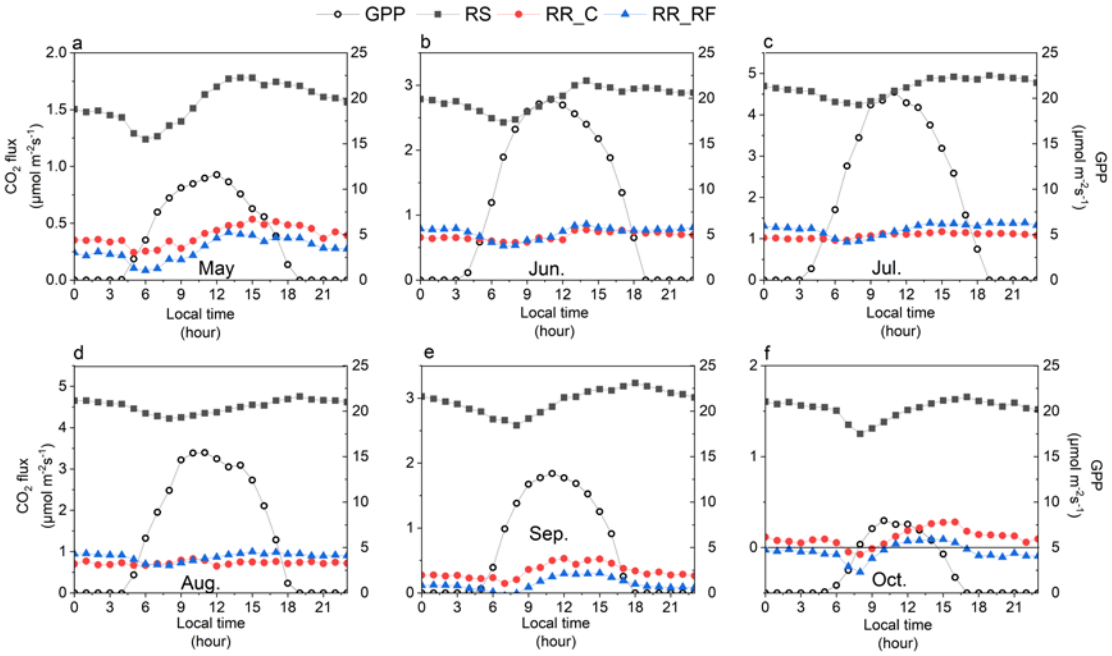

Figure 29. Diurnal trend of GPP, RS, RR_C and RR_RF in 2022. Black, red, and blue points demote RS, RR_RF, and RR_C, respectively. Hollow points indicate GPP.

3.6.2 Time lag estimated by CCF method

De-noised hourly GPP and two RRs, which were averaged from R3, R4, and R5 chambers, were used to calculate autocorrelation factors (ACF) (Figures 30-33), and the highest ACF in each month was shown in Table 12.

Objectively speaking, the fitting ability of the cross-correlation function (CCF) method was poor, with the highest ACF of only 0.52 (GPP over 2-hour lagged RR_C in September 2022, Table 15). Some unnatural results appeared, like the ACF of -0.16 for RR_RF in August 2021, indicating that GPP was five hours late after RR_RF (Table 15, Figure 32). It is unnatural for RR to precede GPP. Fitting of CCF was worse especially in July and August than in other months in 2021, and fitting in 2022 was generally worse than that in 2021; minus lags and negative ACFs commonly appeared for RR_RF (Table 15). Overall, however, lags between GPP and RR could be estimated to be approximately 3-5 hours using the ACF method, because the lags of 3, 4 and 5 hours had the highest ACF in common.

Table 15. Time lag with the highest ACF in each month

Month	Lag of GPP/RR_C [a] (hours)	ACF [b]	Lag of GPP/RR_RF [a] (hours)	ACF [b]
2021				
May	4	0.44	5	0.21
Jun	4	0.36	4	0.33
Jul	−12	0.13	5	0.19
Aug	8	0.08	−5	−0.16
Sep	2	0.30	4	0.22
Oct	4	0.46	6	0.28
2022				
May	5	0.37	4	0.26
Jun	−5	−0.16	−5	−0.25
Jul	4	0.21	6	0.32
Aug	3	0.10	−5	−0.29
Sep	2	0.52	2	0.22
Oct	4	0.43	−5	−0.26

[a] Lag was set to −12-12 hours. Minus lag indicates RR lead, while positive lag indicates GPP lead.

[b] ACF ranges from −1 (absolute negatively correlated) to 1 (absolute positively correlated). Absolute value of ACF reflects the correlation between GPP and lagged RR.

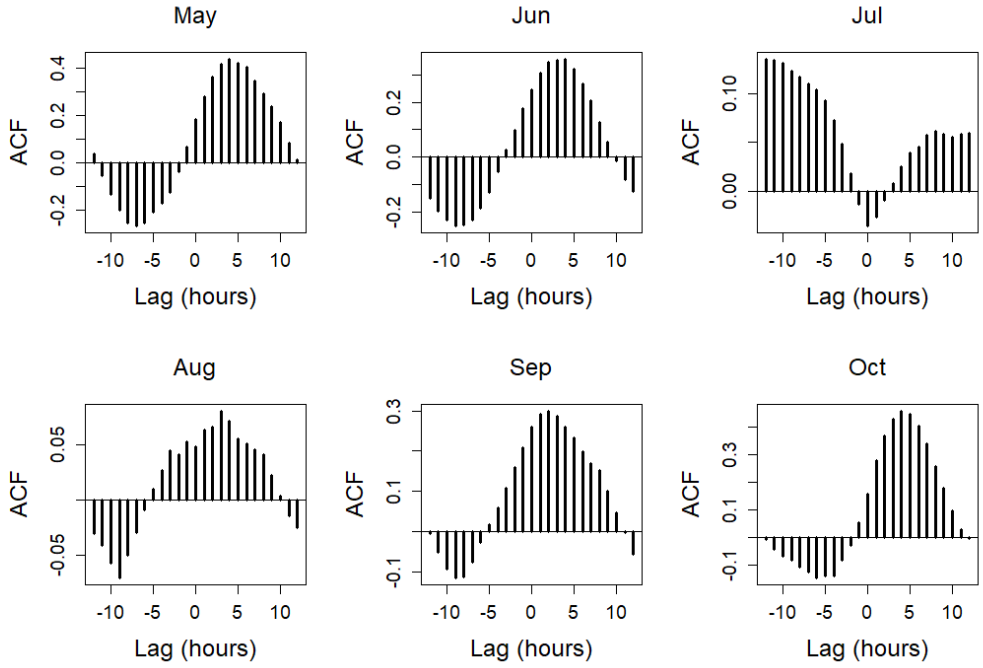

Figure 30. ACF of different lags between GPP and RR_C in each month in 2021. Positive and negative ACF indicate positive and negative correlations, respectively.

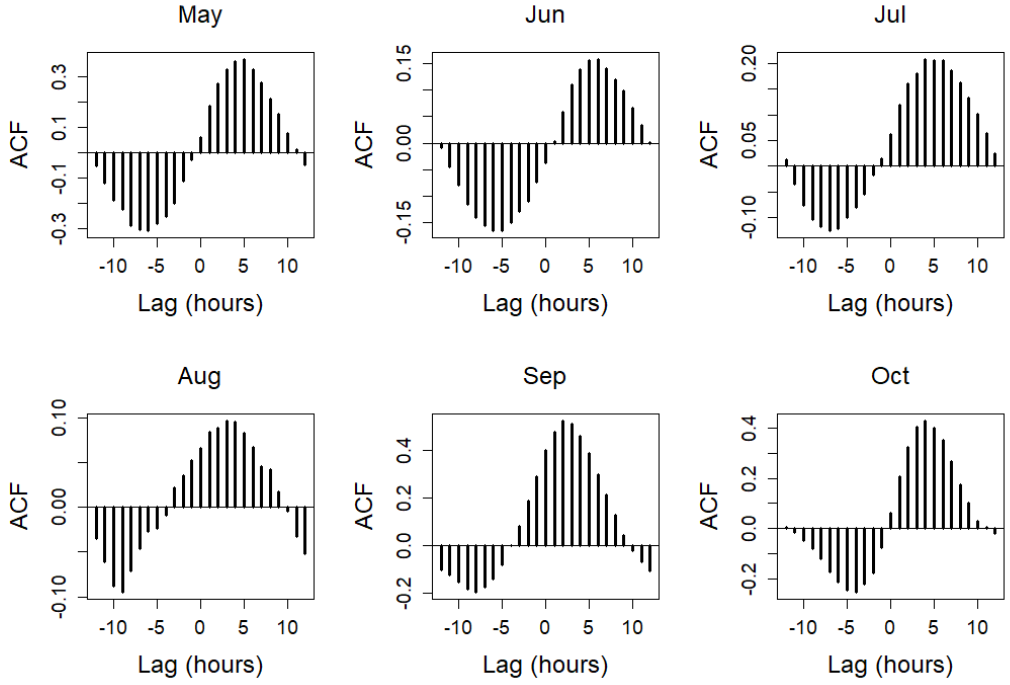

Figure 31. ACF of different lags between GPP and RR_C in each month in 2022. Positive and negative ACF indicate positive and negative correlations, respectively.

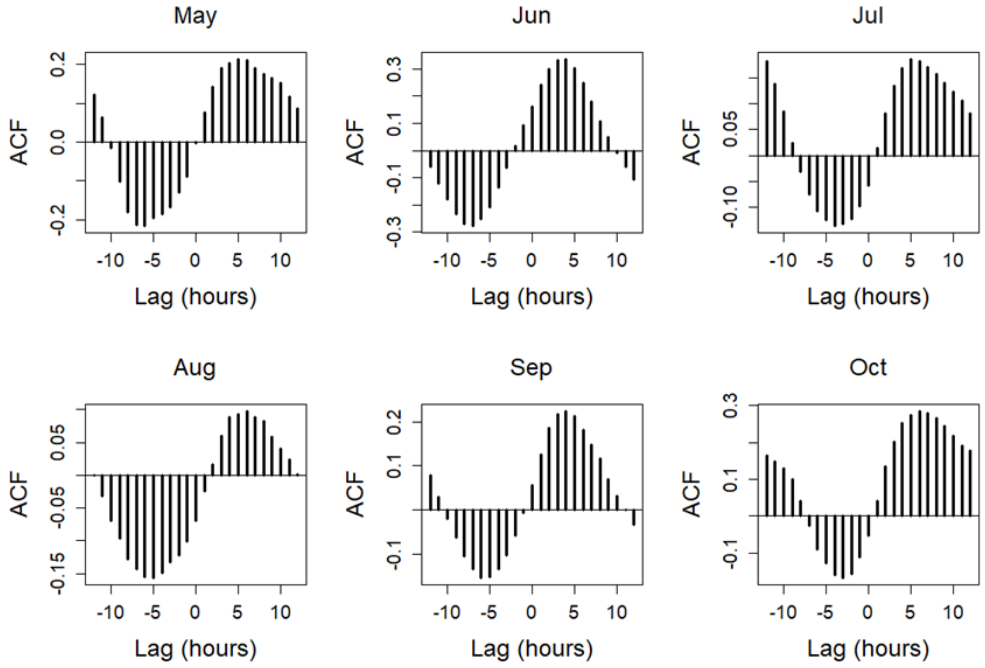

Figure 32. ACF of different lags between GPP and RR_RF in each month in 2021. Positive and negative ACF indicate positive and negative correlations, respectively.

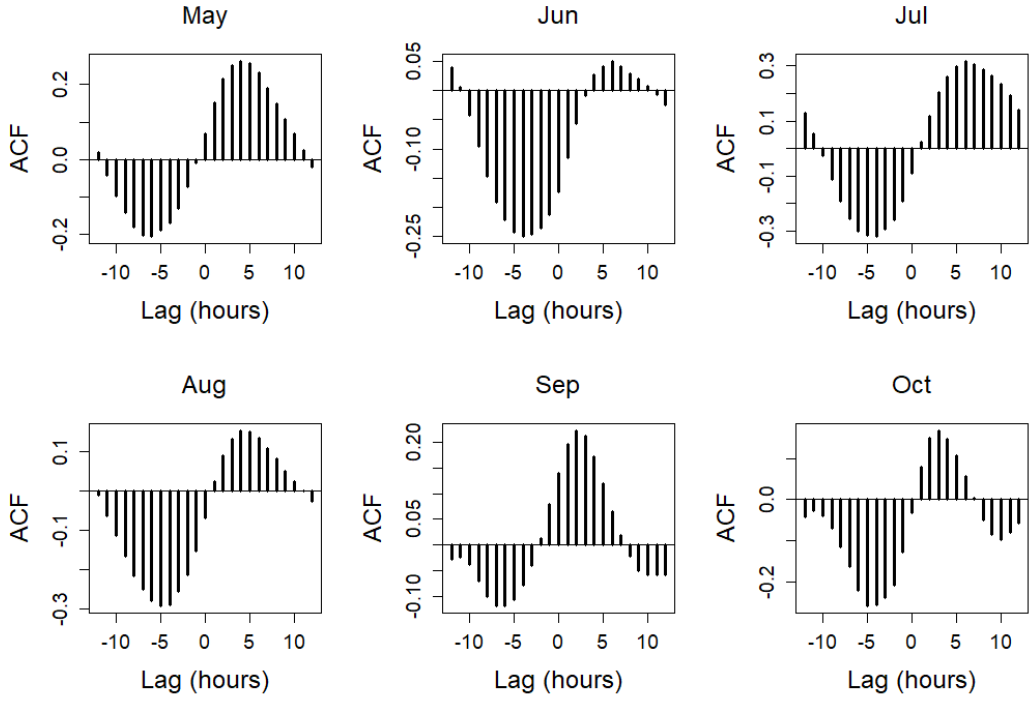

Figure 33. ACF of different lags between GPP and RR_RF in each month in 2022. Positive and negative ACF indicate positive and negative correlations, respectively.

3.6.3 Time lag estimated by wavelet phase difference method

Valid hourly instant lags with a significant wavelet cross power ($P < 0.05$) were extracted from the results of wavelet cross power analysis (3.5.3) in a one-day period and averaged daily to calculate daily means (Table 16, Figure 34). In theory, time lag between GPP and RR should be stable in a relative short-term time window if the ecosystem was not disturbed, which could be reflected in lags between GPP and RS, RR_RF in Table 16. Compared with RR_C, lags for RR_RF was relatively stable at around 5 hours in two years while lags for RS was around 6.5 hours. The lag for RR_C showed a significant annual variation ($P < 0.001$) with the seasonal means of 1.83 ± 5.85 hours in 2021 and 4.11 ± 4.10 hours in 2022; the interannual difference of 2.23 hours was much larger than that for RR_RF (0.42 hour) or RS (0.31 hour). In addition, lags were minus in July and August 2021 for RR_C, suggesting that the result for RR_C was unreliable (Figure 34 b). Significant seasonal variation appeared in lags between GPP and RR ($P < 0.05$, Table 16), but the seasonal variation was a bit inconsistent between two years; the shortest lag (3.59 ± 4.35 hours) appeared in June in 2021 for RR_RF, whereas it increased to 6.71 ± 4.41 hours, the second longest lag, in 2022 (Table 16). Compared with lags for RR_RF, that for RR_C was significantly shorter by 72.4% in 2022 even without minus lags. Significant seasonal variation appeared in lags of GPP/RS in 2021 ($P < 0.05$), but not showed in 2022 ($P > 0.05$, Table 16), indicating that time delay between GPP and soil respiration basically kept stable in two years (Figure 34 a). Significant seasonal variation ($P < 0.05$) of the lag of GPP/RR_RF suggests that lag between GPP and root respiration changed according to season changes, but insignificant interannual variation ($P > 0.05$) indicates the delay of root respiration to GPP kept stable in different years (Table 14).

Table 16. Lags extracted from one-day period with significant wavelet cross power (mean ± SD) [a]

Month	Lag of GPP/RS [b] (hours)	Lag of GPP/RR_C [b] (hours)	Lag of GPP/RR_RF [b] (hours)
2021			
May	5.65 ± 2.66	6.36 ± 2.55	5.28 ± 4.73
Jun	5.63 ± 1.98	3.06 ± 1.45	3.59 ± 4.35
Jul	7.05 ± 4.34	−5.55 ± 5.15	5.22 ± 6.08
Aug	7.05 ± 4.56	−0.95 ± 5.55	5.72 ± 5.79
Sep	7.16 ± 1.60	1.80 ± 5.21	4.55 ± 3.20
Oct	7.79 ± 1.10	6.42 ± 2.68	7.81 ± 1.76
Mean [c]	6.72 ± 3.10	1.83 ± 5.85	5.35 ± 4.71
P [d]	0.032	$< 2e^{-16}$	0.015
2022			
May	5.52 ± 1.73	5.57 ± 2.15	4.47 ± 4.32
Jun	6.75 ± 1.36	5.59 ± 3.14	6.71 ± 4.41
Jul	7.77 ± 1.44	4.53 ± 3.94	8.28 ±1.45
Aug	6.16 ± 6.46	1.83 ± 6.30	4.33 ± 6.16
Sep	7.23 ± 1.83	2.75 ± 1.62	4.45 ± 2.99
Oct	4.80 ± 6.83	4.06 ± 4.21	1.38 ± 4.38
Mean [c]	6.41 ± 4.06	4.11 ± 4.10	4.93 ± 4.69
P [d]	0.055	$< 2e^{-16}$	$< 2e^{-16}$
2-y Mean	6.56 ± 3.58	2.97 ± 5.00	5.12 ± 4.70
P [d]	0.413	$< 2e^{-16}$	0.459

[a] Significance level of wavelet cross power was set at 0.05 ($P < 0.05$).

[b] Daily lags were averaged from instant hourly lags.

[c] One-way ANOVA within the treatment ($n = 3$, Chambers R3, R4, and R5).

[d] *t*-test between mean daily lags of GPP/RS, GPP/RR_C and GPP/RR_RF in 2021 and 2022 (two-tailed).

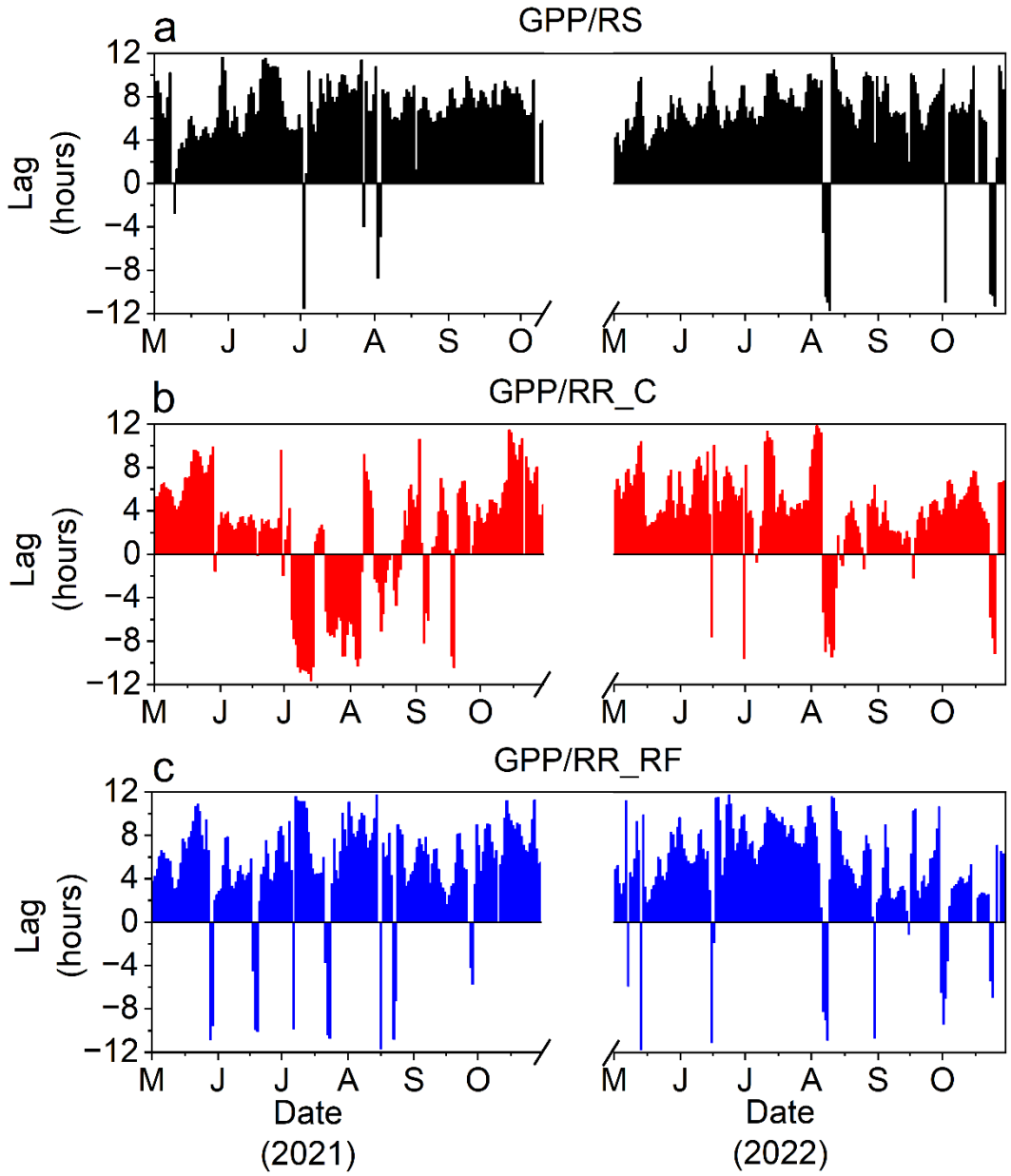

Figure 34. Mean daily lags of GPP/RS (a), GPP/RR_C (b) and GPP/RR_RF (c) in two years (from May 1st to October 31st). Mean daily lags were averaged from hourly instant phase differences with significant wavelet cross power ($P < 0.05$) and selected period was one day (24 hours).

3.7 Time lags estimated based on temperature-normalized RS and RR

To exclude the effect of soil temperature on correlation between GPP and RS, RR, hourly RS and RRs from chamber R3, R4 and R5 were normalized using Eq. (9), respectively, and then normalized RS and RRs were averaged to estimate time lags of GPP/RS, GPP/RR_C and GPP/RR_RF using wavelet cross power analysis and phase difference method (see 3.5 and 3.6). Since CCF method had a poor performance in estimating time lags between GPP and RR (see 3.6.2), normalized data would not be fitted using CCF method.

3.7.1 Diurnal trend of normalized RS, RR_C and RR_RF

After normalization, RS and RR almost lost diurnal trend. Only in May and October, normalized RS showed a typical diurnal trend, which corresponded to GPP roughly in each (Figures 35 a, 35 f and Figures 36 a, 36 f). Compared with normalized RR_RF, normalized RR_C had a more insignificant diurnal variation and showed a nearly flat trend at a daily scale (Figures 35 and 36). This result suggested that the diurnal trend of RS and RR might be mainly controlled by soil temperature.

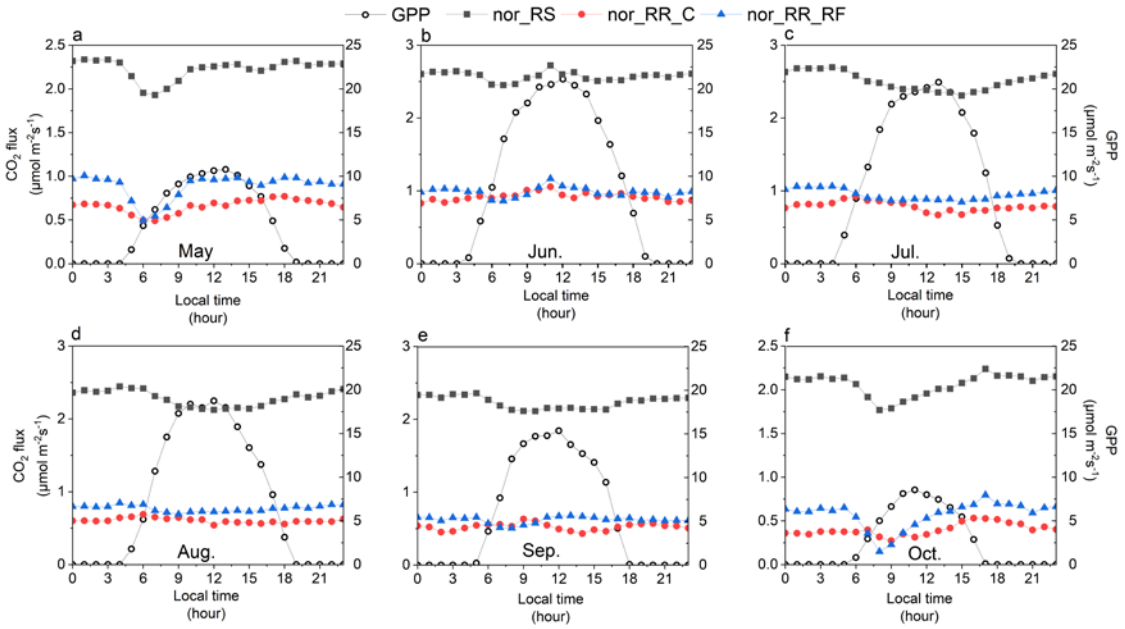

Figure 35. Diurnal trend of GPP, normalized RS, RR_C and RR_RF (at base soil temperature of 15 °C) in 2021. Black, red, and blue points demote normalized RS, RR_RF, and RR_C, respectively. Hollow points indicate GPP.

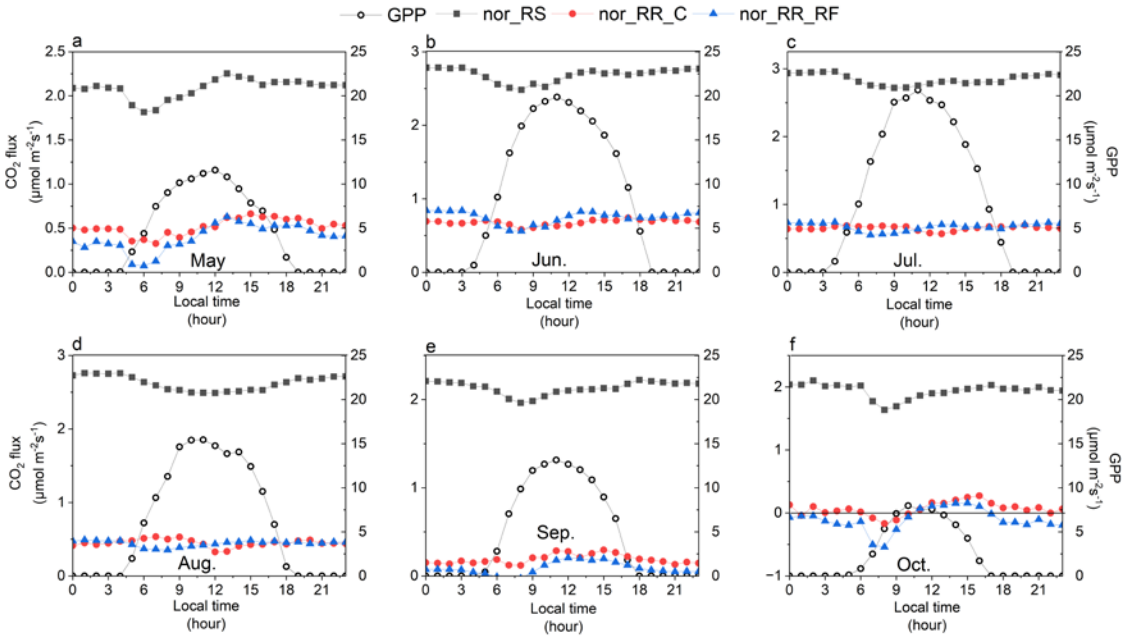

Figure 36. Diurnal trend of GPP, normalized RS, RR_C and RR_RF (at base soil temperature of 15 °C) in 2022. Black, red, and blue points demote normalized RS, RR_RF, and RR_C, respectively. Hollow points indicate GPP.

3.7.2 Time lags estimated based on soil temperature normalized data

Time lag between GPP and RS, RR calculated based on normalized data was shown in Table 17 and Figure 37. Compared with unnormalized data, lags of GPP/normalized RS and GPP/normalized RR_C showed more minus values from June to August in 2021, and July, August in 2022 (Table 17, Figure 37), which made the results unreliable. Lags between GPP and normalized RR_RF were slightly higher credibility, but minus values still commonly appeared in June, July and August in 2021 (Table 17). Both significant interannual variation between two years and seasonal variation within each year emerged in lags of GPP/RS, GPP/RR_C and GPP/RR_RF, which was unreasonable. This result also suggested that soil temperature was the main regulating factor even for root respiration in Tomakomai site because that time lag between GPP and root respiration (expected to keep stable) changed frequently at short-and-long-term scale when impacts from soil temperature were excluded.

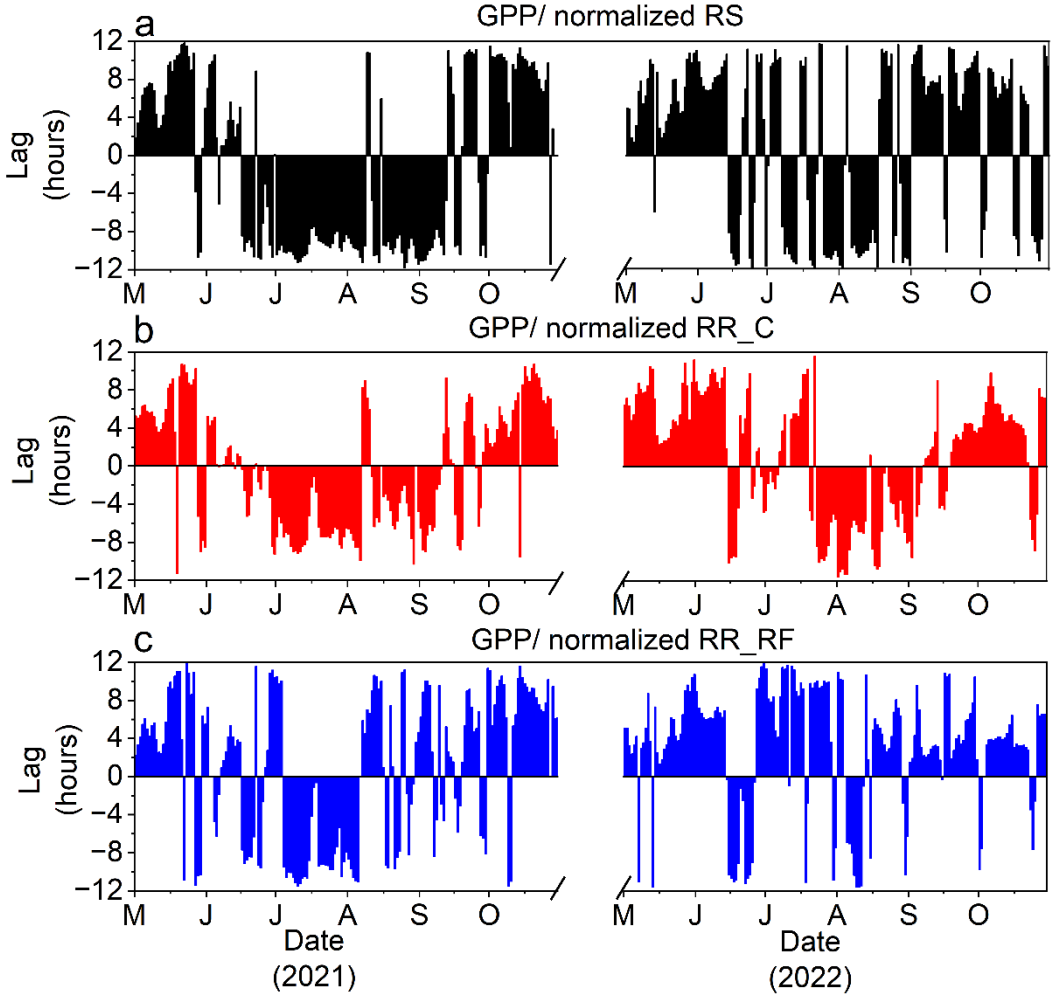

Figure 37. Mean daily lags of GPP/normalized RS (a), GPP/normalized RR_C (b) and GPP/normalized RR_RF (c) in two years (from May 1st to October 31st). Mean daily lags were averaged from hourly instant phase differences with significant wavelet cross power ($P < 0.05$) and selected period was one day (24 hours).

Table 17. Lags extracted from one-day period with significant wavelet cross power (mean ± SD) [a]

Month	Lag of GPP/normalized RS [b] (hours)	Lag of GPP/normalized RR_C [b] (hours)	Lag of GPP/normalized RR_RF [b] (hours)
2021			
May	5.80 ± 5.76	4.86 ± 5.67	4.25 ± 6.64
Jun	−1.33 ± 7.44	−0.50 ± 3.41	−0.13 ± 6.77
Jul	−9.33 ± 1.99	−7.05 ± 1.98	−6.37 ± 6.99
Aug	−7.88 ± 5.86	−3.87 ± 5.19	−0.30 ± 8.23
Sep	−3.17 ± 9.29	−1.62 ± 5.71	2.30 ± 6.09
Oct	7.87 ± 4.87	5.70 ± 3.87	7.07 ± 5.44
Mean [c]	−1.47 ± 8.91	−0.37 ± 6.37	1.15 ± 7.90
P [d]	$< 2e^{-16}$	$< 2e^{-16}$	$< 2e^{-16}$
2022			
May	5.72 ± 3.54	6.26 ± 2.52	3.93 ± 4.72
Jun	3.00 ± 8.66	3.76 ± 6.87	1.03 ± 8.28
Jul	−2.75 ± 9.68	−0.43 ± 6.65	7.23 ± 5.97
Aug	−4.18 ± 9.08	−6.44 ± 3.36	0.44 ± 7.63
Sep	7.00 ± 5.94	0.17 ± 4.46	4.35 ± 3.73
Oct	1.69 ± 8.39	4.00 ± 4.64	2.51 ± 4.33
Mean [c]	1.71 ± 8.76	1.21 ± 6.47	3.26 ± 5.35
P [d]	$< 2e^{-16}$	$< 2e^{-16}$	$< 2e^{-16}$
2-y Mean	0.13 ± 8.88	0.47 ± 6.38	2.66 ± 7.06
P [d]	0.001	0.019	0.005

[a] Significance level of wavelet cross power was set at 0.05 ($P < 0.05$).

[b] Daily lags were averaged from instant hourly lags.

[c] One-way ANOVA within the treatment (n = 3, Chambers R3, R4, and R5). RS, GPP/RR_C and GPP/RR_RF in 2021 and 2022 (two-tailed).

4. Discussion

4.1 Soil carbon flux

4.1.1 Seasonal variation of soil carbon flux

The soil CH_4 uptake rate and CO_2 emission rate showed clear seasonal variations according to the seasonality of WFPS and soil temperature, respectively (Figures 5, 6, 8, and 12), which are similar to previous studies (Mazzola et al., 2021; Sch¨afer et al., 2012; Sakabe et al., 2016; Lang et al., 2019; Goodrick I et al., 2016; Fang et al., 2010). The peak of CO_2 emission appeared at DOY of 220 in two years (early August, Figure 12) when soil temperature was high. This result agrees with and Lu et al. (2022), who reported that CO_2 emission rate increases in subsequent hot conditions. Different from CO_2 emission rate, CH_4 uptake rate showed no typical peaks in summer in 2022 (Figures 8 c and d), which was consistent with seasonal trend of WFPS in 2022 (Figure 6 c and d), emphasizing the important impact of soil moisture on CH_4 uptake (Sakabe et al., 2015). Higher mean daily precipitation in range of DOY 200-250 in 2022 led to a high soil moisture in this period (see 3.1.2), resulting in a lower CH_4 uptake rate.

4.1.2 Spatial variation of soil carbon flux

Significant spatial variation of the soil CH_4 uptake rate and CO_2 emission rate appeared both among chambers within each treatment and between two treatments (Table 8, 9, 11 and 12). Spatial variation between two treatments can be explained by the variation of soil properties. Higher porosity in Root chambers ensured a better soil aeration which allowed atmospheric CH_4 and O_2 to enter into the soil and faster CO_2 emission to the atmosphere, leading to the higher soil CH_4 uptake rate and CO_2 emission rate in Root chambers (Table 3). Higher soil moisture measured in Root chambers was expected to decrease the soil CH_4 uptake rate (Table 6). However, existence of fine roots might increase the absorption of soil inorganic N, leading to a decrease in soil inorganic nitrogen, decreasing the osmotic stress and toxic inhibition to methanotrophs, and then further increasing the methanotrophic gene abundance, thus leading to an increase in soil CH_4 uptake rates (Jing et al., 2021; Xiong et al., 2024). Nitrogen content

shown in Table 3 was the total N content, which showed no significant difference between two treatments, suggesting a need to separate total N content into organic and inorganic N content in the further study. Overall, the inhibiting effect on soil CH_4 uptake of high soil moisture in Root chambers was buffered by the promoting effect of the existence of fine roots.

Small-scale spatial variation (also known as “hot spot”) was mainly consistent with small-scale variation of soil physical properties (Stoyan et al., 2000; Jordan et al., 2009). For example, chambers T3 and R4 had the lowest bulk density (T3: 0.621 ± 0.119 kg m^{-3}, R4: 0.627 ± 0.060 kg m^{-3}) and the highest porosity (T3: 0.767 ± 0.045 m^3 m^{-3}, R4: 0.765 ± 0.028 m^3 m^{-3}) in each treatment, indicating these two chambers had the best diffusion condition, allowing a higher CH_4 uptake rate CO_2 emission rate (Table 2). Additionally, the canopy was also very important for explaining small-scale spatial variation of soil carbon dynamics (Penne et al., 2015). Chambers R4 and R5 were installed in a woody area with the high canopy (Figure 2), which led to the relative low soil temperature among five Root chambers because of shade cover from surrounding trees. However, high production in the woody area also increased root biomass in these two chambers, which helped increase root respiration in a direct way.

The automated chamber system provided a high-accuracy continuous measurement of soil carbon flux and the soil environment factors of temperature and moisture at a small scale, proving an outstanding advantage in explaining the “hot spot” phenomenon which was acknowledged as a difficult problem (Boudoire et al., 2018). Clear relationship between soil carbon dynamics and environmental variables would help to understand feedbacks and interactions between soils and the atmosphere, which is important for improving the accuracy of forecasting future global climate change.

4.1.3 Controls on soil carbon flux

In CH_4 models, two water-related factors, O_2 diffusion rate and WFPS had a similar high relative importance, suggesting that soil CH_4 uptake was mainly controlled by soil moisture (Figure 10). This result is also consistent with many previous studies

(Liu et al., 2019; Xiu-jun et al., 2000; Venturini et al,m 2022; Duan et al., 2022). Higher soil moisture decreases the soil air-filled porosity, resulting in low gas diffusion below the soil surface (Wu et al., 2010). Therefore, soil moisture has been widely reported as the main factor controlling CH_4 dynamics in forest soils (Shoemaker et al., 2014; Lohila et al., 2016; Lang et al., 2019). Ambient CH_4 concentration had a moderately high importance and positive influence in both treatments (higher than soil temperature but lower than soil moisture, physical properties and root dynamics, Figure 10), representing that the supply of atmospheric CH_4 to methanotrophs (Subke et al., 2018) was a relatively important factor (not a main limited factor) for soil CH_4 uptake in this study, which means soil in our site had not reached saturated as a CH_4 sink. Soil temperature is considered an important driver of CH_4 dynamics, mainly by stimulating microbial activities (Yvon-Durocher et al., 2014; Helbig et al., 2017). Specifically, soil temperature has promoting effects on both methanogens and methanotrophs within a temperature range, and methanogenesis seems to be more sensitive to changes in soil temperature (Koh et al., 2009). Therefore, the final effect of soil temperature on CH_4 flux can be explained as a balance of synergistic and antagonistic effects regulating other environmental factors in direct and indirect ways (Feng et al., 2020). In Trench chambers, soil temperature showed a positive effect on soil CH_4 uptake, while the effect of soil temperature was both positive and negative in Root chambers. These different results can be explained by the relatively simple environment of bare soil in Trench chambers. The activities of methane-oxidizing bacteria were accelerated by the increase of soil temperature with low soil moisture, which enhanced CH_4 uptake (Balser et al., 2010). However, promoting effect of increasing soil temperature on soil CH_4 uptake might be buffered by high soil moisture at a specific temperature range (10-15 °C, Figure 11 b). Within this temperature range, the positive effect on methanogens was stronger than that on methane-oxidizing bacteria, resulting a negative relationship between soil temperature and the CH_4 uptake rate in Root chambers. Overall, soil temperature had an enhancement on soil CH_4 uptake in Root chambers (Praeg et al., 2017; Benstead et al., 1997). Moreover, some studies also reported that rhizosphere

might compete with methanotrophs for diffused soil O_2 (Van et al., 2001; Lee et al., 2011; Chowdhury et al., 2013). Increased soil temperature promoted the growth of fine roots, which would lead to an increased activity of rhizosphere, causing a decrease of CH_4 oxidation efficiency.

In contrast with CH_4 models, soil temperature was the dominating factor (contributing for approximately 35% relative importance, Figure 14) in CO_2 models in both treatments, indicating that soil CO_2 emission was almost totally controlled by soil temperature. Compared with the complex physical and chemical processes involved in the soil-atmosphere CH_4 cycle, the soil CO_2 cycle mechanism is relatively simple. Increase in soil temperature speeds up the decomposition of SOM and the turnover rate of fine roots, corresponding to the increase of RH (Hartley et al., 2008; Paré et al., 2006; Karhu et al., 2010) and RR (Badraghi et al, 2021; Jian et al., 2022), respectively. However, the effects of soil moisture on soil CO_2 dynamics are more complicated. On one hand, increased soil moisture will decrease the diffusivity, which makes it difficult for CO_2 to be emitted to the atmosphere. Davidson et al. (2000) reported that RS declined significantly in saturated soils. On the other hand, soil microbial oxygen utilization efficiency might decrease significantly if the soil moisture decreased to a certain low level, resulting in the decrease of RS (Borken et al., 2006). In this study, WFPS showed no typical trends in regulating CO_2 flux, reflecting the complex relationship between soil moisture and soil CO_2 dynamics.

4.2 Machine learning models and wavelet analysis

4.2.1 Accuracy of RF and GBM models

In this study, the RF algorithm had higher accuracy than GBM models in both CH_4 and CO_2 flux prediction (Table 10 and 13), which is consistent with previous studies (Abbasian et al., 2022; Ghosh et al., 2021). These two algorithms are both based on decision tree models, but many differences exist in dataset re-sampling, tree construction and parallel computing (Bentéjac et al., 2021). Compared with GBM, the requirements for data quality of RF algorithm are relatively low, and even some outliers

can have a positive effect on the model regularization process, making RF algorithm widely used in flux estimation and data gap-filling in recent years (Irvin et al., 2021; Cui et al, 2021; Kim et al., 2020). For datasets with large standard deviations, like our dataset, the RF algorithm is very useful to decrease the estimation error. However, for datasets with small standard deviations but large bias, a boosting algorithm might be more suitable to effectively reduce prediction bias (Derbentsev et al., 2021; Das et al., 2022). Higher accuracy of Root models can be explained by the addition of two more important explanatory variables of fine root biomass and production. Performance of machine learning models is expected to increase with the increase of observations (Bui et al., 2020). Trench models had more observations than Root models, but performance of Trench models is worse than that of Root models, which indicates that increasing observations to improve prediction accuracy has reached a boundary effect. That is to say, using more explanatory variables (fine root dynamics used in Root models) would be more effective to increase model accuracy than introducing more observations into the model in this study (Chen et al., 2020).

Although RF and GBM modeling showed good performance, there are some potential limitations, including robustness, high requirement for data quantity (especially for GBM algorithm), data gap-filling, and dependence on feature selection. In this study, filling data gaps was avoided to maintain the original data pattern. As a result, four long-term data gaps (> a week) probably increased uncertainty in predicting the seasonal variation of soil carbon dynamics. In addition, ML approach is a kind of black box method with opacity in interpreting the fitted models (Orlenko and Moore, 2021). Although some useful tools, such as partial dependence plots, Shapley Additive exPlanations, feature contribution, have been developed to explain interactions between outcomes and variables, ML approach still has limitation to explain the dynamic variation of non-stationary data, especially time-series data (Kim et al., 2020; Hu et al., 2021; Greenwell, 2017; Kim and Kim, 2022).

4.2.2 Advantages and disadvantages of wavelet analysis

As a useful time-series data analysis tool, wavelet provides a detailed examination of both high-frequency and low-frequency signals in a given time series data, which is very important to capture the detailed changing trends of data at a short-term (diurnal) or long-term (seasonal) period (Maraun et al., 2004). In this study, CCF models showed poor performance with hourly data (Table 15, Figure 30-33). As a linear model, the performance of the CCF model greatly depends on the correlation between two time series data (Rehfeld et al., 2011). GPP data had a typical diurnal trend, but the daily variation of RS and RR data were not as significant as GPP, resulting in that the simple linear correlation method failed to explain the complex corresponding trend changes at a high time resolution. In contrast, the wavelet method decomposed seasonal-scale hourly datasets into a 24-hour period, which provided a relatively reliable periodic pattern to the seasonal dataset. Additionally, the wavelet cross power method, combining with the instant phase difference method, provided time lags between GPP and RR, which has a great potential to increase fitting accuracy in many models. Alternatively, R package “TSLSTM” provides a convenient Long Short-Term Memory modelling method, which has been widely acknowledged as a very accurate deep learning method in estimating time-series data. However, a very specific parameter “tsLag” is needed for this model training, which requires an accurate estimation for time lag between target time series data and variables (Paul et al., 2021).

Main disadvantages of wavelet analysis in this study can be concluded as follows (Sleziak et al., 2015; Guo et al., 2022),

1) Data Integrity: Wavelet analysis does not allow data gaps, indicating that all gaps must be filled before the analysis, which inevitably introduces errors and bias to the dataset. Especially for field measurement data, gaps are very common, which increases the uncertainty in models.
2) Selection of wavelet functions: Balance between the time resolution of raw dataset and wavelet period, time step, and the method for generating surrogate time series directly decide the fitting quality. After several attempts, a 24-hour period in a

monthly time scale window was selected in this study.

3) Detrending of raw data: Abnormal signals have significant impacts on data characteristics extraction in wavelet analysis. In this study, although GPP and RR data had been de-noised and standardized, few abnormal signals still made the result unreliable, especially in RR_C.

4.3 Root respiration

4.3.1 Separation of soil respiration

Root respiration mainly comes from root metabolism, which means it is very difficult to directly measure RR in the field for a long term. Thus, separating RS has become a common indirect method to estimate RR. Conventionally, spatially-mean RR is estimated as a difference between mean RS and mean RH measured by a trenching method. The conventional method has two disadvantages to separate RS in this study. Firstly, the conventional method used the mean CO_2 flux from five Trench chambers as a common RH of Root chambers, ignoring the spatial variation of RH. However, the small-scale spatial variation of soil properties had significant effects on soil carbon dynamics in high-time-resolution and small-spatial-scale studies (Comeau et al., 2018; Mei-Yee 2023). Secondly, the conventional method requires a high-accuracy measurement of soil CO_2 flux to avoid unreasonable minus RR appearing in R1 chamber. Unlike the conventional method, the RF modelling approach took the soil properties of each chamber into consideration to estimate RH in each Root chamber, resulting in a more reliable performance. Better fitting result with soil temperature and GPP proved the reliability of the RF modelling method, which suggests that the RF method is applicable to other study sites as a reliable method to estimate RR.

4.3.2 Relationship between GPP and root respiration

Ecosystem photosynthesis (GPP) has been widely reported to regulate RS in a short-term time scale of several hours (Tang et al., 2005, Riveros-Iregui et al., 2007, Davidson and Holbrook, 2009; Han et al., 2014), but few studies focused on the

relationship between GPP and RR. In general, RS lagged photosynthetic activity on hourly scales (Baldocchi et al., 2006; Bahn et al., 2008). In this study, time lag between GPP and RS was estimated to be 6.56 ± 3.58 hours (two-year mean daily lag, Table 16), which was consistent with previous studies (Liu et al., 2020). Short lags between GPP and RS can be explained by two reasons according to the previous studies. Firstly, there might be a fast transport of recent photosynthate from the canopy to the soil (Bahn et al., 2009; Vargas et al., 2011). High transport rates of assimilates from leaves into roots and their subsequent loss in the processes of root respiration have been demonstrated by previous laboratory experiments (Gregory and Atwell, 1991; Kuzyakov et al., 2010). Secondly, RR may dominate the total RS signal on a diurnal scale during the growing season (Vargas et al., 2011), which means diurnal trend of root respiration was the main reason for explaining the diurnal trend of soil respiration which matched the diurnal trend of GPP in growing seasons. Differently, RR in this study was lower than that of RH in our young generating forest (Figure 17) even in summer, which means RS in this forest was mainly affected by RH. However, strong cross power between GPP and RS appeared in July and August, corresponding to the strong cross power between GPP and RR_RF (Figures 25 and 27), indicating that the impact of RR on RS in summer was more significant than in other seasons.

In this study, time lag between GPP and RR estimated by a RF model (5.12 ± 4.70 hours, two-year mean daily lag, Table 16) was found from wavelet analysis, shorter than the lag between GPP and RS. In principle, autotrophic soil respiration is a direct consequence of RR, so it is coupled to rates of photosynthesis (Baldocchi et al., 2006). Meanwhile, the flux of recent photosynthate supports substantial microbial activity in the rhizosphere, which can in turn influence the relative fraction of RH (Cardon et al., 2002, Tang et al., 2005; Han et al., 2014). However, RR and RH had different sensitivity to tree canopy photosynthesis (Hopkins et al., 2013) because they respond to ecosystem productivity in different ways. As mentioned above, RS in this study was mainly affected by RH, which was more related to abiotic factors (Yu et al., 2015). As a whole, the response of RS to GPP might be slowed down by lower response rate of RH to GPP.

As a contrast, RR could respond to GPP in a direct and faster way.

Temperature-normalized data had a poor performance in estimating time lag between GPP and RS, RR, which could be explained by that: 1) Poor fitting accuracy of CO_2 flux to soil temperature. R^2 of RR to soil temperature was around 0.5 (Figure 18), which was hardly to be acknowledged as a precise fitting, leading to the normalization of RR was not accurate enough. 2) Some important hidden variables, like community structure and functions of soil microorganisms, were ignored in this study. When the key factor, soil temperature, was excluded but no other important explanatory variables were taken into consideration, poor estimation results based on temperature-normalized data could be understood.

5. Limitation, future plan and conclusions

5.1 Limitation and future research plan

Although some important innovations, like developing a reliable Random Forest modelling method to estimate heterotrophic respiration and separate soil respiration into root respiration and figuring out the relationship between ecosystem gross primary production and root respiration, some limitations still exist in this study. First, fitting accuracy of soil methane flux and environmental variables were relatively low, which indicates some important hidden explanatory variables were not used in the model (e.g. litter accumulation). Similarly, soil microorganism activities should also be taken into consideration for a more detailed and precise explanation for soil carbon dynamics. Second, prediction of heterotrophic respiration using random forest model was not accurate enough. Some abnormal minus values still appeared when soil respiration and root respiration were low in October. Third, lag between ecosystem productivity and soil dynamics should be viewed on a long-term scale, especially the interannual variation in a stable and undisturbed ecosystem. A certain degree of randomness might exist in the two-year observation data in this study.

According to the limitations mentioned above, future research plan can be concluded as follows:

1) Increasing quantity of explanatory variables in machine learning models. Variables like litter accumulation and soil microorganism activities should be taken into consideration. Also, more reliable fitting algorithms should be explored.

2) Adding regulation and error correction in prediction of heterotrophic respiration. In this study, heterotrophic respiration was mainly controlled by soil temperature, which was relatively high in October, leading to the overestimation of heterotrophic respiration and minus root respiration. If time could be considered as an explanatory variable, overestimation of heterotrophic respiration in the end of growing season could be corrected.

3) Maintaining the long-term observation of Tomakomai site for soil dynamics and ecosystem energy cycle. Also, a more accurate observation of fine root dynamics should

be considered. Root dynamics measured by soil core sampling method might not be enough to explain soil carbon dynamics.

5.2 Conclusion

Based on the automated chamber system measured soil carbon flux data and machine learning, wavelet analysis methods, soil carbon dynamics in Tomakomai site in 2021 and 2022 can be concluded as follows: firstly, soils in Tomakomai site functioned as a net CH_4 sink and a CO_2 source in 2021 and 2022, and soil CH_4 uptake rate and CO_2 emission rate had a typical spatiotemporal variation which can be explained by spatiotemporal variation of soil temperature and moisture. Secondly, main controlling factor for soil CH_4 uptake and CO_2 emission was soil moisture and temperature, respectively. Soil temperature had a positive effect on soil CH_4 uptake and CO_2 emission, while soil moisture had a negative effect on CH_4 uptake and a complicated both positive and negative impact on soil CO_2 emission. Existence of fine roots significantly improved soil CH_4 uptake and CO_2 emission. Thirdly, Random Forest modelling method had a higher accuracy in predicting CH_4 and CO_2 flux than GBM algorithm. Accuracy of Root models was higher than Trench models, with accuracy of CO_2 models were higher than that of CH_4 models. Fourthly, soil respiration was separated using conventional trenching method and RF modelling method. Conventional method tended to underestimate root respiration by 15.1%, and RR estimated by the conventional trenching method performed worse when fitted with soil temperature and gross primary production data than that by RF modelling method, indicating RF modelling method was a more reliable method to separate soil respiration. Fifthly, GPP and RS, RR data had a typical common diurnal period, indicating that GPP changed synchronously with soil respiration and root respiration. In addition, wavelet cross power of GPP/RR_RF was more significant and regulated than that of RR_C, emphasizing the credibility of RF modelling method in separating soil respiration. Last, linear CCF method had a poor performance in estimating time delay between GPP and RS, RR. As a contrast, phase difference method extracted time lag between GPP and

RS was around 6.5 hours (GPP lead), while lag between GPP and RR was approximate 5 hours (GPP lead, based on RR estimated by RF modelling method). RR estimated by conventional method had a poor performance in estimating time lags.

Acknowledgement

Doctoral life is fleeting, while I vaguely remember the first day I entered into the Lab of Ecological and Environmental Physics at December 2nd in 2021. Three years' study and research in Hokkaido University would be one of the most unforgettable experiences in my life. During these three years, I have experienced concerns about the unknown research fields, confusion about research directions, and distress of exploring complicated new research methods, making my doctoral course quite a struggling trip in my life. However, fortunately, my academic supervisor, Professor Hirano Takashi, helped me with great patience and warmth in study, research and getting myself, a foreigner student, used to the daily life in Japan. Here, I would like to send my deepest gratitude to Hirano sensei for his consistent and illuminating instruction, without which this thesis might be finished smoothly. At the same time, I also wish my dear sensei a good health and more achievements in academic research.

I am also grateful to Professor Toma Yo from Lab of Soil Science, School of Agriculture, Hokkaido University and Professor Kato Tomomichi from Lab of Terrestrial Ecosystem Modeling, Graduate School of GLOBAL FOOD RESOURCE, Hokkaido University for their useful advice and comments for this thesis.

I would also send my special thanks to Doctor Liang Naishen and Doctor Sun Lifei from National Institute for Environmental Studies, who guided me how to conduct field experiments of flux measurement using automated chamber system in Tomakomai site. Also, I would like to thank to Doctor Ookubo Shinjirou from Hokkaido Research Organization, who provided many useful advice about data processing and analysis to the study. Same gratitude also goes to Lecture Okada Keiji and Lecture Yamada Hiroyuki from School of Agriculture, Hokkaido University. They gave me practical suggestions in regular seminars of our lab.

Thanks also go to my dear lab members, they are Doctor Cui Rui (graduated in 2023), Miss Sakaguchi Kaho (graduated in 2023), Mr. Urano Kenta (M2), Mr. Iga Atsushi (M2), Miss Kambe Yui (M1), Mr. Suzuki Kouta (M1), Mr. Takagi Hiroshi, Mr. Miyazaki Ryota, and Mr. Ootsuki Naoya. In the past three years, reliable seniors and

juniors helped me a lot in studies, and also helped me to adapt to Japanese lifestyle. I would always remember your kindness and our friendship. Also, I would like to thank the staff of our lab, Ms. Sasaki Mami, who always helped me with a big smile.

My Ph.D Course was funded by Japanese Government Scholarship (MEXT) program. I am grateful to the Ministry of Education, Culture, Sports, Science and Technology, Japan. I sincerely thank them for giving me the financial support.

Last but not least, I would send thanks to my family members and friends. Thanks to my parents for bringing me up and supporting me to study abroad. Thanks to my sister for cheering me up when I was down and taking a good caring for parents when I was not at home. Thanks to Miss. Yang Mengfan and Mr. Ma Ruiqi for helping me in many ways in daily life.

Reference

Abbasian H, Solgi E, Hosseini S M, et al. Modeling terrestrial net ecosystem exchange using machine learning techniques based on flux tower measurements[J]. Ecological Modelling, 2022, 466: 109901.

Aguiar-Conraria L, Soares M J. The continuous wavelet transform: A primer[R]. NIPE-Universidade do Minho, 2011.

Ahirwal J, Kumari S, Singh A K, et al. Changes in soil properties and carbon fluxes following afforestation and agriculture in tropical forest[J]. Ecological indicators, 2021, 123: 107354.

Azam A, Akhtar M S, Rukh S, et al. Changes in soil organic carbon fractions across a loess toposequence[J]. Journal of Soil Science and Plant Nutrition, 2020, 20: 1193-1202.

Badraghi A, Ventura M, Polo A, et al. Soil respiration variation along an altitudinal gradient in the Italian Alps: Disentangling forest structure and temperature effects[J]. PLoS One, 2021, 16(8): e0247893.

Bahn M, Rodeghiero M, Anderson-Dunn M, et al. Soil respiration in European grasslands in relation to climate and assimilate supply[J]. Ecosystems, 2008, 11(8): 1352-1367.

Bahn M, Schmitt M, Siegwolf R, et al. Does photosynthesis affect grassland soil-respired CO_2 and its carbon isotope composition on a diurnal timescale? [J]. New phytologist, 2009, 182(2): 451-460.

Baldocchi D, Tang J, Xu L. How switches and lags in biophysical regulators affect spatial-temporal variation of soil respiration in an oak-grass savanna[J]. Journal of Geophysical Research: Biogeosciences, 2006, 111(G2).

Baldocchi D. ‘Breathing’of the terrestrial biosphere: lessons learned from a global network of carbon dioxide flux measurement systems[J]. Australian Journal of Botany, 2008, 56(1): 1-26.

Baldocchi D. Measuring fluxes of trace gases and energy between ecosystems and the atmosphere–the state and future of the eddy covariance method[J]. Global change

biology, 2014, 20(12): 3600-3609.

Balser T C, Gutknecht J L M, Liang C. How will climate change impact soil microbial communities? [J]. Soil microbiology and sustainable crop production, 2010: 373-397.

Basri M H A, McCalmont J, Kho L K, et al. Reducing bias on soil surface CO_2 flux emission measurements: Case study on a mature oil palm (Elaeis guineensis) plantation on tropical peatland in Southeast Asia[J]. Agricultural and Forest Meteorology, 2024, 350: 110002.

Benstead J, King G M. Response of methanotrophic activity in forest soil to methane availability[J]. FEMS Microbiology Ecology, 1997, 23(4): 333-340.

Bentéjac C, Csörgő A, Martínez-Muñoz G. A comparative analysis of gradient boosting algorithms[J]. Artificial Intelligence Review, 2021, 54: 1937-1967.

Beer Cetal. Terrestrial gross carbon dioxide uptake: global distribution and covariation with climate[J]. Science, 2010, 329:834–838

Boudoire G, Finizola A, Di Muro A, et al. Small-scale spatial variability of soil CO_2 flux: Implication for monitoring strategy[J]. Journal of Volcanology and Geothermal Research, 2018, 366: 13-26.

Breiman L. Random forests[J]. Machine learning, 2001, 45: 5-32.

Brevik E C. Soils and climate change: gas fluxes and soil processes[J]. Soil Horizons, 2012, 53(4): 12-23.

Borken W, Savage K, Davidson E A, et al. Effects of experimental drought on soil respiration and radiocarbon efflux from a temperate forest soil[J]. Global Change Biology, 2006, 12(2): 177-193.

Bui D T, Tsangaratos P, Nguyen V T, et al. Comparing the prediction performance of a Deep Learning Neural Network model with conventional machine learning models in landslide susceptibility assessment[J]. Catena, 2020, 188: 104426.

Burges C J C. From ranknet to lambdarank to lambdamart: An overview[J]. Learning, 2010, 11(23-581): 81.

Busman N A, Maie N, Ishak C F, et al. Effect of compaction on soil CO_2 and CH_4 fluxes

from tropical peatland in Sarawak, Malaysia[J]. Environment, Development and Sustainability, 2021, 23: 11646-11659.

Cai W, Wei R, Xu L, et al. A method for modelling greenhouse temperature using gradient boost decision tree[J]. Information Processing in Agriculture, 2022, 9(3): 343-354.

Campbell G S. Soil physics with BASIC: transport models for soil-plant systems[M]. Elsevier, 1985.

Cardon Z G, Czaja A D, Funk J L, et al. Periodic carbon flushing to roots of Quercus rubra saplings affects soil respiration and rhizosphere microbial biomass[J]. Oecologia, 2002, 133: 215-223.

Carmona R, Hwang W L, Torresani B. Practical Time-Frequency Analysis: Gabor and wavelet transforms, with an implementation in S[M]. Academic Press, 1998.

Castaldi S, Fierro A. Soil-atmosphere methane exchange in undisturbed and burned Mediterranean shrubland of southern Italy[J]. Ecosystems, 2005, 8: 182-190.

Cazelles B, Chavez M, Berteaux D, et al. Wavelet analysis of ecological time series[J]. Oecologia, 2008, 156: 287-304.

Cha G W, Moon H J, Kim Y C. Comparison of random forest and gradient boosting machine models for predicting demolition waste based on small datasets and categorical variables[J]. International Journal of Environmental Research and Public Health, 2021, 18(16): 8530.

Chen S, Wang W, Xu W, et al. Plant diversity enhances productivity and soil carbon storage[J]. Proceedings of the National Academy of Sciences, 2018, 115(16): 4027-4032.

Chen R C, Dewi C, Huang S W, et al. Selecting critical features for data classification based on machine learning methods[J]. Journal of Big Data, 2020, 7(1): 52.

Chowdhury T R, Dick R P. Ecology of aerobic methanotrophs in controlling methane fluxes from wetlands[J]. Applied soil ecology, 2013, 65: 8-22.

Comeau L P, Lai D Y F, Cui J J, et al. Separation of soil respiration: a site-specific comparison of partition methods[J]. Soil, 2018, 4(2): 141-152.

Cui X, Goff T, Cui S, et al. Predicting carbon and water vapor fluxes using machine learning and novel feature ranking algorithms[J]. Science of the Total Environment, 2021, 775: 145130.

Currie J A. Gaseous diffusion in porous media Part 1.-A non-steady state method[J]. British Journal of Applied Physics, 1960, 11(8): 314.

Das A, Purakayastha T J, Ahmed N, et al. Influence of clay mineralogy on soil organic carbon stabilization under tropical climate, India[J]. Journal of Soil Science and Plant Nutrition, 2023, 23(1): 1003-1018.

Das B, Rathore P, Roy D, et al. Comparison of bagging, boosting and stacking algorithms for surface soil moisture mapping using optical-thermal-microwave remote sensing synergies[J]. Catena, 2022, 217: 106485.

Davidson E A, Janssens I A. Temperature sensitivity of soil carbon decomposition and feedbacks to climate change[J]. Nature, 2006, 440(7081): 165-173.

Davidson E A, Verchot L V, Cattânio J H, et al. Effects of soil water content on soil respiration in forests and cattle pastures of eastern Amazonia[J]. Biogeochemistry, 2000, 48: 53-69.

Davidson E A, Holbrook N M. Is temporal variation of soil respiration linked to the phenology of photosynthesis? [J]. Phenology of Ecosystem Processes: Applications in Global Change Research, 2009: 187-199.

Derbentsev V, Babenko V, Khrustalev K, et al. Comparative performance of machine learning ensemble algorithms for forecasting cryptocurrency prices[J]. International Journal of Engineering, 2021, 34(1): 140-148.

Díaz-Hernández J L. Is soil carbon storage underestimated? [J]. Chemosphere, 2010, 80(3): 346-349.

Drigo B, Kowalchuk G A, Van Veen J A. Climate change goes underground: effects of elevated atmospheric CO_2 on microbial community structure and activities in the rhizosphere[J]. Biology and Fertility of Soils, 2008, 44: 667-679.

Duan B, Cai T, Man X, et al. Different variations in soil CO_2, CH_4, and N_2O fluxes and their responses to edaphic factors along a boreal secondary forest successional

trajectory[J]. Science of The Total Environment, 2022, 838: 155983.

Dusenge M E, Duarte A G, Way D A. Plant carbon metabolism and climate change: elevated CO_2 and temperature impacts on photosynthesis, photorespiration and respiration[J]. New Phytologist, 2019, 221(1): 32-49.

Eviner V T, Chapin III F S. Functional matrix: a conceptual framework for predicting multiple plant effects on ecosystem processes[J]. Annual Review of Ecology, Evolution, and Systematics, 2003, 34(1): 455-485.

Fang C, Moncrieff J B. The dependence of soil CO_2 efflux on temperature[J]. Soil Biology and Biochemistry, 2001, 33(2): 155-165.

Fang H J, Yu G R, Cheng S L, et al. Effects of multiple environmental factors on CO_2 emission and CH_4 uptake from old-growth forest soils[J]. Biogeosciences, 2010, 7(1): 395-407.

Feizienė D, Feiza V, Vaidelienė A, et al. Soil surface carbon dioxide exchange rate as affected by soil texture, different long-term tillage application and weather[J]. 2010.

Feng H, Guo J, Han M, et al. A review of the mechanisms and controlling factors of methane dynamics in forest ecosystems[J]. Forest Ecology and Management, 2020, 455: 117702.

Ganot Y, Dragila M I, Weisbrod N. Impact of thermal convection on CO_2 flux across the earth–atmosphere boundary in high-permeability soils[J]. Agricultural and Forest Meteorology, 2014, 184: 12-24.

Gatti L V, Basso L S, Miller J B, et al. Amazonia as a carbon source linked to deforestation and climate change[J]. Nature, 2021, 595(7867): 388-393.

Gessler A, Zweifel R. Beyond source and sink control–toward an integrated approach to understand the carbon balance in plants[J]. New Phytologist, 2024.

Ghosh S M, Behera M D, Jagadish B, et al. A novel approach for estimation of aboveground biomass of a carbon-rich mangrove site in India[J]. Journal of Environmental Management, 2021, 292: 112816.

Golden C E, Rothrock Jr M J, Mishra A. Comparison between random forest and

gradient boosting machine methods for predicting Listeria spp. prevalence in the environment of pastured poultry farms[J]. Food research international, 2019, 122: 47-55.

Greenwell B M. pdp: An R package for constructing partial dependence plots[J]. R J., 2017, 9(1): 421.

Gregory P J, Atwell B J. The fate of carbon in pulse-labelled crops of barley and wheat[J]. Plant and Soil, 1991, 136: 205-213.

Grinsted A, Moore J C, Jevrejeva S. Application of the cross wavelet transform and wavelet coherence to geophysical time series[J]. Nonlinear processes in geophysics, 2004, 11(5/6): 561-566.

Goodrick I, Connor S, Bird M I, et al. Emission of CO_2 from tropical riparian forest soil is controlled by soil temperature, soil water content and depth to water table[J]. Soil Research, 2016, 54(3): 311-320.

Guo T, Zhang T, Lim E, et al. A review of wavelet analysis and its applications: Challenges and opportunities[J]. IEEE Access, 2022, 10: 58869-58903.

Hamrani A, Akbarzadeh A, Madramootoo C A. Machine learning for predicting greenhouse gas emissions from agricultural soils[J]. Science of The Total Environment, 2020, 741: 140338.

Han G, Luo Y, Li D, et al. Ecosystem photosynthesis regulates soil respiration on a diurnal scale with a short-term time lag in a coastal wetland[J]. Soil Biology and Biochemistry, 2014, 68: 85-94.

Hartley I P, Ineson P. Substrate quality and the temperature sensitivity of soil organic matter decomposition[J]. Soil Biology and Biochemistry, 2008, 40(7): 1567-1574.

Helbig M, Quinton W L, Sonnentag O. Warmer spring conditions increase annual methane emissions from a boreal peat landscape with sporadic permafrost[J]. Environmental Research Letters, 2017, 12(11): 115009.

Hiederer R, Köchy M. Global soil organic carbon estimates and the harmonized world soil database[J]. EUR, 2011, 79(25225): 10.2788.

Hirano T, Suzuki K, Hirata R. Energy balance and evapotranspiration changes in a larch

forest caused by severe disturbance during an early secondary succession[J]. Agricultural and forest meteorology, 2017, 232: 457-468.

Hirano T, Ohkubo S, Itoh M, et al. Large variation in carbon dioxide emissions from tropical peat swamp forests due to disturbances[J]. Communications Earth & Environment, 2024, 5(1): 221.

Hirano T, Kim H, Tanaka Y. Long-term half-hourly measurement of soil CO_2 concentration and soil respiration in a temperate deciduous forest[J]. Journal of Geophysical Research: Atmospheres, 2003, 108(D20).

Hopkins F, Gonzalez-Meler M A, Flower C E, et al. Ecosystem-level controls on root-rhizosphere respiration[J]. New Phytologist, 2013, 199(2): 339-351.

Hu S, Li Y, Chang S X, et al. Soil autotrophic and heterotrophic respiration respond differently to land-use change and variations in environmental factors[J]. Agricultural and Forest Meteorology, 2018, 250: 290-298.

Hu W H, Rea C, Yuan Q P, et al. Real-time prediction of high-density EAST disruptions using random forest[J]. Nuclear Fusion, 2021, 61(6): 066034.

Iqbal J, Ronggui H, Lijun D, et al. Differences in soil CO_2 flux between different land use types in mid-subtropical China[J]. Soil biology and biochemistry, 2008, 40(9): 2324-2333.

Irvin J, Zhou S, McNicol G, et al. Gap-filling eddy covariance methane fluxes: Comparison of machine learning model predictions and uncertainties at FLUXNET-CH_4 wetlands[J]. Agricultural and Forest Meteorology, 2021, 308: 108528.

Jandl R, Lindner M, Vesterdal L, et al. How strongly can forest management influence soil carbon sequestration? [J]. Geoderma, 2007, 137(3-4): 253-268.

Janzen H H. The soil carbon dilemma: shall we hoard it or use it? [J]. Soil Biology and Biochemistry, 2006, 38(3): 419-424.

Jhariya M K, Banerjee A, Meena R S, et al. Agriculture, Forestry and Environmental Sustainability: a way forward[J]. Sustainable agriculture, forest and environmental management, 2019: 1-29.

Jian J, Frissell M, Hao D, et al. The global contribution of roots to total soil respiration[J]. Global Ecology and Biogeography, 2022, 31(4): 685-699.

Jing H, Liu Y, Wang G, et al. Contrasting effects of nitrogen addition on rhizosphere soil CO2, N2O, and CH4 emissions of fine roots with different diameters from Pinus tabulaeformis forest using laboratory incubation[J]. Science of The Total Environment, 2021, 780: 146298.

Jordan A, Jurasinski G, Glatzel S. Small scale spatial heterogeneity of soil respiration in an old growth temperate deciduous forest[J]. Biogeosciences Discussions, 2009, 6(5): 9977-10005.

Karhu K, Fritze H, Hämäläinen K, et al. Temperature sensitivity of soil carbon fractions in boreal forest soil[J]. Ecology, 2010, 91(2): 370-376.

Kang M, Cho S. Progress in water and energy flux studies in Asia: A review focused on eddy covariance measurements[J]. Journal of Agricultural Meteorology, 2021, 77(1): 2-23.

Kim H. A Study on CO_2 Emissions from Leaf Litter Accumulation in Deciduous Forests. Hokkaido University, School of Agriculture, Doctoral thesis, 2005. (in Japanese)

Kim Y, Johnson M S, Knox S H, et al. Gap-filling approaches for eddy covariance methane fluxes: A comparison of three machine learning algorithms and a traditional method with principal component analysis[J]. Global Change Biology, 2020, 26(3): 1499-1518.

Kim Y, Kim Y. Explainable heat-related mortality with random forest and SHapley Additive exPlanations (SHAP) models[J]. Sustainable Cities and Society, 2022, 79: 103677.

Kluber L A, Johnston E R, Allen S A, et al. Constraints on microbial communities, decomposition and methane production in deep peat deposits[J]. PLoS One, 2020, 15(2): e0223744.

Koh H S, Ochs C A, Yu K. Hydrologic gradient and vegetation controls on CH_4 and CO_2 fluxes in a spring-fed forested wetland[J]. Hydrobiologia, 2009, 630: 271-286.

Kondo M, Ichii K, Patra P K, et al. Plant regrowth as a driver of recent enhancement of terrestrial CO_2 uptake[J]. Geophysical Research Letters, 2018, 45(10): 4820-4830.

Koulelis P P, Proutsos N, Solomou A D, et al. Effects of climate change on greek forests: A review[J]. Atmosphere, 2023, 14(7): 1155.

Kuzyakov Y, Gavrichkova O. Time lag between photosynthesis and carbon dioxide efflux from soil: a review of mechanisms and controls[J]. Global Change Biology, 2010, 16(12): 3386-3406.

Lang R, Goldberg S, Blagodatsky S, et al. Converting forests into rubber plantations weakened the soil CH_4 sink in tropical uplands[J]. Land degradation & development, 2019, 30(18): 2311-2322.

Latte N, Colinet G, Fayolle A, et al. Description of a new procedure to estimate the carbon stocks of all forest pools and impact assessment of methodological choices on the estimates[J]. European Journal of Forest Research, 2013, 132: 565-577.

Law B E, Ryan M G, Anthoni P M. Seasonal and annual respiration of a ponderosa pine ecosystem[J]. Global Change Biology, 1999, 5(2): 169-182.

Launiainen S, Katul G G, Leppä K, et al. Does growing atmospheric CO_2 explain increasing carbon sink in a boreal coniferous forest? [J]. Global Change Biology, 2022, 28(9): 2910-2929.

Lee J, Oh Y, Lee S T, et al. Soil organic carbon is a key determinant of CH_4 sink in global forest soils[J]. Nature communications, 2023, 14(1): 3110.

Lee S Y, Lee S H, Jang J K, et al. Comparison of methanotrophic community and methane oxidation between rhizospheric and non-rhizospheric soils[J]. Geomicrobiology Journal, 2011, 28(8): 676-685.

Li Y, Li Y, Chang S X, et al. Biochar reduces soil heterotrophic respiration in a subtropical plantation through increasing soil organic carbon recalcitrancy and decreasing carbon-degrading microbial activity[J]. Soil Biology and Biochemistry, 2018, 122: 173-185.

Liang N, Hirano T, Zheng Z M, et al. Soil CO_2 efflux of a larch forest in northern Japan[J]. Biogeosciences, 2010, 7(11): 3447-3457.

Liang N, Teramoto M, Takagi M, et al. High-resolution data on the impact of warming on soil CO_2 efflux from an Asian monsoon forest[J]. Scientific Data, 2017, 4(1): 1-11.

Liang N, Nakadai T, Hirano T, et al. In situ comparison of four approaches to estimating soil CO_2 efflux in a northern larch (*Larix kaempferi Sarg.*) forest[J]. Agricultural and Forest Meteorology, 2004, 123(1-2): 97-117.

Liang N, Inoue G, Fujinuma Y. A multichannel automated chamber system for continuous measurement of forest soil CO_2 efflux[J]. Tree physiology, 2003, 23(12): 825-832.

Lindgren A. The effect of natural disturbances on the carbon balance of boreal forests[J]. Lunds universitets Naturgeografiska institution-Seminarieuppsatser, 2011.

Liu L, Estiarte M, Peñuelas J. Soil moisture as the key factor of atmospheric CH_4 uptake in forest soils under environmental change[J]. Geoderma, 2019, 355: 113920.

Liu X, Liang J, Gu L. Photosynthetic and environmental regulations of the dynamics of soil respiration in a forest ecosystem revealed by analyses of decadal time series[J]. Agricultural and Forest Meteorology, 2020, 282: 107863.

Lohila A, Aalto T, Aurela M, et al. Large contribution of boreal upland forest soils to a catchment-scale CH4 balance in a wet year[J]. Geophysical Research Letters, 2016, 43(6): 2946-2953.

Lu B, Song L, Zang S, et al. Warming promotes soil CO_2 and CH_4 emissions but decreasing moisture inhibits CH4 emissions in the permafrost peatland of the Great Xing'an Mountains[J]. Science of The Total Environment, 2022, 829: 154725.

Ludwig S M, Natali S M, Mann P J, et al. Using machine learning to predict inland aquatic CO_2 and CH_4 concentrations and the effects of wildfires in the Yukon-Kuskokwim Delta, Alaska[J]. Global Biogeochemical Cycles, 2022, 36(4): e2021GB007146.

Malhi Y, Meir P, Brown S. Forests, carbon and global climate[J]. Philosophical Transactions of the Royal Society of London. Series A: Mathematical, Physical

and Engineering Sciences, 2002, 360(1797): 1567-1591.

Mayer M, Prescott C E, Abaker W E A, et al. Tamm Review: Influence of forest management activities on soil organic carbon stocks: A knowledge synthesis[J]. Forest Ecology and Management, 2020, 466: 118127.

McCandless T, Gagne D J, Kosović B, et al. Machine learning for improving surface-layer-flux estimates[J]. Boundary-Layer Meteorology, 2022, 185(2): 199-228.

Mei-Yee C, Lau S Y L, Midot F, et al. Root exclusion methods for partitioning of soil respiration: Review and methodological considerations[J]. Pedosphere, 2023, 33(5): 683-699.

Mikan C J, Schimel J P, Doyle A P. Temperature controls of microbial respiration in arctic tundra soils above and below freezing[J]. Soil biology and biochemistry, 2002, 34(11): 1785-1795.

Mazzola V, Perks M P, Smith J, et al. Seasonal patterns of greenhouse gas emissions from a forest-to-bog restored site in northern Scotland: Influence of microtopography and vegetation on carbon dioxide and methane dynamics[J]. European Journal of Soil Science, 2021, 72(3): 1332-1353.

Maraun D, Kurths J. Cross wavelet analysis: significance testing and pitfalls[J]. Nonlinear Processes in Geophysics, 2004, 11(4): 505-514.

Mukul S A, Halim M A, Herbohn J. Forest carbon stock and fluxes: Distribution, biogeochemical cycles, and measurement techniques[J]. Life on land, encyclopedia of the UN sustainable development goals, 2021: 365-380.

Nave L E, Vance E D, Swanston C W, et al. Harvest impacts on soil carbon storage in temperate forests[J]. Forest ecology and management, 2010, 259(5): 857-866.

Noormets A, Epron D, Domec J C, et al. Effects of forest management on productivity and carbon sequestration: A review and hypothesis[J]. Forest Ecology and Management, 2015, 355: 124-140.

Orlenko A, Moore J H. A comparison of methods for interpreting random forest models of genetic association in the presence of non-additive interactions[J]. BioData mining, 2021, 14: 1-17.

Paul R K, Garai S. Performance comparison of wavelets-based machine learning technique for forecasting agricultural commodity prices[J]. Soft Computing, 2021, 25(20): 12857-12873.

Pan Y, Birdsey R A, Phillips O L, et al. The structure, distribution, and biomass of the world's forests[J]. Annual Review of Ecology, Evolution, and Systematics, 2013, 44: 593-622.

Paré D, Boutin R, Larocque G R, et al. Effect of temperature on soil organic matter decomposition in three forest biomes of eastern Canada[J]. Canadian Journal of Soil Science, 2006, 86(Special Issue): 247-256.

Payn T, Carnus J M, Freer-Smith P, et al. Changes in planted forests and future global implications[J]. Forest Ecology and Management, 2015, 352: 57-67.

Phillips C L, Bond-Lamberty B, Desai A R, et al. The value of soil respiration measurements for interpreting and modeling terrestrial carbon cycling[J]. Plant and Soil, 2017, 413: 1-25.

Penne C, Ahrends B, Deurer M, et al. The impact of the canopy structure on the spatial variability in forest floor carbon stocks[J]. Geoderma, 2010, 158(3-4): 282-297.

Praeg N, Wagner A O, Illmer P. Plant species, temperature, and bedrock affect net methane flux out of grassland and forest soils[J]. Plant and Soil, 2017, 410: 193-206.

Pritchard S G. Soil organisms and global climate change[J]. Plant Pathology, 2011, 60(1): 82-99.

Ramesh T, Bolan N S, Kirkham M B, et al. Soil organic carbon dynamics: Impact of land use changes and management practices: A review[J]. Advances in agronomy, 2019, 156: 1-107.

Reay D S, Radajewski S, Murrell J C, et al. Effects of land-use on the activity and diversity of methane oxidizing bacteria in forest soils[J]. Soil Biology and Biochemistry, 2001, 33(12-13): 1613-1623.

Rehfeld K, Marwan N, Heitzig J, et al. Comparison of correlation analysis techniques for irregularly sampled time series[J]. Nonlinear Processes in Geophysics, 2011,

18(3): 389-404.

Remy E, Gasche R, Kiese R, et al. Edge effects on N_2O, NO and CH_4 fluxes in two temperate forests[J]. Science of the total environment, 2017, 575: 1150-1155.

Riveros-Iregui D A, Emanuel R E, Muth D J, et al. Diurnal hysteresis between soil CO_2 and soil temperature is controlled by soil water content[J]. Geophysical Research Letters, 2007, 34(17).

Sakabe, Ayaka, et al. "One year of continuous measurements of soil CH_4 and CO_2 fluxes in a Japanese cypress forest: Temporal and spatial variations associated with Asian monsoon rainfall." Journal of Geophysical Research: Biogeosciences 120.4, 2015: 585-599.

Sakabe A, Kosugi Y, Okumi C, et al. Impacts of riparian wetlands on the seasonal variations of watershed-scale methane budget in a temperate monsoonal forest[J]. Journal of Geophysical Research: Biogeosciences, 2016, 121(7): 1717-1732.

Sakaguchi Kaho. 機械学習による土壌呼吸の分離に関する研究[D]. Hokkaido University, School of Agriculture, Master's thesis, 2023. (in Japanese)

Sano T, Hirano T, Liang N, et al. Carbon dioxide exchange of a larch forest after a typhoon disturbance[J]. Forest Ecology and Management, 2010, 260(12): 2214-2223.

Savage K, Davidson E A, Tang J. Diel patterns of autotrophic and heterotrophic respiration among phenological stages[J]. Global Change Biology, 2013, 19(4): 1151-1159.

Schaufler G, Kitzler B, Schindlbacher A, et al. Greenhouse gas emissions from European soils under different land use: effects of soil moisture and temperature[J]. European Journal of Soil Science, 2010, 61(5): 683-696.

Schäfer C M, Elsgaard L, Hoffmann C C, et al. Seasonal methane dynamics in three temperate grasslands on peat[J]. Plant and soil, 2012, 357: 339-353.

Sha L, Teramoto M, Noh N J, et al. Soil carbon flux research in the Asian region: Review and future perspectives[J]. Journal of Agricultural Meteorology, 2021, 77(1): 24-51.

Shen C. Analysis of detrended time-lagged cross-correlation between two nonstationary time series[J]. Physics Letters A, 2015, 379(7): 680-687.

Shoemaker J K, Keenan T F, Hollinger D Y, et al. Forest ecosystem changes from annual methane source to sink depending on late summer water balance[J]. Geophysical Research Letters, 2014, 41(2): 673-679.

Sleziak P, Hlavčová K, Szolgay J. Advantages of a time series analysis using wavelet transform as compared with a fourier analysis[J]. Slovak Journal of Civil Engineering, 2015, 23(2): 30-36.

Smith P, Soussana J F, Angers D, et al. How to measure, report and verify soil carbon change to realize the potential of soil carbon sequestration for atmospheric greenhouse gas removal[J]. Global Change Biology, 2020, 26(1): 219-241.

Stoyan H, De-Polli H, Böhm S, et al. Spatial heterogeneity of soil respiration and related properties at the plant scale[J]. Plant and soil, 2000, 222(1): 203-214.

Stuart Chapin III F, McFarland J, David McGuire A, et al. The changing global carbon cycle: linking plant–soil carbon dynamics to global consequences[J]. Journal of Ecology, 2009, 97(5): 840-850.

Subke J A, Moody C S, Hill T C, et al. Rhizosphere activity and atmospheric methane concentrations drive variations of methane fluxes in a temperate forest soil[J]. Soil Biology and Biochemistry, 2018, 116: 323-332.

Suseela V, Conant R T, Wallenstein M D, et al. Effects of soil moisture on the temperature sensitivity of heterotrophic respiration vary seasonally in an old-field climate change experiment[J]. Global Change Biology, 2012, 18(1): 336-348.

Tan W F, Zhang R, Cao H, et al. Soil inorganic carbon stock under different soil types and land uses on the Loess Plateau region of China[J]. Catena, 2014, 121: 22-30.

Tang J, Baldocchi D D, Xu L. Tree photosynthesis modulates soil respiration on a diurnal time scale[J]. Global Change Biology, 2005, 11(8): 1298-1304.

Tavares R L M, Oliveira S R M, Barros F M M, et al. Prediction of soil CO_2 flux in sugarcane management systems using the Random Forest approach[J]. Scientia Agricola, 2018, 75(4): 281-287.

Torrence, Christopher, and Gilbert P. Compo. "A practical guide to wavelet analysis." Bulletin of the American Meteorological society 79.1, 1998: 61-78.

Trumbore S. Carbon respired by terrestrial ecosystems–recent progress and challenges[J]. Global Change Biology, 2006, 12(2): 141-153.

Vargas R, Baldocchi D D, Bahn M, et al. On the multi-temporal correlation between photosynthesis and soil CO_2 efflux: reconciling lags and observations[J]. New Phytologist, 2011, 191(4): 1006-1017.

Vargas, Rodrigo, et al. "Multiscale analysis of temporal variability of soil CO_2 production as influenced by weather and vegetation." Global Change Biology 16.5, 2010: 1589-1605.

Van Bodegom P, Stams F, Mollema L, et al. Methane oxidation and the competition for oxygen in the rice rhizosphere[J]. Applied and Environmental Microbiology, 2001, 67(8): 3586-3597.

Van't Hoff, Jacobus Henricus, and Robert Alfred Lehfeldt. "Lectures on theoretical and physical chemistry." 1900.

van Verseveld C J W, Gebert J. Effect of compaction and soil moisture on the effective permeability of sands for use in methane oxidation systems[J]. Waste management, 2020, 107: 44-53.

Venturini A M, Dias N M S, Gontijo J B, et al. Increased soil moisture intensifies the impacts of forest-to-pasture conversion on methane emissions and methane-cycling communities in the Eastern Amazon[J]. Environmental research, 2022, 212: 113139.

Veleda D, Montagne R, Araujo M. Cross-wavelet bias corrected by normalizing scales[J]. Journal of Atmospheric and Oceanic Technology, 2012, 29(9): 1401-1408.

Vogelsang A, Borg M. Requirements engineering for machine learning: Perspectives from data scientists[C]. 2019 IEEE 27th International Requirements Engineering Conference Workshops (REW). IEEE, 2019: 245-251.

Walker A P, De Kauwe M G, Bastos A, et al. Integrating the evidence for a terrestrial

carbon sink caused by increasing atmospheric CO_2[J]. New phytologist, 2021, 229(5): 2413-2445.

Wang H, Yu L, Chen L, et al. Carbon fluxes and soil carbon dynamics along a gradient of biogeomorphic succession in alpine wetlands of Tibetan Plateau[J]. Fundamental Research, 2023, 3(2): 151-159.

Wang J Y, Ren C J, Feng X X, et al. Temperature sensitivity of soil carbon decomposition due to shifts in soil extracellular enzymes after afforestation[J]. Geoderma, 2020, 374: 114426.

Wilmoth J L, Schaefer J K, Schlesinger D R, et al. The role of oxygen in stimulating methane production in wetlands[J]. Global Change Biology, 2021, 27(22): 5831-5847.

Wong G X, Hirata R, Hirano T, et al. Micrometeorological measurement of methane flux above a tropical peat swamp forest[J]. Agricultural and Forest Meteorology, 2018, 256: 353-361.

Wu L, Kato T, Sato H, et al. Sensitivity analysis of the typhoon disturbance effect on forest dynamics and carbon balance in the future in a cool-temperate forest in northern Japan by using SEIB-DGVM[J]. Forest Ecology and Management, 2019, 451: 117529.

Wu X, Yao Z, Brüggemann N, et al. Effects of soil moisture and temperature on CO_2 and CH_4 soil–atmosphere exchange of various land use/cover types in a semi-arid grassland in Inner Mongolia, China[J]. Soil Biology and Biochemistry, 2010, 42(5): 773-787.

Xiong J, Wang G, Sun X, et al. Effects of litter and root inputs on soil CH_4 uptake rates and associated microbial abundances in natural temperature subalpine forests[J]. Science of The Total Environment, 2024, 912: 168730.

Xiu-jun Z, Hui X, Guan-xiong C. Effects of soil moisture and temperature on CH_4 oxidation and N_2O emission of forest soil[J]. Journal of Forestry Research, 2000, 11: 203-206.

Yao H, Peng H, Hong B, et al. Seasonal and diurnal variation in ecosystem respiration

and environmental controls from an alpine wetland in arid northwest China[J]. Journal of Plant Ecology, 2022, 15(5): 933-946.

Yazaki T, Hirano T, Sano T. Biomass accumulation and net primary production during the early stage of secondary succession after a severe forest disturbance in northern Japan[J]. Forests, 2016, 7(11): 287.

Yvon-Durocher G, Allen A P, Bastviken D, et al. Methane fluxes show consistent temperature dependence across microbial to ecosystem scales[J]. Nature, 2014, 507(7493): 488-491.

Yu J C, Chiang P N, Lai Y J, et al. High rainfall inhibited soil respiration in an Asian monsoon forest in Taiwan[J]. Forests, 2021, 12(2): 239.

Yu L, Wang Y, Wang Y, et al. Quantifying components of soil respiration and their response to abiotic factors in two typical subtropical forest stands, southwest China[J]. PloS one, 2015, 10(2): e0117490.

Yu X, Zhou W, Wang Y, et al. Effects of land use and cultivation time on soil organic and inorganic carbon storage in deep soils[J]. Journal of Geographical Sciences, 2020, 30: 921-934.

Yuan K, Zhu Q, Li F, et al. Causality guided machine learning model on wetland CH_4 emissions across global wetlands[J]. Agricultural and Forest Meteorology, 2022, 324: 109115.

Yuping Y, Liqing S, Min C, et al. Fluxes of CH_4 and N_2O from soil under a tropical seasonal rain forest in Xishuangbanna, Southwest China[J]. Journal of Environmental Sciences, 2008, 20(2): 207-215.

Zhang L, Wu X. On the application of cross correlation function to subsample discrete time delay estimation[J]. Digital Signal Processing, 2006, 16(6): 682-694.

Zhang L, Lin W, Sardans J, et al. Soil warming-induced reduction in water content enhanced methane uptake at different soil depths in a subtropical forest[J]. Science of the Total Environment, 2024, 927: 171994.

Zhang Y, Gu F, et al. Variations of carbon stock with forest types in subalpine region of southwestern China[J]. Forest Ecology and Management, 2013, 300: 88-95.